

Transcriptomic profiling and regulatory pathway modeling in a renal allograft transplantation model



**Dissertation der Fakultät für Biologie der
Ludwig-Maximilians-Universität München**

Christine von Törne

München

2009

Erstgutachter: Prof. Dr. Elisabeth Weiß

Zweitgutachter: Prof. Dr. Peter Becker

Tag der mündlichen Prüfung: 19.11.2009

Die vorliegende Arbeit wurde unter der Anleitung von PD Dr. Peter Nelson im Forschungslabor der Medizinischen Poliklinik der Ludwig-Maximilians-Universität München durchgeführt.

Das Projekt wurde gefördert durch das Graduierten Kolleg 438 „Vaskuläre Biologie“ der LMU und durch die Deutsche Forschungsgemeinschaft im Rahmen des Sonderforschungsbereiches 571 „Autoimmunreaktionen: von den Manifestationen über die Mechanismen zur Therapie“.

Table of contents

Abstract	1
Zusammenfassung	2
1 Introduction	3
1.1 Chronic allograft dysfunction (CAD)	3
1.1.1 Inflammation and fibrosis in CAD	4
1.1.2 Myofibroblasts	4
1.1.3 Pathways activated in epithelial to mesenchymal transition (EMT)	5
1.1.3.1 The TGFB pathway	6
1.1.3.2 The NOTCH pathway	7
1.1.3.3 The hedgehog (HH) pathway	8
1.1.3.4 The WNT pathway	10
1.2 Preceding experiments.....	12
1.2.1 CAD in a Fisher to Lewis rat model	12
1.2.2 Effects of retinoic acid treatment	13
1.2.3 Working mechanism of retinoic acid.....	14
2 Aim of the present study	17
2.1 Transcriptomic profiling of kidney transplants.....	17
3 Material	18
3.1 Microarrays.....	18
3.1.1 CEL files.....	19
3.2 Kidney samples	20
3.2.1 RNA isolated from kidney sections.....	20
3.2.2 Kidney sections for immunohistochemistry	20
3.3 Cells	20
3.3.1 Human fibroblast cell line K4IM.....	20
3.3.2 Media used for K4IM	21
3.4 Oligonucleotides.....	21
3.4.1 Oligonucleotides for qPCR of cDNA.....	21
3.4.1.1 AoD Assays	21
3.4.1.2 QuantiTect Primer Assays	21
3.4.1.3 Oligonucleotides for qPCR, self-designed.....	21
3.4.2 Oligonucleotides for PCR of genomic DNA, self designed.....	22
3.5 Enzymes, enzyme solutions, and inhibitors.....	22
3.6 Antibodies.....	22
3.6.1 Primary antibodies.....	22
3.6.2 Secondary antibodies.....	22
3.7 Kits	22
3.8 Chemicals, reagents, and additives.....	23
3.9 Buffers and Solutions	24
3.10 Consumables	25
3.11 Instruments.....	26
3.12 Software	27

3.12.1	Commercial software.....	27
3.12.2	Freeware and databases.....	27
4	Methods	28
4.1	Microarray analysis	28
4.1.1	ChipInspector analysis of CEL Files.....	28
4.1.2	BiblioSphere and GO analysis	29
4.1.3	Pathway analysis	29
4.1.4	Robust multichip average (RMA) analysis.....	30
4.1.5	Cluster analysis.....	30
4.2	Verification of microarray results on the mRNA level	31
4.2.1	RNA Cleanup	31
4.2.2	Quantification of RNA.....	31
4.2.3	Reverse Transcription	31
4.2.4	Quantitative PCR (qPCR).....	32
4.2.5	Calculation of regulation.....	33
4.3	Verification of microarray and qPCR results on the protein level.....	34
4.3.1	Histology	34
4.3.2	Immunohistochemistry	34
4.3.2.1	Sample preparation.....	35
4.3.2.2	Detection of the antigen	35
4.4	Identification of the working mechanism of 13cRA on the DNA level	37
4.4.1	Cell cultivation	37
4.4.1.1	Counting of viable cells	37
4.4.1.2	Cryo-conservation of cells	37
4.4.1.2.1	Freezing of cells.....	37
4.4.1.2.2	Thawing of cells	38
4.4.2	Cell culture and stimulation experiments.....	38
4.4.3	Enzyme-linked immunosorbent assay (ELISA)	39
4.4.4	Chromatin immunoprecipitation (ChIP)	39
4.4.4.1	Chromatin preparation	39
4.4.4.1.1	Formaldehyde fixation.....	39
4.4.4.1.2	Lysis of cells.....	40
4.4.4.1.3	Sonication	40
4.4.4.1.4	Gel electrophoresis	40
4.4.4.2	Immunoprecipitation.....	41
4.4.4.2.1	Preparation of Pansorbin (StaphA) cells	41
4.4.4.2.2	Blocking of Staphylococcus A cells.....	41
4.4.4.2.3	Preparation of samples	41
4.4.4.2.4	Precipitation	42
4.4.4.2.5	Decrosslinking and ethanol precipitation.....	42
4.4.4.2.6	Protease K digestion.....	42
4.4.4.3	DNA analysis.....	43
4.4.4.3.1	Phenol-chloroform extraction	43
4.4.4.3.2	Ethanol precipitation	43
4.4.5	PCR analysis.....	44
4.5	Statistical analyses	44

5	Results	45
5.1	Transcriptomic profiling identifies progressive changes in the transplantation model during CAD	45
5.1.1	Inflammation associated gene expression in CAD	49
5.1.2	EMT and fibrosis associated gene expression in CAD	52
5.1.3	Pathways regulated during progression of CAD	54
5.1.3.1	Specific activation of the hedgehog pathway	55
5.1.3.2	Specific and progressive changes of WNT genes and pathways ..	59
5.1.3.2.1	Regulation of the canonical WNT pathway	61
5.1.3.2.2	Changes in the WNT-Ca ²⁺ pathway	67
5.1.3.2.3	The WNT planar cell polarity pathway	70
5.2	13cRA is a master regulator of CAD induced transcriptomic alterations	71
5.2.1	Cluster analysis of overall gene expression	71
5.2.2	The retinoic acid – HH – WNT axis	73
5.2.2.1	HH pathway	73
5.2.2.2	WNT pathway	74
5.2.3	13cRA influences the proinflammatory and profibrotic milieu	78
5.2.4	Working mechanism of 13cRA at the promoter level	83
5.2.4.1	13cRA mediates inhibition of TNFA stimulated <i>CCL5</i> promoter activation	83
5.2.4.2	Nuclear corepressor (NCOR) binding to promoters	83
5.2.4.2.1	Establishing the ChIP	83
5.2.4.2.2	NCOR binding to the <i>CCL5</i> promoter	85
6	Discussion	87
6.1	Transcriptomic analysis	87
6.2	Alterations in gene expression during disease progression	89
6.3	Therapeutic intervention of disease progression by 13cRA	96
7	Abbreviations	103
8	References	105
9	Supplementary data	113
	Supplementary table 1:	113
	Supplementary table 2:	116
	Supplementary table 3:	117
	Supplementary table 4:	118
	Supplementary figure 1:	119
	Supplementary figure 2:	121
	Supplementary figure 3:	123
	Supplementary figure 4:	125
10	Publications	126
11	Acknowledgements	127
12	Curriculum vitae	128

Abstract

Chronic allograft dysfunction (CAD) following kidney transplantation is characterized by progressive fibrosis and a smoldering inflammatory infiltrate. A modified Fischer 344 (RT1^{lv}) to Lewis (RT1^l) rat renal allograft model was used to study transcriptomic changes during the initiation and progression of CAD and to identify potential therapeutic modes of action of treatment with 13cRA previously shown to limit the development of CAD. Transcriptomic profiling was performed using Affymetrix DNA arrays at time points 0, 7, 14 and 56 days after transplantation. The animal model showed development of significant chronic fibrotic damage with accompanying inflammatory infiltrate by day 56 after transplantation. Regulatory pathways were identified by the *Database for Annotation, Visualization, and Integrated Discovery* (DAVID) and modulated, based on the *Kyoto Encyclopedia of Genes and Genomes* (KEGG) pathways database.

Microarray analysis revealed dramatic changes in the mRNA expression levels of genes associated with inflammation and fibrosis, as well as the hedgehog and WNT pathways, with a gradual increase in the number of differentially regulated genes during progression of tissue damage. Disease phenotype, as well as differential regulation of select components of the hedgehog, canonical WNT and WNT-Ca²⁺ signaling pathways could be verified by quantitative PCR (qPCR) and immunohistochemistry. Treatment with 13cRA, not only attenuated disease progression, but even reversed early effects of CAD. The overall effects of the treatment are mediated by a potentially direct influence on fibrosis and inflammation associated gene expression, as well as by a specific modulation, observed for hedgehog and WNT pathway activations. The results identify a series of potential pathways that may represent therapeutic targets in chronic allograft dysfunction.

Zusammenfassung

Die chronische Transplantat Dysfunktion (CAD), als Folge einer Nierentransplantation, ist charakterisiert durch voranschreitende Fibrose begleitet von einem entzündlichen Infiltrat. Um Veränderungen auf transkriptomischer Ebene im Krankheitsverlauf der CAD zu untersuchen wurde ein renales Transplantations-Modell verwendet, in dem Fisher344(RT1^{lv})-Rattennieren in Lewis(RT^{1l}) Ratten transplantiert wurden. Zusätzlich dazu sollten die Mechanismen untersucht werden, die dem zuvor beobachteten therapeutischen Effekt einer Isotretionin-Behandlung der Ratten nach Transplantation zugrunde liegen. Die Charakterisierung des Transkriptoms wurde durchgeführt unter der Verwendung von Affymetrix Microarrays, von den Zeitpunkten null (untransplantierte Kontrollen), 7, 14 und 56 Tagen nach Explantation. Ein chronischer Schaden, begleitet von einem entzündlichen Infiltrat wurde 56 Tage nach Explantation im Tiermodell beobachtet. Regulatorische Signalwege wurden mit Hilfe der *Database for Annotation, Visualization, and Integrated Discovery* (DAVID) und basierend auf Signalwegen der *Kyoto Encyclopedia of Genes and Genomes* (KEGG) Datenbank identifiziert.

In der Microarray-Analyse zeigten sich deutliche Veränderungen der Genexpression von Entzündungs- und Fibrose-assoziierten Genen. Desweiteren wurden Veränderungen beobachtet die Hedgehog- und WNT-Signalwege betreffend, mit einem steten Anstieg der Anzahl differentiell regulierter Gene während des Krankheitsverlaufs. Die differentielle Regulation sowohl Krankheits-assoziiertes Gene als auch bestimmter Komponenten des Hedgehog-, kanonischen WNT- und WNT-Ca²⁺-Signalweges konnte mittels quantitativer PCR (qPCR) und teilweise auch auf der Proteinebene verifiziert werden. Die Isotretionin-Behandlung schwächte den Krankheitsverlauf nicht nur generell ab, sondern machte frühe Veränderungen sogar rückgängig. Die Effekte der Behandlung setzten sich aus einer möglicherweise direkten Beeinflussung der Fibrose bzw. Entzündung und einer spezifischen Modulation der beobachteten Aktivierung der Hedgehog- und WNT-Signalwege zusammen. Unsere Ergebnisse präsentieren Kandidaten für mögliche Zielgene einer Therapie der chronischen Transplantat Dysfunktion.

1 Introduction

1.1 Chronic allograft dysfunction (CAD)

Renal transplantation represents the only therapy option for individuals with end-stage renal disease. While short-term graft survival increased and acute rejection decreased dramatically within the last 20 years, late graft loss remains to be a critical issue. Chronic allograft dysfunction (CAD) is a major long-term complication following kidney transplantation and is now the principle reason for loss of allografts [1]. CAD is a complex disease process resulting from the cooperation of humoral and cellular immune responses and nonimmunological factors [2-4]. Clinically, CAD is manifested by a gradual deterioration of renal function accompanied by hypertension and proteinuria [5].

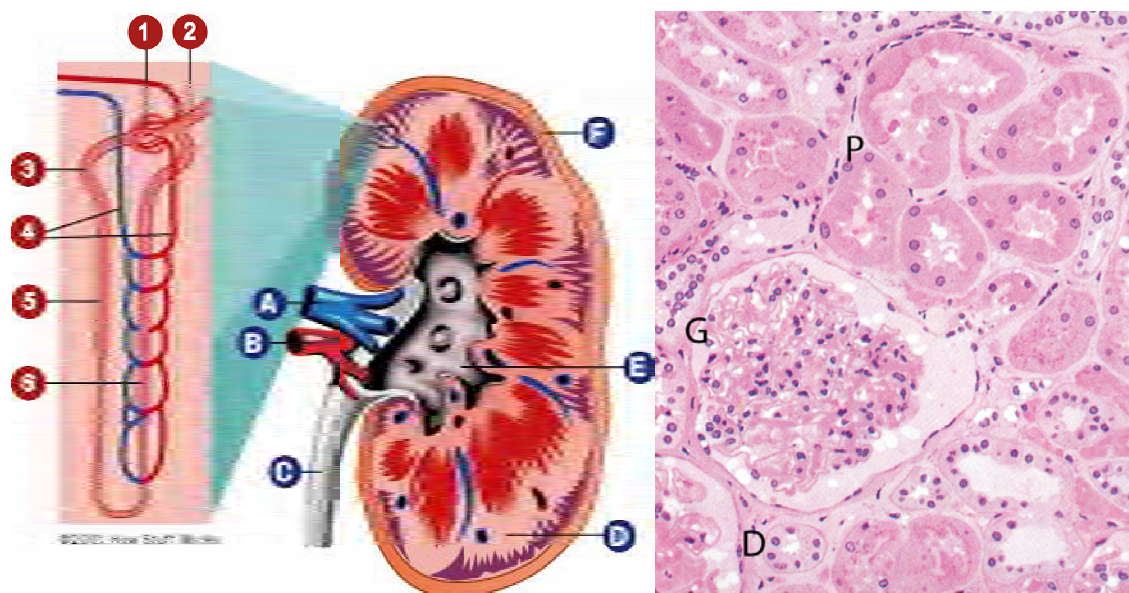


Fig. 1: Kidney and Nephron. The left figure displays parts of the kidney and the nephron; 1: Glomerulus, consisting of Bowman's capsule and Glomerular capillaries, 2: Distal tubule; 3: Proximal tubule, 4: Peritubular capillaries, 5: Descending limb of loop of Henle, 6: Ascending limb of loop of Henle, A: Renal vein, B: Renal artery, C: Ureter, D: Medulla, E: Pelvis, F: Cortex. From Freudenrich, Ph.D., Craig. "How Your Kidneys Work." 10 January 2001. <http://www.howstuffworks.com/kidney.htm>

The right part of the figure originates from the "Sobotta Atlas of Human Anatomy" [6] and shows a section of a human kidney cortex. Staining with hematoxylin-eosin, 100x, P: Proximal tubule, G: Glomerulus, D: Distal tubule

Histopathologically, CAD is characterized by hyalinosis and fibrosis of preglomerular vessels, transplant glomerulopathy, glomerulosclerosis, interstitial fibrosis with a variable degree of mononuclear cell infiltrates, and tubular atrophy [3, 4]. Importantly, many of the pathophysiologic features found in CAD can also be seen in other chronic fibrosing renal diseases such as diabetic nephropathy [7, 8].

Thus, CAD can be regarded as a useful model for processes associated with progressive renal disease. Figure 1 shows the general compartments of the kidney in humans.

1.1.1 Inflammation and fibrosis in CAD

The kidney's response to injury resembles a generalized wound healing response. The focus of wound healing is restoration of tissue architecture and recovery of function. For reasons that are not well understood, this is only partially successful in the adult [9]. In response to sustained inflammation fibrosis, an increased scarring of the tissue, is observed over time and is believed to be the central cause of the progressive decline and final loss of transplant in CAD [9]. A number of proinflammatory and fibrogenic mediators such as interleukin 6 (IL6; nomenclature for human protein symbols in accordance with the "Guidelines for human gene nomenclature" [10]), tumor necrosis factor alpha (TNFA), interferon gamma (IFNG) and transforming growth factor beta 1 (TGFB1) have been shown to be involved in various stages of the chronic inflammatory and reparative process [2].

There are indications that chemokines such as chemokine ligand 5 (CCL5) and interferon inducible protein 10 (CXCL10/IP10) also contribute to CAD [11]. These proteins are synthesized and secreted by tissue-infiltrating inflammatory cells as well as by activated graft parenchymal cells [4].

1.1.2 Myofibroblasts

Fibrosis is associated with an excess synthesis of extracellular matrix (ECM), usually collagen. During renal fibrosis ECM is produced by activated fibroblasts, so called myofibroblasts, as evidenced by their *de novo* synthesis of alpha smooth muscle actin [12]. The origin of myofibroblasts in chronic renal fibrosis is a matter of conjecture. It has been suggested that myofibroblasts migrate either from the perivascular regions [13] or that their progenitors are recruited from bone marrow [14]. An emerging paradigm suggests that myofibroblasts may also originate from either the transition of tubular epithelial cells via epithelial to mesenchymal transition (EMT) [15], or by the transformation of resident fibroblasts [16]. EMT would be consistent with the hypothesis that a recapitulation of developmental programs is activated in response to tissue injury [9]. During EMT, epithelial cells have been described to lose polarity and cell-cell contacts, and to acquire mesenchymal cell expression profiles, and a migratory phenotype [9].

1.1.3 Pathways activated in epithelial to mesenchymal transition (EMT)

To better understand and potentially prevent organ loss due to chronic fibrosis, it is important to identify the underlying molecular mechanisms that drive these processes. Complex signal transduction between resident kidney cells and the infiltrate takes place and orchestrates changes in the phenotype of the kidney cells. If it was possible to correlate changes in the signal transduction to pathology one would possess a tool for manipulating early stages of the disease and might be able to change the outcome.

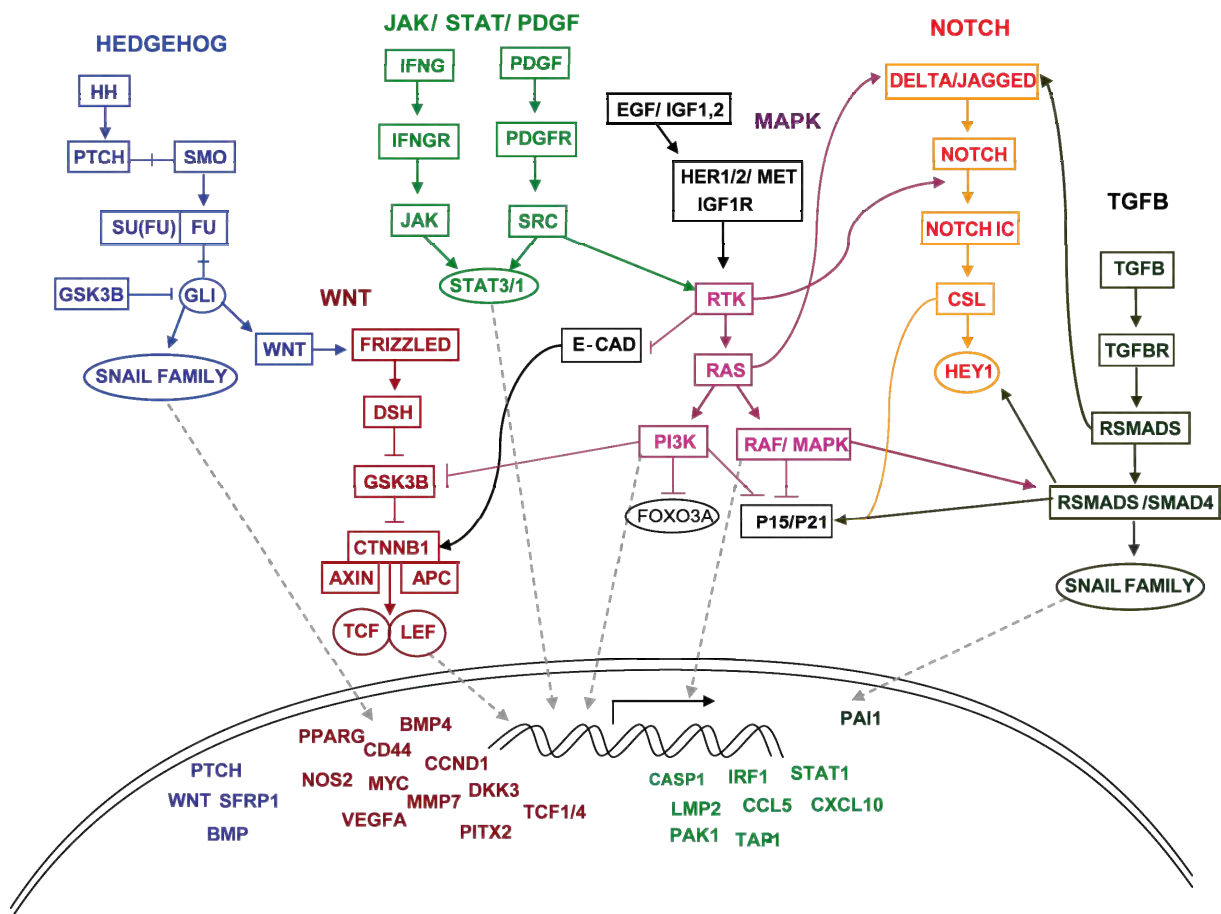


Fig. 2: Pathways in EMT. This figure overviews crosstalk of pathways discussed in the context of EMT, including HEDGEHOG, WNT, JAK-STAT/PDGF, MAPK, NOTCH and TGFβ pathways (discussed in 1.1.3). Boxes indicate gene products of canonical signaling of the individual pathways. Colors are uniform for the pathways and the target genes. Transcriptional activation of pathway genes leads to protein interaction, subsequently, target gene transcription. Arrows indicate positive interaction of gene products, symbols are used as defined in Abbreviations. Modified from [17].

Since in wound healing and fibrosis, steps of development seemed to have been recapitulated, it is not surprising that many of the signal transduction pathways, discussed in the context of EMT and fibrosis, were originally identified in developmental biology.

1.1.3.1 The TGFB pathway

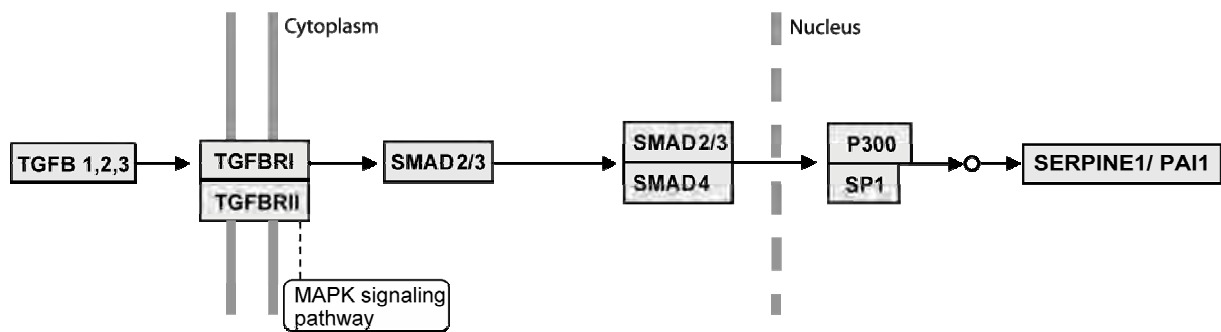


Fig. 3: The TGFB pathway. The diagram displays the main components of canonical TGFB signaling (discussed in detail in 1.1.3.1). Boxes indicate gene products, arrows indicate positive interaction of gene products, and the circle represents additional molecules involved. The white box indicates possible crosstalk with other pathways. Other symbols are used, as defined in Abbreviations. After binding of TGFB1,2,3 to the receptors TGFBR1/II signal transducers (SMAD) are activated and translate the signal into the nucleus. TGFB1,2,3-induced transcription factors bind to the DNA and activate transcription of TGFB1,2,3 target genes, one example of a TGFB1 target gene is PAI1. This scheme is a modification from the KEGG database pathway view (<http://www.genome.jp/kegg/kegg2.html>).

TGFB1 is a secreted cytokine that regulates embryonic development and adult tissue homeostasis [18]. The TGFB family includes TGFB1, TGFB2 and TGFB3. The ligands bind to heteromeric complexes of type I and II receptor serine/threonine kinases (TGFBR1, TGFBR2) [19]. This leads to phosphorylation and activation of the TGFBR1. This pathway signals via phosphorylation of cytoplasmic SMAD proteins. The SMAD proteins are homologs of the *drosophila* protein “mothers against decapentaplegic” (Mad) and the *C. elegans* protein SMA. SMADs are divided into two types, the receptor-regulated SMADs (rSMADs) and the coSMADs. In the TGFB pathway, signaling is mediated by the rSMADs SMAD2 and SMAD3, as well as the coSMAD SMAD4. The phosphorylated rSMADs bind a coSMAD with high affinity and enter the nucleus as rSMAD/coSMAD complex. The complex binds to cofactors or promoters and regulates the transcription of DNA.

Alternative signaling of TGFB include the mitogen-activated protein kinase (MAPK) and protein kinase B (PKB) pathways [20]. TGFB1 is a major mediator of renal fibrosis [21, 22] [23] and known to stimulate EMT *in vitro* [24]. Figure 3 summarizes the basic steps in canonical TGFB signaling.

1.1.3.2 The NOTCH pathway

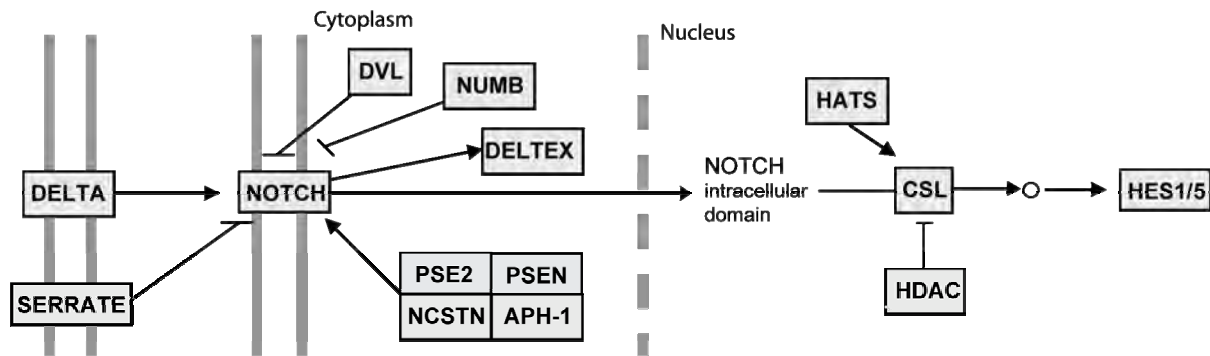


Fig. 4: The NOTCH pathway. The diagram displays the main components of the NOTCH signaling pathway (discussed in detail in 1.1.3.2). Boxes indicate gene products, arrows indicate positive interaction of gene products, and the circle represents additional molecules involved. Other symbols are used as defined in Abbreviations. After the binding of DELTA to NOTCH, the intracellular domain of NOTCH is cleaved and enters the nucleus. The intracellular domain can, involving further signaling steps, activate transcription factors of the HES family. This scheme is a simplified modification from the KEGG database pathway view.

The notch gene was discovered almost 90 years ago, but only in the early eighties was it identified to encode a single-pass transmembrane receptor. Vertebrates possess four different notch receptors, referred to as NOTCH1 to NOTCH4 and five transmembrane ligands: jagged 1, jagged 2, delta-like 1, delta-like 3, and delta-like 4 (JAG1, JAG2, DLL1, DLL3 and DLL4). NOTCH signaling is activated upon cell-to-cell contact as a result of interactions between NOTCH receptors and their ligands. At the molecular level, triggering of NOTCH receptor by ligand binding promotes two proteolytic cleavage events at the NOTCH receptor that result in the separation of the NOTCH intracellular domain (NICD) into the cytoplasm. NICD cannot directly bind to DNA but instead, heterodimerizes with the recombination signal sequence-binding protein Jk (RBP-J). NICD first displaces corepressors from RBP-J, resulting in de-repression of promoters containing RBP-J binding sites and subsequently, recruits a coactivator complex to activate transcription of NOTCH target genes [25]. The hairy/enhancer of split (HES) genes are highly conserved proteins that are regulated by NOTCH in multiple cell types [26]. These transcription factors are the best-described NOTCH target genes [27]. NOTCH pathway activation has been observed in the pathogenesis of glomerular diseases [28] and in EMT in development and tumorigenesis [29, 30]. Figure 4 summarizes the basic steps in canonical NOTCH signaling.

1.1.3.3 The hedgehog (HH) pathway

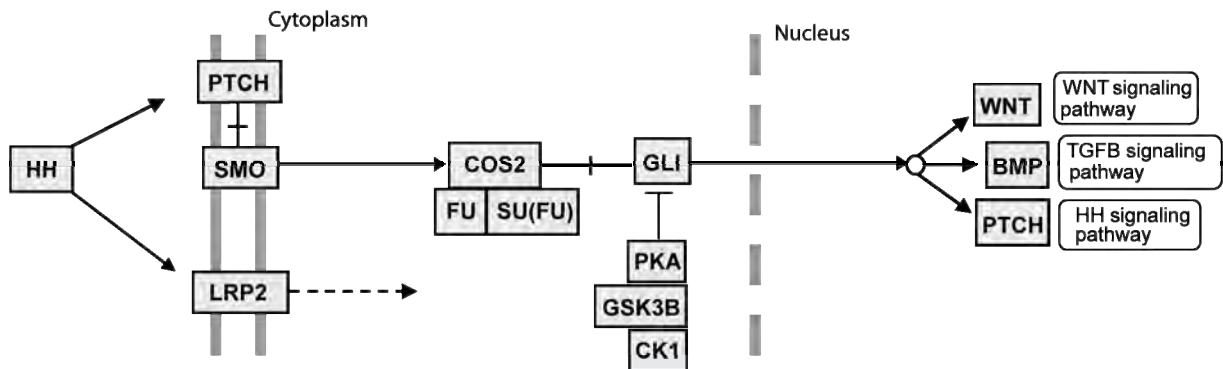


Fig. 5: The hedgehog pathway. The diagram displays the main components of canonical HH signaling (discussed in detail in 1.1.3.3). Boxes indicate gene products, arrows indicate positive interaction of gene products, and the circle represents additional molecules involved. The white boxes indicate possible crosstalk with other pathways. Other symbols are used as defined in Abbreviations. After binding of HH to the receptor PTCH, the inhibition of the SMO receptor is relieved. Subsequent activation of GLI transcription factors leads to nuclear enrichment of GLI and activation of transcription of Hedgehog target genes such as the receptor PTCH. This scheme is a simplified modification from the KEGG database pathway view.

Mammals have three secreted hedgehog (HH) protein isoforms: sonic (SHH), indian (IHH) and desert (DHH). The HHs bind to their receptors patched 1 or 2 (PTCH1, PTCH2) which then release their repression of the 7-transmembrane protein smoothed (SMO). SMO regulates activity of the HH specific transcription factors GLI family zinc finger 1, 2 and 3 (GLI1, GLI2 and GLI3) by stabilizing the GLIs and stopping the GLI-inhibitor suppressor-of-fused (SU(FU)). Stabilized GLIs can enter the nucleus and activate transcription of HH target genes [31]. Similar to the other pathways discussed here, the HH pathway also plays critical roles in development and in adult tissue homeostasis. Moreover, this pathway has been discussed in the context of tissue repair during chronic persistent inflammation and EMT in tumorigenesis [17, 31]. In a mouse model, HH could be demonstrated to be essential for normal wound healing [32]. In addition to patched, the so called megalin receptor (LRP2/Megalin) has been shown to bind SHH and mediate endocytosis [33, 34]. Figure 5 summarizes the basic steps in canonical HH signaling.

Megalin is a large (600 kDa), single spanning transmembrane glycoprotein which belongs to the low-density lipoprotein receptor family [35]. Megalin is an endocytotic scavenger receptor that mediates non-specific uptake of protein [36] (see figure 6) and is internalized after ligand binding. This receptor is of special interest, because it is expressed in cells of the kidney proximal tubule brush border, in addition to its association with the HH pathway. Also, megalin expression is put into context with

the TGFB pathways and seems to play an important role in chronic kidney diseases [37-39].

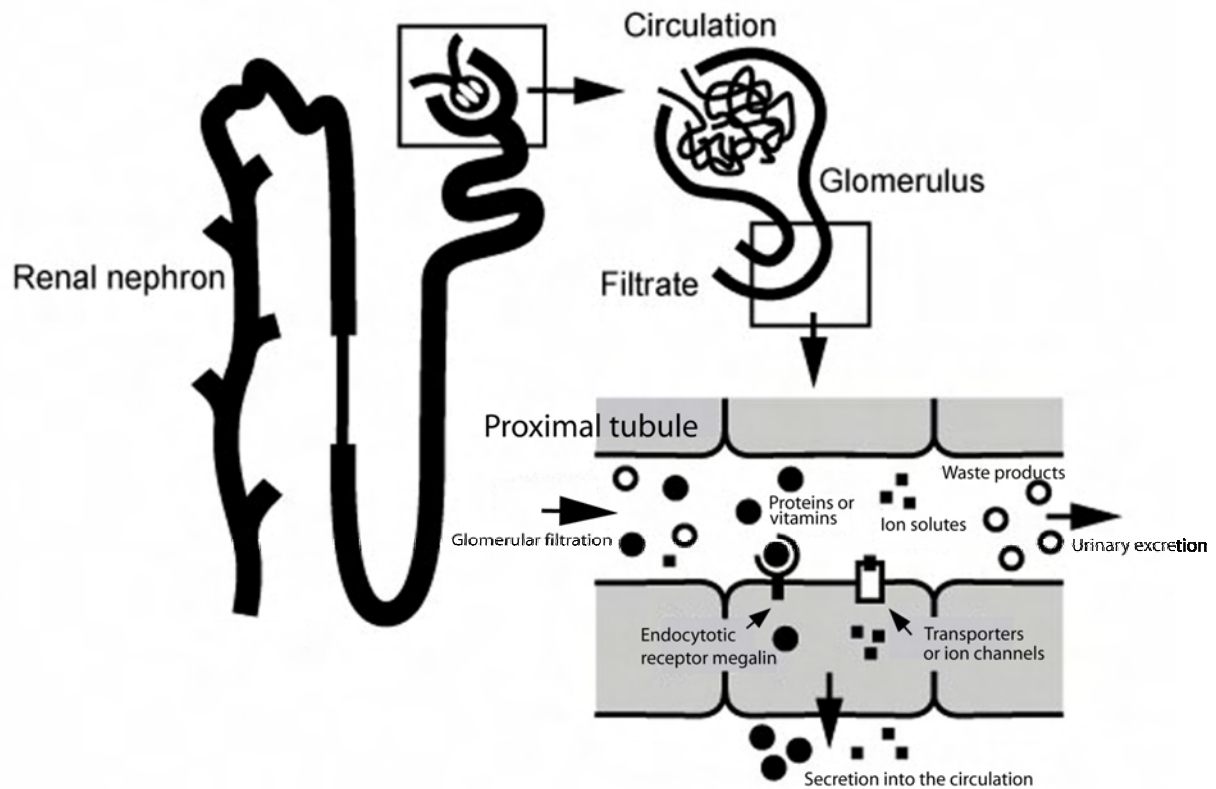


Fig. 6: LRP2/Megalin. The scheme gives an overview of the LRP2/Megalin localization within the renal nephron, as a functional unit of the kidney. After glomerular filtration; the primary excretion fluid is channeled through the tubule and through active transport, or passive processes along the tubule, the urine is generated. Megalin is an endocytotic scavenger receptor of the proximal tubule that binds low weight molecules such as certain proteins or vitamins and transports them from the apical side of the tubule cells to the basal side. The scheme is adapted from [Recepticon Aps \(www.recepticon.com\)](http://www.recepticon.com).

1.1.3.4 The WNT pathway

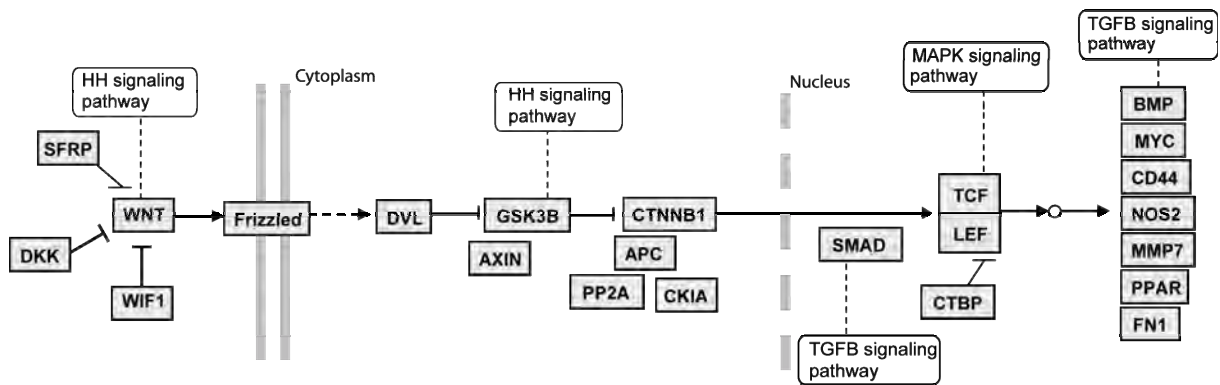


Fig. 7: The canonical WNT pathway The diagram displays the main components of canonical WNT signaling (discussed in detail in 1.1.3.4). Boxes indicate gene products, arrows indicate positive interaction of gene products, and the circle represents additional molecules involved. The white boxes indicate possible crosstalk with other pathways. Other symbols are used as defined in Abbreviations. After binding of WNT to the receptor frizzled degradation of CTNNB1 is inhibited, resulting in nuclear enrichment of CTNNB1. Complexes of CTNNB1 and WNT-dependent transcription factors such as LEF1 bind to the DNA and activate WNT target genes expression. Known targets are amongst others FN1, MMP7 and CD44. This scheme is a simplified modification from the KEGG database pathway view.

Two decades ago investigators discovered the homology between the *Drosophila* wingless gene (*wg*) and the vertebrate oncogene integrase 1 (*INT1*). They named the family of secreted glycoproteins, known as WNTs (*wg-INT1s*). To date 19 WNT-proteins have been identified in human, mouse and rat. Members of the WNT superfamily activate at least three distinct pathways. The WNT pathways, originally characterized as essential components in early development, are implicated in many physiological and pathophysiological processes. It has been proposed that WNT signaling may be recapitulated in the progressive damage associated with chronic organ failure [40]. Of the three WNT pathways, canonical WNT, WNT-Ca²⁺ and WNT planar cell polarity, the canonical WNT pathway, acting through activation of beta-catenin (CTNNB1), is best understood. In the absence of WNT, CTNNB1 becomes phosphorylated and then degraded by the proteasome. If select WNT proteins bind to so called frizzled receptors (FZD), the resulting signaling cascade inhibits CTNNB1 degradation, leading to beta-catenin accumulation in the nucleus, where the CTNNB1-T-cell specific transcription factor (CTNNB1-TCF) complex activates Wnt target gene transcription.

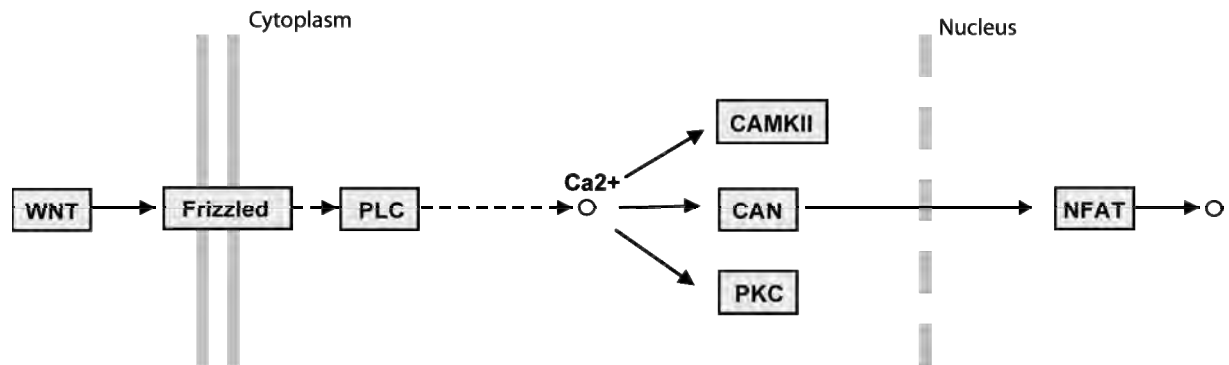


Fig. 8: The WNT-Ca²⁺ pathway The diagram displays the main components of WNT –Ca²⁺ signaling (discussed below). Boxes indicate gene products, arrows indicate positive interaction of gene products, and the circle represents additional molecules involved. Other symbols are used as defined in Abbreviations. After binding of WNT to the FZD receptor, activation of phospholipase C, calmodulin kinase II and protein kinase C is involved in the signaling process. Ca²⁺-dependent signaling finely leads to activation of transcription factors of the NFAT-family. This scheme is a simplified modification from the KEGG database pathway view.

The WNT-Ca²⁺ pathway acts in a beta-catenin independent manner, through calmodulin kinase II, protein kinase C, and the subsequent activation of transcription factors of the nuclear factor of activated T-cells (NFAT) family [41]. Figure 8 summarizes the basic steps in WNT-Ca²⁺ signaling.

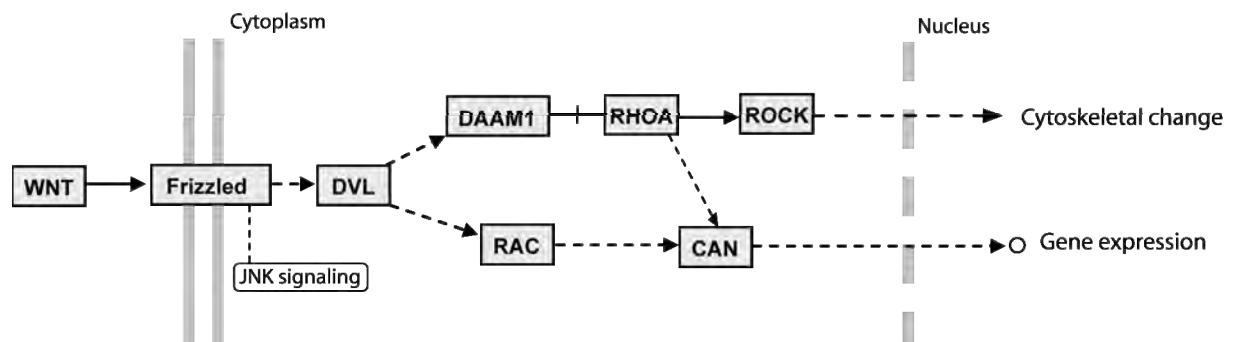


Fig. 9: The WNT planar cell polarity pathway The diagram displays the main components of WNT–PCP signaling (discussed below). Boxes indicate gene products, arrows indicate positive interaction of gene products, and the circle represents additional molecules involved. Other symbols are used as defined in Abbreviations. This scheme is a simplified modification from the KEGG database pathway view.

The third pathway, the WNT planar cell polarity (PCP) pathway signals independently from beta-catenin. The PCP pathway activates either the ras homologue gene-family member A (RHOA) – Rho-associated coiled-coil-containing protein kinase (ROCK) pathway, or signals through Jun N-terminal kinases (JNK) and is thought to regulate changes in the cytoskeleton [42, 43]. Figure 9 summarizes the basic steps of the WNT planar cell polarity pathway. Based on the proposed targets of these pathways, each could potentially contribute to pathophysiologic events associated with fibrosis.

1.2 Preceding experiments

1.2.1 CAD in a Fisher to Lewis rat model

In the original Fisher to Lewis rat renal allograft model as described by Lee et al. [44], Fisher kidneys were transplanted into Lewis rats. These rat strains differ in their major histocompatibility complex (RT1) RT1-C/E/M region. The Fisher strain represents the RT1^{l^v} and the Lewis strain the RT1^l haplotype variant of the RT1-C/E/M region [45, 46]. This model also made use of low doses of cyclosporine A and right kidney nephrectomy seven to ten days after transplantation. Without the right, healthy kidney, the recipient animal is solely dependent on the function of the allograft. We, and others, have reported that this allograft model does not show evidence of CAD, including rejection in preglomerular vessels, glomeruli and tubulointerstitium, and displays only small areas of unspecific acute and chronic fibrosing lesions, probably due to ischemia reperfusion injury and surgical trauma [5, 47, 48]. To this end a modification of this model was used. Cyclosporine A and right nephrectomy of the recipient's own kidney were omitted after kidney transplantations from Fisher to Lewis rats, performed in collaboration with Prof. Herrmann-Josef Gröne (Deutsches Krebsforschungszentrum Heidelberg) [5]. These modifications of the model were found to lead to a well-defined, acute phase (day 0 to day 14) of vascular rejection manifested in endothelialitis, interstitial rejection with tubulitis, and transplant glomerulitis [5, 47, 49]. Importantly, during the chronic rejection-phase of this modified model (day 14 to day 56), morphologic phenomena, characteristic of allograft rejection in humans, are observed. The preglomerular arteries show an increase in subendothelial matrix and an infiltration of the subendothelium and media by mononuclear cells (displayed in figure 10). Due to immunosuppression this latter phenomenon is only seen in relatively few cases of human allografts with CAD. Transplant glomerulopathy, as well as changes in the tubulointerstitium that are characteristic of CAD show tubular atrophy and matrix increase, as well as focal low level tubulitis in differentiated tubules (see figure 10). In summary, major morphologic phenomena commonly observed during the progression of CAD in patients can be documented in this model.

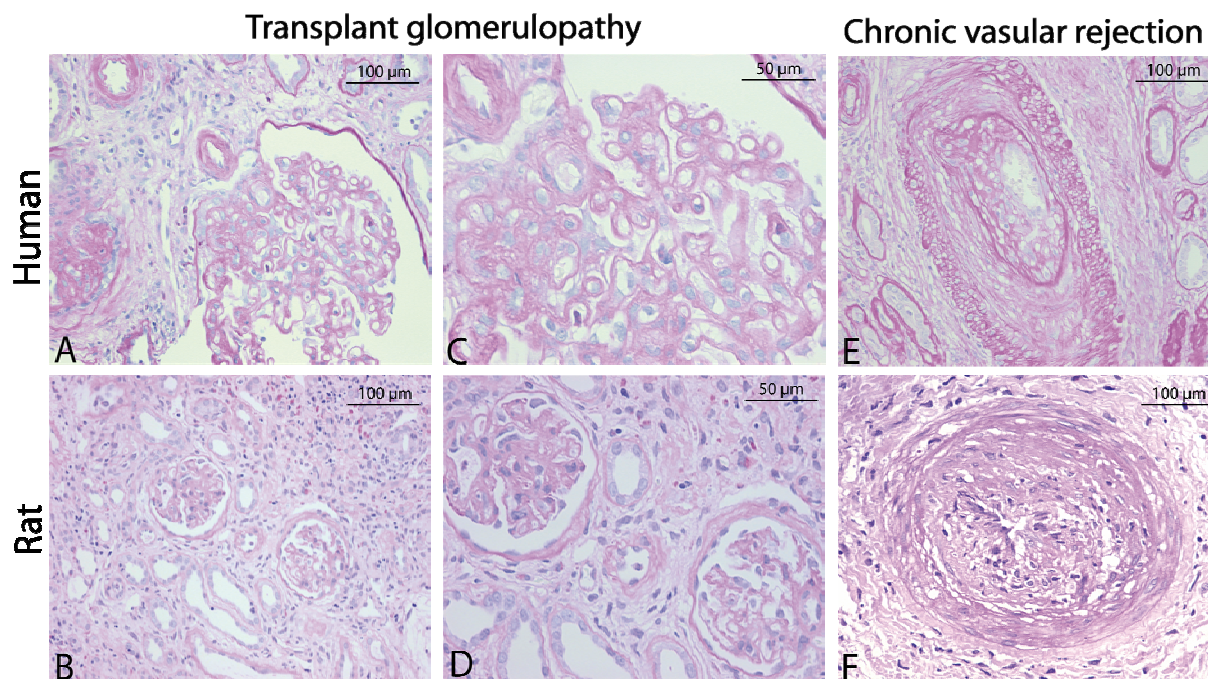


Fig. 10: Allograft morphology. Periodic-acid Schiff (PAS) staining was performed on kidney sections by Ms. Gabrielle Schmidt from the DKFZ, Heidelberg, as described in 4.3.1. **A-D:** figures A to D display transplant glomerulopathy (A- human, B- fisher to lewis (FL) rat- allografts; C,D - are higher magnifications. The glomeruli show mesangial matrix expansion. The capillary walls are thickened and focally duplicated with few adherent mononuclear cells in the capillary lumen (glomerulitis). The surrounding tubulointerstitium presents chronic changes such as tubular atrophy and interstitial fibrosis, with an additional inflammatory cell infiltrate. **E, F:** figures E and F display chronic vascular rejection (E- human, F- FL rat- allograft). Arteries show an increase in the subendothelial matrix, with a severe obliteration of the vessel lumen and an infiltration of the subendothelium and media by mononuclear cells. Numbers range from few cells in the human (E) to more prevalent ones in the rat (F) (A,B and E,F: 200x; C,D: 400x).

1.2.2 Effects of retinoic acid treatment

In order to find alternatives to the conventional immunosuppressive therapies, the effect of retinoic acid to prevent allograft rejection was tested in this model. 13-cis-retinoic acid (13cRA) has been reported to ameliorate rejection phenomena and to preserve graft function in acute models of renal transplantation [50]. Based on these results, it was hypothesized that 13cRA could prevent or moderate CAD.

The anti-inflammatory and anti-proliferative actions of retinoids (derivatives of vitamin A) have long been known [49]. The receptors of retinoids belong to the superfamily of nuclear receptors (NRs). NRs form a class of transcription factors regulated by steroids, thyroid hormone, retinoids and vitamin D [51]. Retinoids act via retinoic acid (RAR) and retinoid X (RXR) receptors, with alpha, beta and gamma subtypes. RAR and RXR receptors are widely expressed in the rat and human kidney as well as in immune cells such as B and T cells and monocytes/macrophages [52-54].

Type 1 nuclear receptors are characterized by the formation of homodimers and include, amongst others, the estrogen receptor. Type 2 nuclear receptors are characterized by the formation of retinoic X receptor heterodimers and include, amongst others, the RAR, RXR and peroxisome-proliferators-activated-receptor (PPAR). Hetero-dimerization increases diversity in the signaling of nuclear receptors. The retinoid receptors regulate expression of target genes, either by direct binding to retinoic acid response-elements, or indirectly, by diverse mechanisms called transactivation or transrepression. They are known to influence transcription factors such as activator protein-1 (AP-1) [55] and nuclear factor-kB (NF-kB) [56].

In experimental models of glomerulonephritis, retinoids have been shown to inhibit proliferation of mesangial cells, lower the number of infiltrating monocytes, and reduce extracellular matrix deposition without signs of vitamin A toxicity [57, 58].

A dose of 2 mg 13cRA/kg body weight/day, corresponding to a dose used in humans, was tested by Prof. Gröne's laboratory as a potential treatment modality in the modified Fisher to Lewis model of rat renal transplantation. The 13cRA was administered orally starting on the day of transplantation. On day 56 after transplantation, a significant preservation of renal function could be observed, while the placebo group showed characteristic histological changes of CAD in the allografts as early as 4 weeks. Morphometric analysis showed inhibition of subendothelial fibrosis. Morphology of glomerular structures was preserved. Infiltration of monocytes and CD8+ T-cells was still observed but to a significantly lesser degree. The mRNA expression of inflammatory cytokines/chemokines was significantly lower in the 13cRA treated animals [5].

1.2.3 Working mechanism of retinoic acid

Retinoic acid could have a protecting effect on cells of the grafted kidney as well as on immune cells, preventing alloreactivity. Adams et al. further investigated the working mechanism of the 13cRA on the DNA level. TNFA - mediated activation of *CCL5* gene expression can be inhibited by 13cRA. Truncated reporter constructs showed that action of 13cRA is not necessarily mediated through direct binding to DNA, since deletion of the consensus sequences did not influence 13cRA suppression of *CCL5* promoter activity [5]. In 2005, Pascual et al. [59] identified a novel molecular pathway of nuclear receptor mediated transrepression. The peroxisome proliferator-activated receptor gamma (PPARG) is a member of the

nuclear receptor family, as well as a receptor for retinoic acid [60]. It could be demonstrated that the PPARG receptor represses the transcriptional activation of inflammatory-response genes.

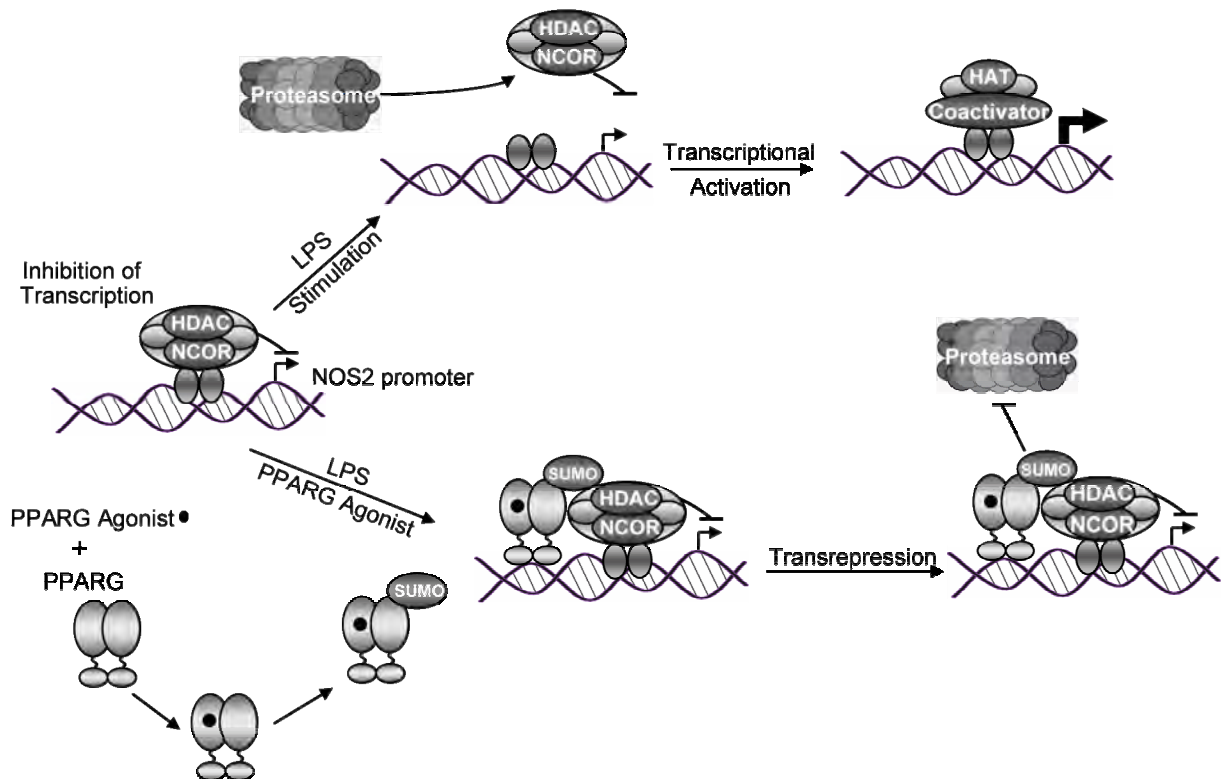


Fig. 11: Transrepression mechanism of PPARG. This scheme displays the basic mechanisms underlying the transrepression of *NOS2* transcription activation by PPARG, as identified by Pascual et al (discussed in 2.1.2). Through sumoylation of the PPARG receptor, the nuclear corepressor complex (NCOR) is retained at the *NOS2* promoter, leading to an inhibition of *NOS2* transcription, despite an inflammatory (LPS) stimulus.

Lipopolysaccharide (LPS) triggered-activation of the inducible nitric oxide gene (*NOS2*) in mouse macrophages could be inhibited by simultaneous stimulation with a PPARG agonist. In the absence of inflammatory stimulation, *NOS2* transcription is repressed by a complex of proteins containing the nuclear receptor corepressor (NCOR). After stimulation, this complex is degraded by the proteasome and replaced by an activator complex, subsequently, transcription can take place. Pascual et al. showed that after ligand binding a posttranscriptional modification of the PPARG receptor takes place. The PPARG is sumoylated and subsequently recruited to the NCOR complex at the *NOS2* promoter. This leads to a repression of the proteasomal degradation of the NCOR and transrepression of *NOS2* gene transcription. The basic steps of this mechanism are displayed in figure 11.

An indirect Transrepression mechanism identical or similar to the mechanism identified by Pascual et al. might be responsible for the inhibition of gene expression of inflammatory mediators such as CXCL10/IP10, as observed by Adams et al. in the retinoic acid treated animal group.

2 Aim of the present study

2.1 Transcriptomic profiling of kidney transplants

The goals of the present study were twofold. First, to characterize by transcriptomic analysis, the development of CAD in the rat animal-model over specified time points by studying changes in exemplary, regulatory pathways previously associated with fibrosis and EMT. For studying complex biological events, the evaluation of single gene expression is generally inferior to a multi-gene analysis. This is also true in the context of signal transduction whereby a higher interpretation scale of the study can be achieved. It was hypothesized that it is possible to identify changes in the activation status of distinct pathways leading to the induction and progression of chronic renal allograft dysfunction.

The second aim of the study was to identify potential therapeutic modes of action of 13cRA in chronic renal fibrosis through analysis of alterations in the same regulatory pathways.

Microarray experiments, analyzed with new bioinformatics approaches and expanded pathway analysis, provided the basis for these studies. Quantitative PCR (qPCR) was used to verify gene expression of genes assigned to the microarray, and to investigate additional genes not present on the array. Additionally, immunohistochemistry (IHC) for select candidates was employed to demonstrate translation of changes on the mRNA into changes on the protein level.

It was further hypothesized that the same, or a similar molecular transrepression mechanism, as observed by Pascual et al. in macrophages, leads to the reduced expression of inflammatory genes observed *in vivo* after 13cRA treatment and *in vitro* after stimulation of fibroblasts. To this end the CHIP technique was established in our lab and experiments on human fibroblasts performed.

3 Material

For general statements, gene and protein nomenclature was employed according to the “Guidelines for Human Gene Nomenclature” [10]. Gene and protein symbols are all uppercase, gene symbols are italicized. No greek symbols are used.

For the transcriptomic profiling, nomenclature for genes and proteins was employed according to the “Guidelines for Nomenclature of Genes, Genetic Markers, Alleles, and Mutations in Mouse and Rat” by the “Rat Genome and Nomenclature Committee” revised, January 2009. Gene symbols begin with an uppercase letter (not a number), followed by italicized lowercase letters. Protein symbols are not italicized.

3.1 Microarrays

Microarrays of transplanted kidneys

Time points	Treatment	Animal number
Control kidney day 0, n=3		N3
		N4
		N5
Transplanted kidney 7d, n=4	Placebo	211
	Placebo	213
	Placebo	539
	Placebo	540
Transplanted kidney 14d, n=5	Placebo	244
	Placebo	246
	Placebo	531
	Placebo	546
Transplanted kidney 56d, n=5	Placebo	248
	Placebo	572
	Placebo	574
	Placebo	592
	Placebo	593
Transplanted kidney 7d, n=4	Placebo	587
	13cRA	1448
	13cRA	1464
	13cRA	1466
	13cRA	1357
Transplanted kidney 14d, n=5	13cRA	561
	13cRA	563
	13cRA	564
	13cRA	527
	13cRA	760
Transplanted kidney 56d, n=4	13cRA	1083
	13cRA	1129
	13cRA	1131
	13cRA	1132

To assess changes, observed in the study of Adams et al. [5] performed in the laboratory of Prof. H.-J. Gröne, on the transcriptomic level, microarray expression data was generated. Total RNA was extracted from the transplanted (left) kidney allografts by the method of Chomczynski and Sacchi as in described [61]. The recipient's right native kidney was not investigated.

Microarray analyses were performed in cooperation with Prof. Gretz at the Zentrum für Medizinische Forschung, Mannheim (ZMF). Samples were hybridized to Affymetrix RG-U34A microarrays and scanned with an Affymetrix scanner controlled by the Affymetrix® GeneChip® Operating Software (GCOS). All reactions were performed essentially according to the Affymetrix protocol (Affymetrix, Sunnydale, CA). A total of 30 arrays were generated, as detailed above.

3.1.1 CEL files

Affymetrix microarray experiments are evaluated using the GCOS software. GCOS interfaces with equipment to run a probe-array experiment, and is also used to generate preliminary analysis data from an experiment. The basic files generated by GCOS are the "Experiment File", "Image Data File", and "Cell Intensity File".

Experiment File *.EXP: This file contains the parameters of the experiment, such as probe-array type, experiment name, equipment parameters, sample description, and others. This file is not used for analysis, but is required to open other GCOS files for the designated chip experiment.

Image Data File *.DAT: This is an image file generated by the scanner from the probe array after processing on the fluidics station. This file can be viewed in GCOS to assess the quality of scanning event or exported as a *.TIFF image. It is used in GCOS to generate the *.CEL file (see following).

Cell Intensity File *.CEL: This binary file is the result of low level analysis performed from the *.DAT image file. It is exported from GCOS and is often used as the base file for further analysis.

A digital version of these files was given to us by Prof. Gröne and subsequent analyses of the CEL files were performed in the lab of the AG Dr. Peter Nelson, Klinische Biochemie, Medizinische Poliklinik der LMU.

3.2 *Kidney samples*

3.2.1 RNA isolated from kidney sections

The RNA samples that built the basis of this thesis were provided by our long term collaborator Prof Dr. Hermann-Josef Gröne.

Prof Dr.Hermann-Josef Gröne is head of the Department of Cellular and Molecular Pathology at the DKFZ in Heidelberg. The major focus of his research is renal physiology and the pathophysiology of renal disease. Over the past ten years he has co-authored 25 papers with PD Dr. Nelson including a series of studies detailing the biology of acute and chronic allograft rejection using the model system as described in the thesis. RNA provided by Prof. Gröne was isolated by the method of Chomczynski and Sacchi and quality controlled as described in [5]. In Munich RNA quality was additionally monitored by agarose electrophoresis for degradation. No degradation could be observed and samples were stored at -80°C.

3.2.2 Kidney sections for immunohistochemistry

Tissue sections were prepared as described in [5].

Subsequent sample preparation was performed in the laboratory of PD Dr. Peter Nelson, Klinische Biochemie, Medizinische Poliklinik der LMU.

3.3 *Cells*

3.3.1 Human fibroblast cell line K4IM

The human fibroblast cell line K4IM, immortalized with the SV40 T large antigen, was generously donated by Professor Haas, Freiburg. This cell line was established in order to study the mechanisms that induce and maintain synovial fibroblast activation [62]. Haas et al. used synoviocytes from a healthy donor and generated the stable synovial fibroblast cell line K4IM with the help of SV40 T antigen mediated immortalization. Analyzing the expression of cell surface markers in the native parental synoviocyte line K4WT, and in the immortal K4IM cells, demonstrated that K4IM cells differ only in part from the parental K4WT phenotype [62]. Therefore, the immortalized K4IM cell line is an ideal tool to study mechanisms that maintain fibroblasts activation during fibrosing and inflammatory diseases [62].

3.3.2 Media used for K4IM

K4IM cells were cultured in culture medium consisting of Dulbecco's Modified Eagles Medium (DMEM, Invitrogen, Karlsruhe) supplemented with 10% heat inactivated FBS (Biochrome AG, Berlin) and 1% of Penicillin/Streptomycin (see 3.9).

As freezing medium, culture medium with the addition of DMSO to a final concentration of 10% was used.

Starving medium equals culture medium without the addition of FBS.

3.4 Oligonucleotides

Supplemental figure 1 summarizes all the oligonucleotides employed in this study, including sequences. Self-designed oligonucleotides were synthesized by Metabion, Martinsried.

3.4.1 Oligonucleotides for qPCR of cDNA

qPCR was performed using either Assays on Demand (AoD) (Applied Biosystems, Darmstadt), pre-developed reagents for 18S rRNA (Applied Biosystems, Darmstadt) or a SYBR green system using self designed primer pairs as well as QuantiTect Primer Assays (Qiagen, Hilden).

3.4.1.1 AoD Assays

Probes of the AoDs were labeled 5-prime with 6-Carboxy-Fluorescein (FAM) and 3-prime with the quencher Tetramethyl-Rhodamin (TAMRA). The probe of the housekeeping gene 18S rRNA was labeled 5-prime with VIC® (Trademark) and 3-prime with the quencher (TAMRA). All primers and probes were provided by the manufacturer as 20x assay solutions.

3.4.1.2 QuantiTect Primer Assays

Each assay for a specific gene was supplied as a lyophilized mix of forward and reverse primers and was reconstituted in water to obtain a 10x assay solution, according to the manufacturers instructions. Information about concentrations was not provided.

3.4.1.3 Oligonucleotides for qPCR, self-designed

Lyophilized oligos are reconstituted in water to reach a 100 pmol/ µl stock solution. The working solution contains primers in a concentration of 10 pmol/µl.

3.4.2 Oligonucleotides for PCR of genomic DNA, self designed

Lyophilized oligos are reconstituted in water to reach a 100 pmol/μl stock solution. The working solution contains primers in a concentration of 10 pmol/μl.

3.5 Enzymes, enzyme solutions, and inhibitors

DNase I	Qiagen, Hilden
Protease XXIV (7-14U/mg), lyophilized	Sigma-Aldrich, Taufkirchen
Protease inhibitor cocktail, complete (No 04693116001) Stock solution (50x)	Roche Diagnostics, Mannheim
Protease K (20 mg/ml)	Sigma-Aldrich, Taufkirchen
RNase A (10 mg/ml)	Roche Diagnostics, Mannheim
Taq DNA – polymerase (5U/μl)	NEB, Frankfurt a.M.
Trypsin – EDTA	PAA Laboratories, Pasching, Austria
Superscript™ II Reverse Transcriptase	Invitrogen, Karlsruhe

3.6 Antibodies

3.6.1 Primary antibodies

Mouse anti-rat beta-catenin	BD Bioscience, Heidelberg
Mouse anti-rat Cd44 H (clone OX-49)	BD Bioscience, Heidelberg
Rabbit anti-rat collagen I	Chemicon, Temecula, USA
Rabbit anti-human fibronectin	DAKO, Glostrup, Denmark
Rabbit anti-acetyl histone (H3, Lys9/18)	Upstate, Lake Placid, USA
Rabbit anti-rat Lef1	Cell Signaling (NEB), Frankfurt a.M.
Rabbit anti-NCOR ChIP grade	Abcam, Cambridge, UK

3.6.2 Secondary antibodies

Biotinylated goat anti-mouse IgG (H+L)	Jackson ImmunoResearch Laboratories, West Grove, USA
Biotinylated goat anti-Rabbit IgG (H+L)	Jackson ImmunoResearch Laboratories, West Grove, USA

3.7 Kits

AEC Substrate kit	Biogenex, San Ramon, USA
Avidin/Biotin Blocking kit	Vector Laboratories, Burlingame, USA
DuoSet RANTES ELISA Development kit	R&D Systems Europe, Wiesbaden

Quant-iT™ RNA Assay kit	Invitrogen, Karlsruhe
RNeasy Mini (50) kit	Qiagen, Hilden
RNase – free DNase Set (50)	Qiagen, Hilden
Taqman® Universal PCR Master mix	Applied Biosystems, Darmstadt
VECTASTAIN® Universal Quick kit	Vector Laboratories, Burlingame, USA

3.8 Chemicals, reagents, and additives

13-cis retinoic acid (13cRA)	Sigma Aldrich, Taufkirchen
3,3'-diaminobenzidine (DAB)	Sigma Aldrich, Taufkirchen
Acetic acid	Sigma Aldrich, Taufkirchen
Acrylamid, linear	Ambion/Applied Biosystems, Darmstadt
Agarose, ultrapure	Invitrogen, Karlsruhe
Aqua ad injectabilia	Braun, Melsungen
β-mercaptoethanol (BME)	Roth, Karlsruhe
Boric acid	Merck, Darmstadt
Bovine serum albumin (BSA), PCR grade	Fermentas, St.Leon-Rot
Chloroform/isoamyl alcohol (49:1)	Merck, Darmstadt
Deoxycholic acid	Sigma Aldrich, Taufkirchen
Dimethylsulfoxid (DMSO)	Merck, Darmstadt
Dithiothreitol (DTT)	Invitrogen, Karlsruhe
Ethanol (EtOH)	Merck, Darmstadt
Ethylenediaminetetraacetic acid (EDTA)	Calbiochem, Darmstadt
Ethidium bromide solution, 1.0% (EtBr)	Merck, Darmstadt
Fetal bovine serum (FBS)	Biochrome AG, Berlin
Formaldehyde, pro analysis, 37%	Merck, Darmstadt
Glycine	AppliChem, Darmstadt
Glycogen	Ambion/Applied Biosystems, Darmstadt
Herring sperm DNA	Roche Diagnostics, Mannheim
Hexanucleotides	Roche Diagnostics, Mannheim
Hydrogen peroxide solution, 30%	Merck, Darmstadt
KCl	Merck, Darmstadt
LiCl	Merck, Darmstadt
Methanol	Merck, Darmstadt

Material

Methyl green	Fluka, Schnelldorf
MgCl ₂	Fermentas, St.Leon-Rot
NaCl	Merck, Darmstadt
NaHCO ₃	Roth, Karlsruhe
NiCl	Sigma Aldrich, Taufkirchen
dNTP set	Fermentas, St.Leon-Rot
NP40	Fluka, Schnelldorf
Piperazine-N,N-bis 2-ethanesulfonic acid (PIPES)	Boehringer Mannheim, Mannheim
RNAasin – ribonuclease inhibitor	Promega, Madison, USA
Rox reference dye (25x)	Invitrogen, Karlsruhe
Roti® –Phenole/C/I	Roth, Karlsruhe
Sodium-N-lauroylsarcosinate (Sarkosyl)	Fluka, Schnelldorf
Sodium acetate	Merck, Darmstadt
Sodium citrate	Merck, Darmstadt
Sodium dodecyl sulfate (SDS)	Roth, Karlsruhe
SYBRgreen I (250x)	Fluka, Schnelldorf
Pansorbin® cells (StaphA), lyophilized	Calbiochem, Darmstadt
Tnf alpha, recombinant, human	ImmunoTools, Friesoythe
Trishydroxymethylaminomethan (Tris)	Merck, Darmstadt
TritonX100	Sigma Aldrich, Taufkirchen
Tween 20	Fluka, Schnelldorf
Immumount	Thermo Fisher Scientific, Bonn
Xylol	Merck, Darmstadt

3.9 Buffers and Solutions

Antibody diluent Dako REALTM	DAKO, Glostrup, Denmark
Antigen unmasking solution	0.1M Sodium citrate, pH 6.0
Cell lysis buffer	5 mM PIPES pH 8.0, 85 mM KCl, 0.5% NP40
Elution buffer	50 mM NaHCO ₃ , 1% SDS (v/v)
First-strand buffer (5x)	Invitrogen, Karlsruhe
Immuno precipitation (IP) dilution buffer	0.01% SDS (v/v), 1,1% TritonX100, 1.2 mM EDTA, 16.7 mM Tris pH 8.1, 167 mM NaCl

Dialysis buffer (1x)	2 mM EDTA, 0.2% Sarkosyl, 50 mM Tris pH 8.1
Streptavidin-Horseradish peroxidase	Vector Laboratories, Burlingame, USA
IP washing buffer	100 mM Tris pH 9.0, 500 mM LiCl, 1% NP40, 1% deoxycholic acid
Loading buffer	0.25% Bromphenol blue, 0.25% Xylene cyanol, 30% glycerol in H ₂ O
Mayers haemalaun	Roth, Karlsruhe
Nuclei lysis buffer	1% SDS (v/v), 10 mM EDTA, 50 mM Tris pH 8.1
Penicillin/Streptomycin (100x)	Penicilin 10000U/ml, Streptomycin 10mg/ml, 0.9% NaCl PAA Laboratories, Pasching, Austria
Phosphate buffered saline (PBS) (1X)	PAA Laboratories, Pasching, Austria
PBS/Tween	PBS (1x), 0.5% Tween 20
PCR Optimizer	Bitop, Witten
PK buffer (5x)	50 mM Tris pH 7.5, 25 mM EDTA, 1.25%, SDS (v/v)
Protease XXIV solution	3-5U/ml in H ₂ O
SYBRgreen I solution	1:100 in H ₂ O with 20% DMSO, -20°C
SYBRgreen Mastermix	20% Taq buffer without detergent, 375 µM NTPs, 4% Rox referencedye, 40% PCR Optimizer, 2% BSA, 0.4% SYBRgreen I solution, 6 mM MgCl ₂
Taq buffer without detergent (10x)	Fermentas, St.Leon-Rot
TBE (1x)	90 mM Tris, 2 mM Boric acid, 10 mM EDTA pH 8.0, 0,015 % EtBr (v/v)
TE buffer (1x)	10 mM Tris pH 7.5, 1 mM EDTA
ThermoPol buffer (10x)	NEB, Frankfurt a.M.
Trypsin – EDTA solution	PAA Laboratories, Pasching, Austria
Trypan Blue	Sigma Aldrich, Taufkirchen

3.10 Consumables

Cell culture plates	TPP AG, Trasadingen, Switzerland
Cell culture flasks	TPP AG, Trasadingen, Switzerland
Cell scraper	TPP AG, Trasadingen, Switzerland
Falcon tubes 15 ml/ 50 ml	BD Bioscience, Heidelberg
Taqman plates	Sarstedt, Nümbrecht

Taqman cover	Sarstedt, Nümbrecht
ELISA plate Maxisorb	Nunc, Roskilde, Denmark

3.11 Instruments

ABIPrism7000 Sequence Detection System	Applied Biosystems, Darmstadt
Plate reader GENiosPlus	Tecan, Crailsheim
Gel electrophoresis apparatus	MBT Brand, Gießen
Geneamp PCR system 9700 PE	Applied Biosystems, Darmstadt
Incubator Modell 400	Brutmaschinen Janeschitz, Hammelburg
Liquid Blocker, Super Pap pen	Daido Sangyo, Tokyo, Japan
Leica microscope Q600 Qwin	Leica, Cambridge, UK
MinifugeT	Heraeus, Hanau
Megafuge 1.0R	Heraeus, Hanau
Micro Centrifuge 5415 D	Eppendorf, Hamburg
Microwave	Milestone Medical, Kalamazoo, USA
Neubauer counting chamber	Braun, Melsungen
Power supply PowerPac300	Biorad, München
Qubit TM fluorometer	Invitrogen, Karlsruhe
Thermomixer comfort	Eppendorf, Hamburg
Sonifier 250	Branson Ultrasonics Corporation, Danbury, USA
Steamer MultiGourmet	Braun, Kronberg
UV Transilluminator	Bachofer, Reutlingen
Water bath Haake SWB20	Thermo Haake, Karlsruhe

3.12 Software

3.12.1 Commercial software

ABI Prism 7000 SDS	Applied Biosystems, Darmstadt
BiblioSphere	Genomatix GmbH, München
ChipInspector	Genomatix GmbH, München
Prism 4.03.	GraphPad Software, La Jolla, USA
Illustrator CS2	Adobe Systems, San Jose, USA
Microsoft Office 2003	Microsoft, Redmont, USA
Photoshop CS2	Adobe Systems, San Jose, USA
XFluor	Tecan, Crailsheim

3.12.2 Freeware and databases

Primer 3 from the Whitehead Institute for Biomedical Research; Cambridge, USA
Genesis Version 1.7.5, Institute for Genomics and Bioinformatics; TU Graz, Austria
Image Processing and Analysis in Java (ImageJ); NIH, USA
David Bioinformatics database, Version 2007 (DAVID); NIAID, NIH, USA
Kyoto Encyclopedia of Genes and Genomes (KEGG); University of Kyoto, Japan
RMAExpress, V. 1.0 beta 10, Ben Bolstad, University of California, Berkeley, USA

4 Methods

4.1 *Microarray analysis*

4.1.1 **ChipInspector analysis of CEL Files**

Transcription profiling using Affymetrix RG-U34A microarrays was performed on RNA from rat kidneys, described in 3.1 and 3.2.

The microarray RG-U43A contained 93725 single probes with different sequences, control mismatch probes are not included. After the hybridization stage, the resulting fluorescent signals are translated into numeric data, the so called CEL files (see 3.1). Standard analysis of microarray data consists of a series of steps. Quality controls are used to detect degradation of the RNA input material. In a normalization step, the background signal levels are defined to allow comparisons between the different arrays. In the final step statistical analyses are used for evaluation of the significance of data.

Due to problems of sensitivity and specificity of this analysis approach (for details see 5.1., figure 12) the resultant CEL files were analyzed using the ChipInspector software [63].

The approach is based on single probes, avoids probe-set definitions, and each analysis is based on the most current single probe annotation. Mismatched probes or probes with known cross-hybridization are excluded from the analysis.

Similar to the standard analysis this tool for microarray data that is comprised of four steps: single probe-transcript annotation, total intensity normalization, Significance Analysis of Microarrays (SAM) [64] (adapted to single probe handling), and transcript identification, based on significantly changed probes. All probes on the array were individually matched against the rat genome and all known transcripts thereof, available at the time of analysis. Only probes that matched uniquely to the genome and to at least one transcript (or overlapping transcripts) were retained for further analysis. SAM analysis was then carried out for each probe individually and the resulting probes showing significantly changed signals were then used to identify the corresponding transcripts (which may be more than one per gene). The expression ratios shown in the result table were calculated from the average expression levels of all significant probes of each individual transcript. Gene identifiers were then attached to each transcript. Analysis was carried out using all default settings,

as recommended by the software provider, except for the expected false discovery rate (FDR) which was set to maximal detection of regulated transcripts with lowest amount of falsely called features (FDR 0%).

4.1.2 BiblioSphere and GO analysis

A network of genes based on literature co-citations was built up using the BiblioSphere software (Genomatix Software GmbH, Munich, Germany). Based on these network, the distribution of differentially regulated genes was grouped according to functional, biological categories. The controlled hierarchical vocabulary of the Gene Ontology (GO) consortium provides a structured language applied to the functions of genes and proteins in all organisms (<http://www.geneontology.org/>) [65], and was used to subgroup them by gene ontology.

4.1.3 Pathway analysis

Pathways were identified using the DAVID bioinformatics database, Version 2007 (DAVID) (<http://david.abcc.ncifcrf.gov/>) [66, 67] and the Kyoto Encyclopedia of Genes and Genomes (KEGG) databases (<http://www.genome.jp/kegg/kegg2.html>) [68-70]. Lists containing genes identified to be differentially regulated by the microarray can be uploaded to the DAVID database. In addition to GO categories, DAVID gives detailed information on every single gene regarding the different pathways it has been assigned to. Through a direct link to the KEGG, the database DAVID makes it possible to gain an overview of the roles of every single gene in different pathways. To analyze alterations in pathways, a version of the individual regulatory pathway was first defined by using the KEGG database. The initial KEGG-defined pathways were then refined to include additional target genes. Genes not yet annotated in the rat database were eliminated and additional points of potential interaction between various pathways were added.

It was always taken into consideration that not every gene assigned to a pathway is necessarily available on the microarray employed. Therefore, the list of genes of interest, according to the pathway but not available on the array, could be obtained.

Microarray data was integrated in schemes of adapted pathways to generate an overview of pathway activation and possible regulation. Primers were designed for genes, included in the arrays that showed regulation in a pathway of interest and for genes that were not present on the array for further analysis by qPCR.

4.1.4 Robust multichip average (RMA) analysis

For the robust multichip average (RMA) analysis, the program RMAExpress Version 1.0 beta 10 was used [71-74]. For each microarray, the manufacturer provides information about probe-set annotations on the array. This so called library file could be downloaded from the Affymetrix support webpage. In the first step of the analysis, the library file was loaded into the RMAExpress program. Only then could the CEL files of all the microarrays be loaded into the program, and be further processed. The analysis was computed automatically using default settings. A graphical output file in the form of boxplots could be generated to control for outliers between the arrays. A numeric output file (.txt format) contained expression values on a normal or a logarithmic scale, after the normalization. The .txt files could be used for further analysis.

4.1.5 Cluster analysis

Cluster analysis was performed using the program Genesis Version 1.7.5 [75]. This tool was developed to simultaneously visualize and analyze a whole set of gene expression experiments. After normalization with RMAExpress, the native text files were loaded as input into the Genesis program. The data of the individual arrays was log₂ transformed and normalized by their genes. Hierarchical, average linkage clustering over genes and arrays was performed in order to show untainted, familiarity linkage. The graphical output was a matrix displaying clusters of co-regulated genes and arrays. The information gained was twofold. First, an overview was gained of the general expression-patterns of genes from the individual animals. The more similar overall gene expression on the arrays, the closer the arrays of the individual animals would cluster together. The end stage of renal disease should cluster further away from the control kidneys. Second, genes with distinct expression patterns will cluster together, which gives an overview of the expression of individual genes or groups of genes and their expression patterns along with disease progression. A possible effect of the treatment on gene expression can easily be observed with this method and candidates for further evaluation can be chosen.

4.2 Verification of microarray results on the mRNA level

4.2.1 RNA Cleanup

RNA was isolated as described in 3.2.1. RNA cleanup was performed to remove residual contamination with genomic DNA. This procedure was performed with the reagents of the RNeasy Mini kit and according to the instructions of the RNeasy Mini Handbook 04/2006. The optional DNase I (Qiagen, Hilden, Germany) digestion step was included. RNA was eluted in 30 µl RNase free water. Elution was repeated once to maximize final RNA concentration.

4.2.2 Quantification of RNA

For quantification of RNA after cleanup, the Quant-iT™ RNA assay for the Qubit™ fluorometer was employed. Quant-iT technology uses fluorescent dyes specifically for RNA. Upon binding to RNA, the fluorescence of the Quant-iT dyes increases several hundred fold, giving a very high signal-to-background ratio that is measured by the Qubit™ fluorometer. This assay is highly selective for RNA. Measurements and calculations were performed according to the manufacturer's protocol.

4.2.3 Reverse Transcription

The isolated total RNA was transcribed into cDNA through reverse transcription. The amount of cDNA was measured in a following qPCR reaction step. Primers designed for qPCR are usually cDNA specific, which means they will only amplify cDNA and not genomic DNA. For some genes, such as the S18-rRNA or genes consisting of just one exon it is not possible to design cDNA specific primers. For this reason, and to exclude a PCR signal from genomic DNA contamination in the sample, the so-called RT- sample was included into the reverse transcription step. Here, 0.1 µg of total RNA, possibly containing genomic DNA contamination, was added to the reaction batch. This batch equaled the RT+ batch with the exception of the reverse transcription enzyme. Since no reverse transcription could take place in this batch and RNA can not be measured in qPCR, each signal that was produced by the RT- had to originate from the combination of a cDNA unspecific primer and genomic DNA contamination.

RT PCR (1x)

Reagent	RT+	RT-
First-strand buffer (5x)	1x	1x
dNTP	1.5 mM	1.5 mM
DTT	13.4 mM	13.4 mM
Rnasin	2.5 U/ μ l	2.5 U/ μ l
Acrylamid, linear	0.7 μ M	0.7 μ M
Hexanucleotides (10x)	0.2x	0.2x
Superscript II	4.4 U/ μ l	-

For the reverse transcription, 1.1 μ g of total RNA, as measured in 4.2.2, was diluted in RNase free water to a final volume of 33 μ l. Of that dilution, 30 μ l were added to the 15 μ l of the RT+ mastermix. The residual 3 μ l were diluted to 31 μ l with RNase free water and added to the 14 μ l of the RT- mastermix. The RT+ mastermix therefore, contained 1 μ g of RNA and the RT- mastermix contained 0.1 μ g of RNA. Both reaction batches were incubated at 42°C, slowly shaken in a thermo block for 1.5 hours. For subsequent qPCR reactions, the RT+ batch had to be diluted 1:10, whereas the RT- batch remained undiluted. Batches and dilutions were stored at -20°C, until further use.

4.2.4 Quantitative PCR (qPCR)

qPCR permitted to calculate the amount of amplification products in a specific PCR reaction. The qPCR is based on fluorescent signals generated through amplification of the sample and on the detection system's laser technology that can measure fluorescence. There are two main concepts of qPCR, the Taqman assay and the SYBRgreen assay. In the case of the Taqman assay, primers and a double-labeled probe anneal to the cDNA. The probe is labeled with a fluorescent dye and a quencher. No fluorescent signal can be emitted, of a probe that is not bound to the cDNA and/or if the cDNA is not amplified. If primers and probe are bound to a specific cDNA and the Taq polymerase amplifies the strand, the 5'-3'- exonuclease activity of the polymerase will hydrolyze the probe and separate the fluorescent dye from the quencher. A fluorescent signal is then generated by the quencher free probe, labeled with FAM or VIC, which can then be measured by the detection system.

In the case of the SYBRgreen primers, the fluorescent signal is generated by intercalation of the SYBRgreen dye in double stranded cDNA. To control that the

signal did not originate from unspecific byproducts, an additional step had been included. After the amplification cycles, the PCR machine gradually increased the temperature up to 95°C. While doing so, the double strands generated through amplification separated again and the system could detect the loss of fluorescence. Each product had a melting temperature depending on its length. A melting curve could be displayed by the system. A single peak at a temperature that fitted the size of the amplicon ensured that the product is specific. Both techniques were employed in this study.

qPCR

Reagent (1x)	AoD	QuantiTect Primer	SYBRgreen Primer
Taqman Universal PCR Mastermix (10x)	1x	-	-
SYBRgreen Mastermix (10x)	-	1x	1x
Taqman Assay (20x)	1x	-	-
QuantiTect Primer	-	1x	-
SYBRgreen Primer Fw	-	-	10 pM
SYBRgreen Primer RV	-	-	10 pM
Taq polymerase	-	0.03 U/ μ l	0.03 U/ μ l

H₂O was added to the mastermix to reach a final volume of 18 μ l. For qPCR 2 μ l of the RT+ (1:10) dilution or 2 μ l of the RT- reaction batch were added to the mastermix, to reach a final volume of 20 μ l per well/taqman plate. Experiments were set up in duplicates. qPCR was performed on an ABIPrism7000 Sequence Detection system. After an initial hold of 2 minutes at 50°C and 10 minutes at 95°C, the samples were cycled 40 times at 95°C for 15 seconds, and 60°C for 60 seconds. All primers are summarized in the supplementary table 1. The expression of candidate genes was normalized to the reference gene 18S rRNA [76]. Primers were tested using pooled cDNA samples from each group of rats to identify significant differential regulation. If dysregulation in expression was observed between one or more groups, the qPCR was repeated using cDNA - samples from kidneys of individual animals. These results were then used for statistical analysis.

4.2.5 Calculation of regulation

The AbiPrism software detects fluorescence above a certain threshold, the so called Cycle Threshold (CT). A high CT indicates a detection of signal in a late cycle of the PCR which stands for low abundance of the mRNA in the original sample. The opposite is true for a low CT.

The CT is determined in the graphical output of the software after the PCR run. For each gene, a baseline was individually adjusted depending on the fluorescence curves. Using the log-scale view, the baseline for every gene was positioned within the area of the curve showing a linear increase. According to this baseline, a CT value was created by the software for every well of the PCR plate measured.

Thereby, the CT represented expression values for the analyzed genes. To be able to analyze regulation of expression, fold changes (FCs) of the various experimental groups were calculated. Values of all the animal groups investigated were divided by the average value of the normal kidney, the control group. This means that all FCs, discussed in this work have to be regarded as changes in expression in relation to the expression level of the average normal kidney.

FCs were generated using the Pfaffl method [77]. When the calculated FCs had values between 0 and 1, they were transformed according to the following formula [$FC = -1 * FC^{-1}$] to achieve negativity of values. Thus, the distribution of expression values could be visualized on equal scales for up and downregulated genes in comparison to the control kidney.

4.3 Verification of microarray and qPCR results on the protein level

4.3.1 Histology

Light microscopy evaluation was performed on 3 μm sections stained by periodic acid-Schiff (PAS). Kidneys were assessed for acute and chronic vascular, glomerular, as well as tubulointerstitial damage, as described [5].

Sirius red staining was used on sections to evaluate fibrotic changes in representative renal allografts [47]. Collagen forms the basic substance of connective tissue. It is composed of three amino-acids and stains strongly with acid red dyes due to the affinity of the cationic groups of the proteins for the anionic reactive groups of the acid dyes. By using the Sirius red staining total collagen could be evaluated in the sections to evaluate the overall fibrotic changes during CAD progression. PAS and Sirius red staining were performed by Ms. Gabrielle Schmidt, DKFZ, Heidelberg.

4.3.2 Immunohistochemistry

Immunohistochemistry (IHC) aims at localizing proteins in cells of a tissue section by specific antibody binding to antigens. Visualizing an antibody-antigen interaction can be accomplished in a number of ways.

In the most common instance, an antibody is conjugated to an enzyme, such as peroxidase, that can catalyze a color-producing reaction, ending with the local precipitation of a water-insoluble stain. Immunohistochemistry was performed on paraffin embedded formaldehyde-fixed tissue sections on glass slides, prepared as described in Adams et al. [5].

4.3.2.1 Sample preparation

To remove the paraffin from the tissue, two washing steps, 10 minutes each, in xylol were performed. Rehydration of the sections was achieved by incubating them three times for 5 minutes in EtOH 100%, twice in EtOH 96%, once in EtOH 80% and once in EtOH 70%. To remove residual EtOH, one washing step with H₂O followed. For unmasking of the antigen, sections were incubated in 0.01 M sodium citrate solution pH 6 or Tris buffer pH 9, in a steamer for 20 minutes approximately 70°C, or in a microwave for 1 hour at 98°C. Exact conditions for each antibody are reported below. The sections were then cooled down to room temperature and washed once in H₂O. Depending on the antibody, an alternative unmasking step had to be performed. Thereby the sections were digested with protease XXIV solution for 10 minutes. Reaction was stopped by two washing steps in EtOH 100%.

After antigen retrieval, sections were allowed to air dry and encircled with a liquid blocker pen to ensure that the small amounts of antibody solutions would remain on the tissue and not blend across the cover slide.

4.3.2.2 Detection of the antigen

Sections were rehydrated by two PBS/Tween washing steps. After rehydration, several blocking steps followed. All incubations were performed in a humid chamber, consisting of a metal box covered with wet pulp and a cover that ensured high humidity within the box and prevented the tissue from dehydrating during incubation periods. To prevent background reaction, it was necessary to block the endogenous peroxidase of the tissue. For this purpose, the sections were incubated in PBS containing 3% of hydrogen peroxide for 10 minutes. The sections were then washed twice with fresh PBS/Tween and blocked again with PBS containing 2% of blocking serum from the VECTASTAIN® Universal Quick kit for 10 minutes, followed again by two PBS/Tween washing steps. Before the antibody could be added endogenous biotin had to be blocked using the Avidin/Biotin Blocking Kit.

The general protocol for the antibody staining consisted of an incubation of the section with a primary antibody, followed by washing steps. Then, the secondary biotinylated antibody was incubated. All antibodies were prepared in antibody diluent (Dako). Concentrations of antibodies are summarized below.

IHC

Primary Antibody	Retrieval	Buffer	Dilutions
Mouse anti-rat beta-catenin	Steamer	Citrate	1/20
Mouse anti-rat Cd44H	Steamer	Citrate	1/500
Rabbit anti-rat collagen I	Protease	-	1/20
Rabbit anti-human fibronectin	Protease	-	1/500
Rabbit anti-rat Lef1	Microwave	Tris	1/100

All primary antibodies were incubated at room temperature for 2 hours.

Incubation was followed by two PBS/Tween washing steps before the second biotinylated antibody, directed against the species of the primary antibody, was added for 30 minutes at room temperature. Concentrations were used as stated below.

IHC

Secondary Antibody	Dilutions
Biotinylated anti mouse	1/150
Biotinylated anti rabbit	1/150

The Avidin-Biotin-Complex method (ABCComplex) was employed. Horse radish peroxidase (HRP) is complexed with streptavidin and conjugated to the biotinylated antibody. Sections were incubated for 60 minutes at room temperature in the ABC-HRP solution. After incubation, the slides were washed twice with PBS/Tween and once with H₂O. Then the slide was incubated using the AEC substrate kit for an initial 3 minutes and the staining was controlled using light microscopy (Laborlux D, Leitz, Wetzlar). If necessary, the staining reaction could be prolonged for up to 10 minutes in total. The AEC substrate was oxidized to a red stain.

Before the counterstaining of the nuclei with Mayers Haemalaun, the slides were washed once with H₂O. Slides were dipped for several seconds in Mayers Haemalaun and then incubated in tap water for about 10 minutes, resulting in a blue staining of the nuclei. A drop of mounting medium and a cover slide were added to protect the section. Slides were stored at room temperature, until investigated by microscopy.

4.4 Identification of the working mechanism of 13cRA on the DNA level

4.4.1 Cell cultivation

The adherently growing K4IM cells were cultured in DMEM medium in a cell culture incubator at 37°C, 100% humidity, and 5% CO₂ until use. Before reaching confluent growth, cells were removed from the culture dish using Trypsin-EDTA. They were split and subcultured. For splitting, the culture medium was completely removed and cells were washed once with PBS. Trypsin-EDTA solution was added to just cover the cell layer. Cells were put back into the incubator until they started to detach. Then the reaction was stopped by the addition of an equal amount of culture medium containing serum. The cell suspension was softly pipetted up and down to ensure detachment of all cells. Then the suspension was transferred to a tube and centrifuged for 3 minutes at 1100 x g. The supernatant was discarded and the pelleted cells were resuspended in fresh culture medium and seeded on new culture plates. K4IM can be splitted up to 1:3. If necessary, cells were counted before splitting.

4.4.1.1 Counting of viable cells

Cells were counted using a Neubauer counting chamber. The cover slip had to be attached to the chamber in such a way so that the “Newton rings” were visible. Then the distance between chamber and slip is defined and the chamber could be used for counting. One part of the cell suspension was mixed with Trypan Blue solution in a 1:1 ratio, staining dead cells blue. 10 µl of this mixture were immediately pipetted into the chamber. Only living cells were counted in all the quadrants of the chamber. The number of cells per ml suspension could then be calculated. The count (x) multiplied by the dilution and divided by the quadrants counted gave a number of $x \cdot 10^4$ cell/ml cell suspension.

4.4.1.2 Cryo-conservation of cells

4.4.1.2.1 Freezing of cells

The freezing medium was prepared by the addition of DMSO to culture medium in a concentration of 20%. After counting and centrifugation, cells were resuspended in the culture medium to reach a cell concentration of $1 \cdot 10^6$ cell/ml.

Cell suspension and freezing medium were now mixed 1:1 and immediately transferred in 2 ml aliquots into cryotubes. This led to 1×10^6 cells per cryotube and a final concentration of 10% DMSO in the freezing medium. The tubes were cooled down to -80°C over 24 to 48 hours and later on transferred to the gas-phase of a liquid nitrogen tank for long-term storage at approximately -130°C .

4.4.1.2.2 Thawing of cells

A cell culture plate with a warm culture medium was prepared. Frozen cells were thawed by dipping the cryotube into a 37°C waterbath until only the core of the suspension was frozen to indicate a temperature of 4°C within the cryotube. When this point was reached the suspension was immediately added to the prepared culture plate. On the next day, if adherent cells were attached to the plate and had time to recover, the whole culture medium and the residual DMSO were removed and replaced by a fresh culture medium.

4.4.2 Cell culture and stimulation experiments

Cells were cultured to 90% confluency on cell culture plates in culture medium. The medium was discarded and replaced by starving medium, followed by further incubation of the cells for 24 hours. After this, cells reached synchronization in the cellular cycle. K4IM were stimulated with TNFA and/or 13cRA, as established in our lab by Ana Belén, in batches of three conditions. All plates were supplied with freshly prepared medium according to the following table and incubated for 24 hours.

Cell stimulation

Medium and Reagents	Control	Stimulation	Inhibition of Stimulation
Starving medium	+	+	+
25 ng/ml TNFA		+	+
13cRA 10^{-5}M			+

After incubation, 2 ml of the supernatants were harvested and frozen at -20°C until they were analyzed by sandwich enzyme-linked immunosorbent assay (ELISA). Cells were further processed as described in 4.4.4.

4.4.3 Enzyme-linked immunosorbent assay (ELISA)

To ensure that stimulation of CCL5 production and the inhibition of this stimulation were successful, undiluted supernatants were tested for CCL5 production using the DuoSet ELISA Development kit, according to the manufacturer's instructions. Optical density was determined using an ELISA reader *GENiosPlus*, set to 450 nm.

The read-out was generated by the XFluor software. Calculation of results was performed using the Microsoft program Excel according to the manufacturer's instructions. Only samples that showed a significant increase in CCL5 protein in the supernatants and a decrease after 13cRA stimulation were employed in ChIP analysis (data not shown).

4.4.4 Chromatin immunoprecipitation (ChIP)

The chromatin immunoprecipitation (ChIP) is a method used to determine the localization of protein of interest at a specific DNA binding site within the genome. This technique gives a picture of the protein-DNA interactions that occur inside the nucleus of living cells or tissues. This technique was used to investigate whether the nuclear co-repressor (NCOR) complex is bound to the *CCL5* promoter under non-stimulated conditions. If our hypothesis holds true, the NCOR should detach from the promoter after stimulation with TNFA but remain there, if the stimulation is inhibited by 13cRA.

4.4.4.1 Chromatin preparation

Cells were stimulated as described in 4.4.2. For the assessment of cell number one, an additional control plate was prepared. Samples were generated with approximately 2×10^6 cell/sample and condition.

4.4.4.1.1 Formaldehyde fixation

Formaldehyde was directly added to the medium to a final concentration of 1%. Samples were fixed at room temperature, gently shaken for ten minutes. The crosslinking reaction was stopped by adding glycine to a final concentration of 125 mM and incubated for another 5 minutes.

Cells were then washed twice with ice-cold PBS, containing 0.1% of a 50x protease inhibitor cocktail. Cells were scraped from the culture dish, transferred into 1.5 ml tubes, centrifuged and the supernatant was discarded.

4.4.4.1.2 Lysis of cells

Cell pellets were resuspended in lysis buffer (600 $\mu\text{l}/1 \times 10^6$ cells) containing 0.1% of a 50x protease inhibitor cocktail. After incubation on ice for ten minutes, the lysates were centrifuged at 2300 x g for 5 minutes at 4°C to pellet the nuclei. Subsequently, the nuclei were resuspended in 200 μl nuclei lysis buffer, containing 0.1% of a 50x protease inhibitor cocktail, and incubated on ice for ten minutes. At this step, samples can be frozen at -80°C.

4.4.4.1.3 Sonication

In order to fragment the DNA to an average length of 500 bp, the samples were exposed to ultrasound. To prevent the sample from being degraded by the developing heat and to prevent foaming, the individual samples were kept on ice during the whole sonication procedure. For sonication, the Sonifier250 was used, put to 20% duty cycle and set at level 2 for the output. Lysates were sonicated in four cycles at 20 pulses each with a 30 second interval between each round. To free samples of cell debris, they were centrifuged at 16000 x g for ten minutes at 4°C. The supernatants were transferred to fresh tubes and the pellets were discarded.

4.4.4.1.4 Gel electrophoresis

The correct size of the DNA fragments was controlled by running 1% of the sample on an agarose gel. Gel electrophoresis is a technique used for the separation of DNA using an electric current applied to an agarose gel matrix. A 2% agarose gel was prepared with a 0.5% TBE buffer. A solution of agarose was achieved by repeated heating of the mixture in the microwave. As soon as the agarose reached a temperature of approximately 50°C, it was cast onto the gel slide of the gel electrophoresis apparatus. After cooling, the solid agarose gel was placed in the running-chamber filled with 0.5% TBE. The sample augmented to 10 μl using H_2O and mixed with 2 μl of loading buffer (6x) before being loaded on the gel. An 1kb size marker (Quick Load, NEB, Frankfurt) was applied to the first lane. A current of 100 – 180 Volt was employed.

After electrophoresis, the bands appearing in the gel were photographed using an UV-transilluminator connected to a gel documentation system (data not shown).

4.4.4.2 Immunoprecipitation

4.4.4.2.1 Preparation of Pansorbin (StaphA) cells

One gram of lyophilized *Staphylococcus A* (Pansorbin; StaphA) cells was resuspended in 10 ml of 1x dialysis buffer and centrifuged at 9300 x g for 5 minutes at 4°C. The supernatant was discarded. This washing step was repeated once. Then the cells were resuspended in 3 ml of 1x PBS plus 3% SDS and 10% BME. This mixture was boiled at 95°C for 30 minutes. After two more washing steps with 1x dialysis buffer, the cells were resuspended in 4 ml of 1x dialysis buffer, divided into 50 µl aliquots, snap frozen and stored at -80°C till use.

4.4.4.2.2 Blocking of *Staphylococcus A* cells

An aliquot of frozen StaphA cells, sufficient to treat a sample originating of up to 5×10^7 fibroblasts, was thawed. To prevent unspecific binding of StaphA cells to DNA or protein, 5 µl of herring sperm DNA and BSA, in concentrations of 10 mg/ml each, were added to the StaphA cells and incubated on a rotating platform at 4°C for at least 3 hours. Before use, the StaphA were washed three times with 1x dialysis buffer and finally resuspended in 50 µl of 1x dialysis buffer again.

4.4.4.2.3 Preparation of samples

The fibroblast samples, consisting of crosslinked and sheared chromatin fragments, dissolved in 200 µl nuclear lysis buffer were diluted 1:10 in the immuno precipitation (IP) dilution buffer to decrease the SDS concentration in the sample. The high SDS content would otherwise impede antibody binding. As total DNA input control, 1% of each sample was taken and frozen at -20°C.

To preclear the samples, 5 µl of preblocked StaphA cells were added to each sample and incubated at 4°C for 15 minutes. The samples were then centrifuged at 16000 x g at 4°C and the supernatants were transferred to fresh tubes.

The following controls were included: a mock control consisting of IP dilution buffer instead of chromatin, a control containing no antibody and an isotype control for each condition. The aim was to check for DNA contaminations within the reagents in use and nonspecific interactions of the antibody.

After sample and control preparation the antibody was added. The active chromatin and the NCOR antibody were whole serum antibodies. On inquiry, the manufacturers stated a concentration of 1 mg/ml (maximum). According to this information, of both

antibodies an estimated 2 µg per IP sample were used. Antibody and samples were incubated over night on a rotating platform at 4°C.

4.4.4.2.4 Precipitation

The over night incubation was followed by the precipitation of the antibody-immune complexes via the StaphA cells. 5 µl of preblocked StaphA cells were added to each sample and incubated on a rotating platform at 4°C for 15 minutes. This was followed by a centrifugation step at 16000 x g at 4°C and several washing steps. The washing procedure included two steps of 1x dialysis buffer and four steps of IP wash buffer. For each washing step, the pellet was dissolved in 600 µl of buffer. An additional 600 µl of buffer was added and the samples were incubated on a rotating platform for three minutes, followed by centrifugation at 16000 x g at 4°C for 4 minutes. It is necessary to remove as much buffer as possible after each wash without aspirating the StaphA cell–antibody complexes. After the last wash, remaining traces of buffer had be completely removed. To separate the StaphA–Antibody–Protein-DNA complexes, the pellet was dissolved in 150 µl IP elution buffer containing SDS. The mix was shaken on a vortexer for at least 15 minutes and was then centrifuged. The supernatant, now containing only Protein - DNA complexes, was transferred to a fresh tube. This step was repeated once and eluted fractions were pooled.

4.4.4.2.5 Decrosslinking and ethanol precipitation

The aim of this step was to reverse the crosslinks generated through the formaldehyde fixation by heat and high salt concentration. Proteins bound to the DNA were denatured and thus, separated in this way from the DNA. The total DNA input controls (see 4.4.4.2.3) were thawed and diluted to a volume of 300 µl. NaCl at a final concentration of 0.3 M and 1 µl of RNase A (10 mg/ml) was applied to all samples. All samples were incubated for four hours or overnight at 65°C. After incubation, 2.5 volumes of 100% EtOH were added to the samples to precipitate chromatin at -20°C overnight.

4.4.4.2.6 Protease K digestion

To ensure removal of most of the chromatin proteins from the sample, a protease K digestion was conducted. Samples were centrifuged at 16000 x g for 20 minutes at 4°C. The ethanol was discarded, samples were centrifuged once again and residual ethanol removed completely. Pellets were allowed to air dry. Dried pellets were

dissolved in 100 µl of TE buffer. 25 µl of 5x PK buffer and 1.5 µl of protease K were added to each sample and incubated at 45°C for 1-2 hours in a heating block.

4.4.4.3 DNA analysis

4.4.4.3.1 Phenol-chloroform extraction

In order to purify the DNA and remove residual RNA, protein or reagents, DNA was extracted once with phenol/chloroform/isoamyl alcohol and once with chloroform/isoamyl alcohol. To keep the loss of DNA as small as possible, the samples were diluted in TE buffer to a volume of 300 µl. One volume of Roti® – Phenol/C/I was added and samples were vortexed and centrifuged at 16000 x g for 3 minutes. The upper aqueous phase containing the DNA was transferred to a fresh tube. One volume of chloroform/isoamyl alcohol was added to this sample, followed again by vortexing and centrifugation at 16000 x g for three minutes. The aqueous phase containing the DNA was transferred to a fresh tube and precipitated using EtOH 100%.

4.4.4.3.2 Ethanol precipitation

Sodium acetate was added to samples and total DNA input controls to a final concentration of 0.3 M. The expected amount of specific, enriched DNA in the eluted samples was marginal. Glycogen is an inert carrier, which is insoluble in ethanolic solutions and forms a precipitate that traps the target nucleic acid. 5 µl of that carrier were added to the samples. Finally, 2.5 volumes of ice cold 100% EtOH were added and all samples were precipitated over night at -20°C.

After precipitation, samples were centrifuged at 16000 x g for 20 minutes at 4°C. The ethanol was discarded and samples were washed with one volume of 70% EtOH to remove residual salt that might influence the following PCR reaction. The samples were centrifuged once and residual ethanol was removed completely. Pellets were allowed to air dry completely. Dried pellets were dissolved in 30 µl of H₂O. It was critical to ensure complete resuspension of DNA. This was achieved by repeated pipetting. Subsequently, the samples remained in a thermo block at 37°C for at least one hour. Repeated freeze and thaw cycles can be necessary to ensure complete dissolving of the DNA.

4.4.5 PCR analysis

PCR analysis was employed as the last step to amplify the precipitated DNA. This was necessary in order to detect enrichment of specific DNA after precipitation. The DNA of interest can only be amplified by the specific primers of the PCR reaction, while the quantity of specific DNA was increased in contrast to the non specific DNA that could not completely be eliminated through the washing steps. Optimal conditions will produce strong signals in the samples compared to the controls. If a signal was detectable after the ChIP, it implied that the precipitated protein under investigation had bound to the DNA sequence under investigation at the moment of DNA fixation.

PCR

Reagent	Batch
ThermoPol buffer (10x)	1x
NTPs (1.25 mM)	0.25 mM
Forward 10pM	0.5 pM
Reverse 10pM	0.5 pM
Taq polymerase	0.25 U/ μ l

H₂O was added to reach a volume of 24 μ l. For the PCR reaction, 1 μ l of the 30 μ l elution sample was added to a 24 μ l PCR batch. PCR was performed on a Geneamp PCR system 9700PE. After an initial denaturing step of 5 minutes at 94°C, the samples were cycled 35 times, for 30 seconds at 94°C, followed by 60 seconds at 65°C for annealing and 30 seconds at 72°C for elongation. All oligonucleotides are summarized in the supplementary table 1.

4.5 Statistical analyses

Statistical analyses were performed using Graph Pad Prism 4.03. For expression values of qPCR data, a non-parametric analysis of variance (ANOVA/ Kruskal–Wallis test) was performed to test for significant differences between the different groups of animals. Analysis of gene expression over time, compared to the control kidney was followed by the Dunn's post test, correcting for multiple testing. Only the results of the post test are displayed. Effects of the treatment were followed by a Mann-Whitney-U Test. Only the results comparing the different groups at specific time points are displayed. P-values of less than 0.05 were considered to indicate statistically significant differences.

5 Results

5.1 Transcriptomic profiling identifies progressive changes in the transplantation model during CAD

CAD results of a complex set of processes that eventually manifests itself as a progressive fibrosing disease. While morphometric analysis can demonstrate progressive changes during CAD, the goal of this study was to characterize features at the transcriptomic level to help identify regulatory networks underlying the initiation and progression of tissue damage.

A problem often associated with oligonucleotide-based Affymetrix DNA-microarrays is appropriate annotation of the probe-sets that are used to define a specific transcript. Regarding this, the annotation provided by the company of a significant number of probe-sets are not in line with our current knowledge of the genome as they might be based on data predating genomic sequencing [78, 79]. In addition, individual probes within the probe-sets can cross-hybridize with other transcripts leading to a skewing of data and an increase in false positive signals. Therefore, in addition to a standard analysis (data not shown), the recently developed ChipInspector software (Genomatix GmbH) was used for the analysis of the Affymetrix DNA microarrays, as described in 4.1. Both analyses yielded comparable numbers of regulated genes. The data outputs are represented by lists of compiled genes containing information about gene regulation and statistical significance. It has been previously demonstrated that this approach effectively reduces background noise and largely eliminates false positives in the analysis, thereby improving the sensitivity and specificity of the biological findings (data not shown and [63]). Figure 12 displays similarities as well as differences of the two microarray analysis approaches. Transcriptomic profiling by microarray analysis demonstrated more than one thousand genes to be significantly regulated in the transplanted kidneys as compared to the control kidneys at the various time points tested (7 days, 14 days and 56 days after transplantation). The time points mark different stages observed in disease progression. The 7 day time point represents acute inflammation and by day 14 this process begins to show chronic and fibrotic alterations. The 56 days time point represents severe chronic damage.

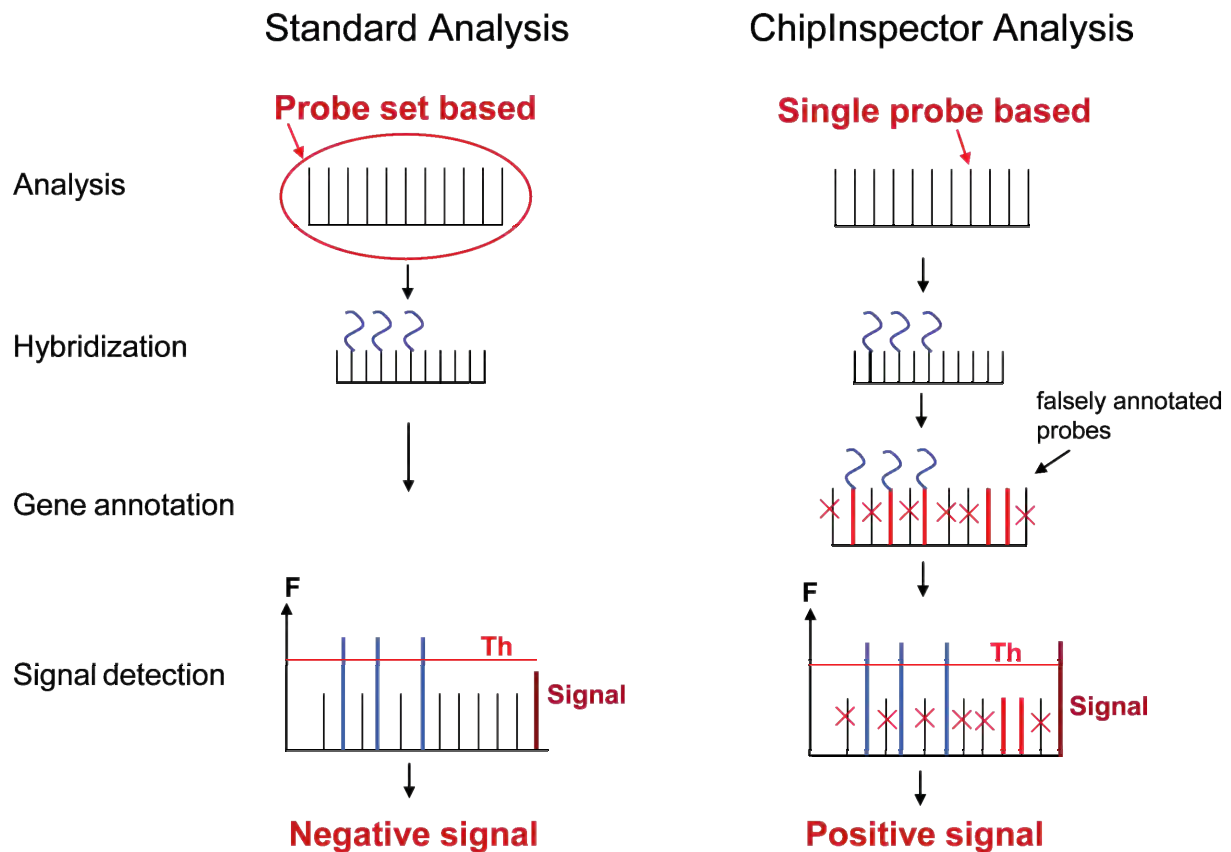


Fig. 12: Differences in microarray analyses. The diagram displays the basic steps of a microarray analysis and the difference between the standard and the ChipInspector (CI) analysis. The standard analysis is based on whole probe-sets, representing genes on the array. The single probe based CI-analysis ignores probe-sets and regards single probes only. After hybridization, the CI performs an up-to-date genome annotation check, for every single probe. Single probes, identified to be falsely assigned to a probe-set or to crosshybridize, are not evaluated for signal detection. Standard methods generate averages of fluorescence (F) intensity over all single probes of the probe-set. A signal is positive if the average overcomes a certain threshold (Th). In our example, this would result in a negative signal. In case of the CI, only verified single probes are taken into consideration for signal calculation which generates a positive signal, as in the example above. The advantage of the CI is fewer false positive or negative signals through up-to-date genome annotation of single probes.

Figure 13 displays the workflow of the bioinformatical analysis and the programs employed.

The lists compiled by the ChipInspector analysis include a gene identification number (GeneID) and a fold change relative to a specific time point. The lists were subsequently analyzed using BiblioSphere software from Genomatix GmbH. This software generates networks of genes connected by literature co-citations. The connection between genes can be graphically observed on different hierarchical levels.

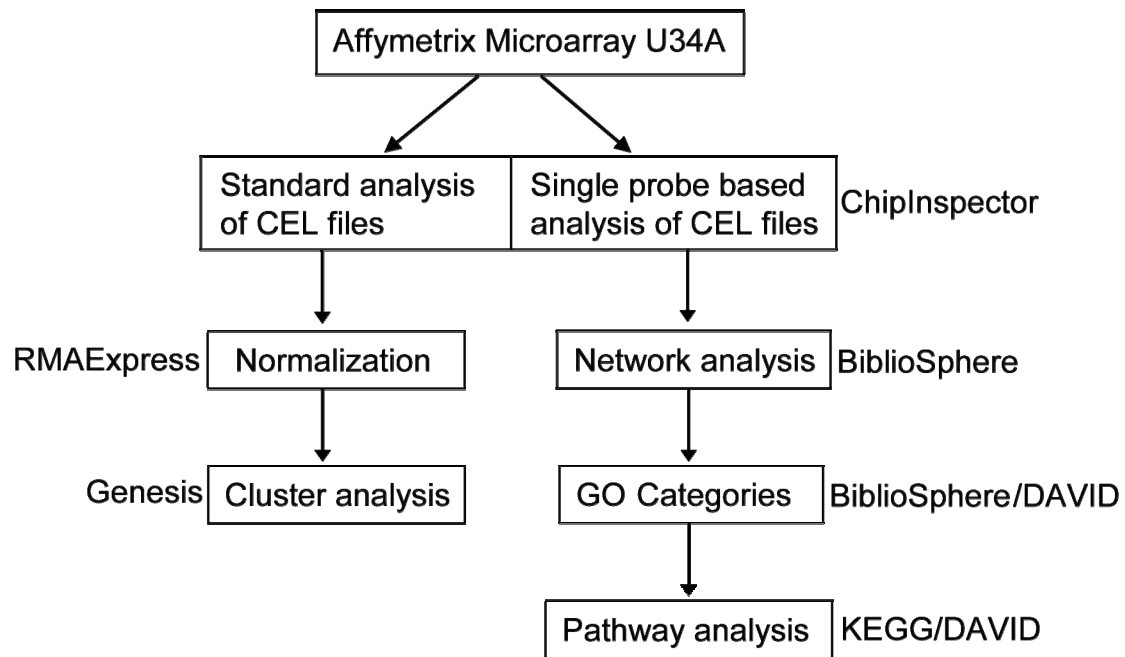


Fig. 13: Bioinformatic analysis. The flowchart summarizes the single analyses performed and displays the workflow. After paralleling standard and CI analysis of CEL files, progressing analyses divide. CI (4.1.1) generated gene lists were loaded into BiblioSphere (4.1.2) and DAVID (4.1.3) Standard microarray analysis results were normalized using RMAExpress (4.1.4) and subsequent hierarchical clustering was performed by the Genesis program (4.1.5).

Due to the high numbers of genes, the standard BiblioSphere analysis was difficult to apply to our experimental data. However, an additional feature of the BiblioSphere software allows the categorization of genes according to the gene ontology (GO) consortium.

The GO filter “biological process” was first employed to dissect and organize the gene lists. Over- or under-representation of genes assigned to a special GO group within the gene lists was automatically calculated and displayed by a “score”. This approach was used to identify groups of genes linked to specific biological processes. GO groups with significant scores for over representation included “response to stress”, “response to stimulus” and several GO groups expected during tissue damage. No GO group regarding signal transduction showed a significant score. Further investigation was performed by applying the DAVID bioinformatics database tool.

DAVID provides a comprehensive set of functional annotation tools that help provide a more detailed biological context behind large lists of genes. DAVID is linked to several databases that allow visualization of genes in pathway maps. These pathways were further studied in the context of gene expression associated with signal transduction by using the Kyoto Encyclopedia of Genes and Genomes (KEGG)

database of pathways. Using the functional annotation chart provided by the DAVID database, the association of individual genes with a regulatory pathway defined by KEGG was investigated. All the gene lists were uploaded and manually searched for pathway associations. Pathways associated with epithelial to mesenchymal transition (EMT, as described in 1.1.3) and fibrosis were evaluated in detail. These included NOTCH, TGFB, HH and WNT pathways. For each pathway, a list of genes, based on KEGG and recent literature was compiled. In many cases, genes playing critical roles in the different pathways were not present on the commercial microarray, which allowed no statement regarding their expression. Finally a list of genes for each pathway was generated for qPCR analysis that consisted of genes observed to be regulated according to the microarray analysis and critical genes not present on the array.

5.1.1 Inflammation associated gene expression in CAD

Transplantation of a kidney initiates a series of complex pathophysiologic processes leading to the recruitment of immune effector cells to the graft. In the absence of sufficient immunosuppressive therapy and genetic match, this leads to persistent inflammation in the kidney tissue and chronic fibrotic damage.

Transplantation of Fisher kidneys into Lewis rats without immunosuppression results in a smoldering inflammatory process. This activity has been linked to the development and progression of allograft dysfunction. In our animal transplantation model for CAD, an infiltrate consisting of monocytes/macrophages and CD8-positive T cells was demonstrated [5]. By morphometry, the inflammatory infiltrate was found to peak at early time points (7 to 14 days) and decrease towards the last time point (56 days).

Transcriptomic profiling, combined with pathway modeling, was used here to characterize networks of genes that underlie the initiation and progression of CAD. The first set of genes examined, represented transcripts linked to inflammation.

The genes investigated included the chemokine ligands 2, 3, 5 (Ccl2, Ccl3, Ccl5), interferon gamma (Ifng), interferon-inducible cytokine 10 (Cxcl10/Ip10), Tnfa, and the interleukins 1 beta and 6 (Il1b, Il6).

With the exception of tumor necrosis factor alpha (Tnfa), the microarray analysis indicated strong upregulation of all investigated genes. qPCR verified that gene expression of these proinflammatory cytokines was upregulated at all tested time points as compared to a normal kidney. The mRNA expression of Ccl2, Ccl3, Ifng and Tnfa remained elevated after 7 days, whereas mRNA expression progressively increased for Ccl5 and Il6 after 14 and 56 days. Il1b and Cxcl10/Ip10 were rapidly upregulated to a peak on day 7 and then slowly declined. Results are summarized in figure 14.

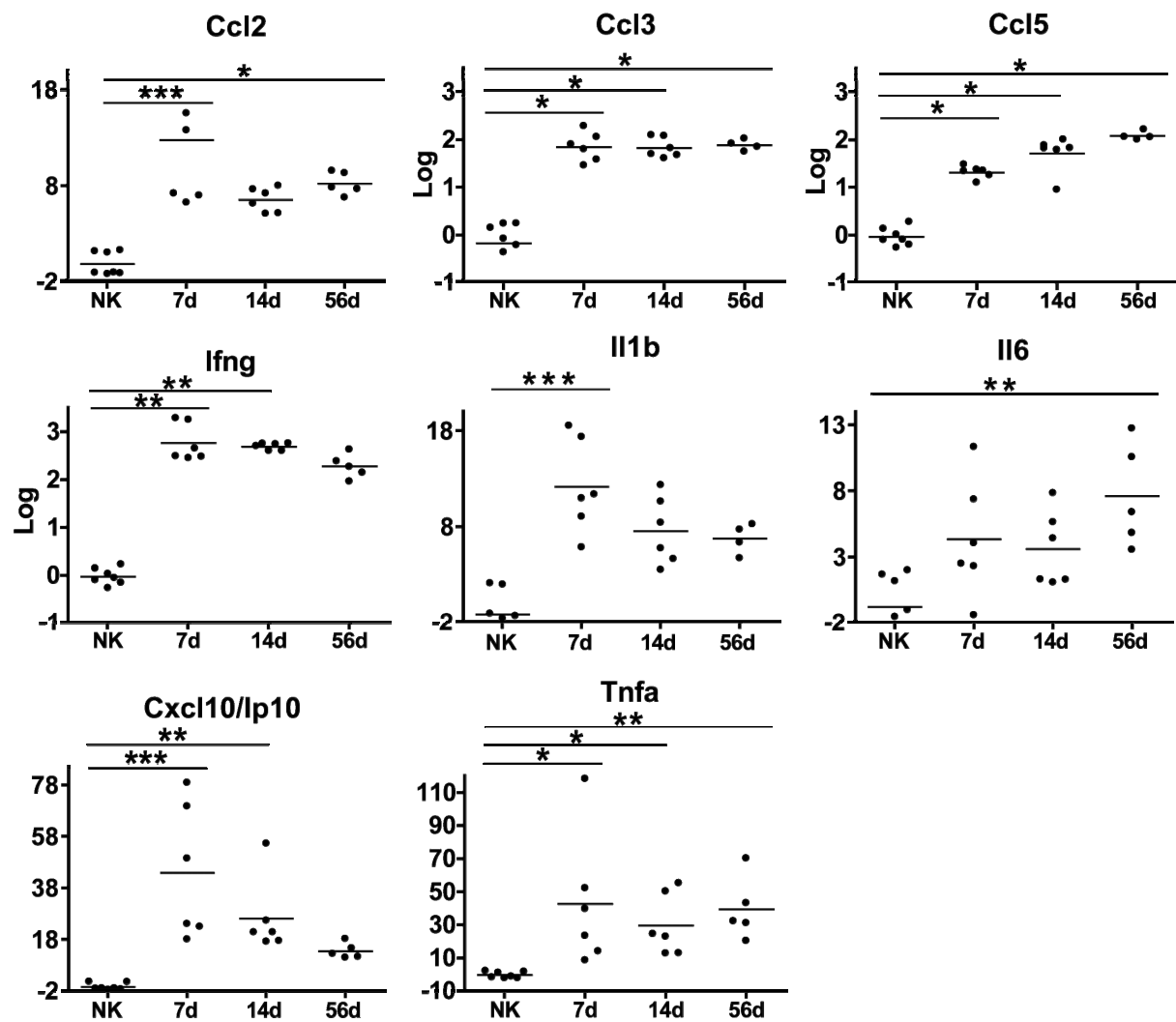


Fig. 14: Inflammatory genes. Expression data of inflammation associated genes after qPCR analysis. Data was generated employing qPCR, as described in 4.2.4 and displayed fold changes were calculated, as described in 4.2.5. “Log” denotes a logarithmic scale, if not noted otherwise the scale is linear. For statistical analysis, the Kruskal-Wallis non-parametric test was applied to analyze the differences between the individual animal groups. Dunn’s post test was applied for multiple testing. Significant differences are denoted by an asterisk. * denotes a statistically significant difference with a p value < 0.05, ** denote a statistically significant difference with a p value < 0.01 and *** denote a statistically significant difference with a p value < 0.0001.

Many of these proinflammatory cytokines have been previously shown to influence downstream signaling events. The activation of genes known to respond to inflammation-associated signal transduction was investigated.

These included signal transducer and activator of transcription 1 (*Stat1*), interferon regulatory factor 1 (*Irf1*) and janus kinase 2 (*Jak2*), which are closely related with *Ifng* stimulated signal transduction. A minor but constant upregulation of *Jak2* was observed. After ligand binding and receptor dimerization, JAKs dissociate from the receptor. This results in phosphorylation and dimerization of STATs which help to activate transcription of genes with specific response elements within their promoters.

The transcription factor *Irf1* is one of these genes. *Stat1* and *Irf1* showed a strong upregulation, peaking on day 7 and decreasing afterwards. qPCR verified the upregulation of genes indicated by the microarray analysis. Other genes associated with inflammatory signal transduction included the toll-like receptor 4 (*Tlr4*), interleukin-1-receptor-associated kinase 3 (*Irak3*) and the nuclear receptor peroxisome proliferator activated receptor gamma (*Pparg*). IRAK3 acts as a downstream inhibitor of TLR4 signaling. Both genes showed a constant upregulation in transplanted kidneys. This expression suggests paralleled expression in certain cell types, such as monocytes/macrophages. *Pparg* showed highest upregulation on day 56. Figure 15 displays the genes assigned to inflammatory signal transduction.

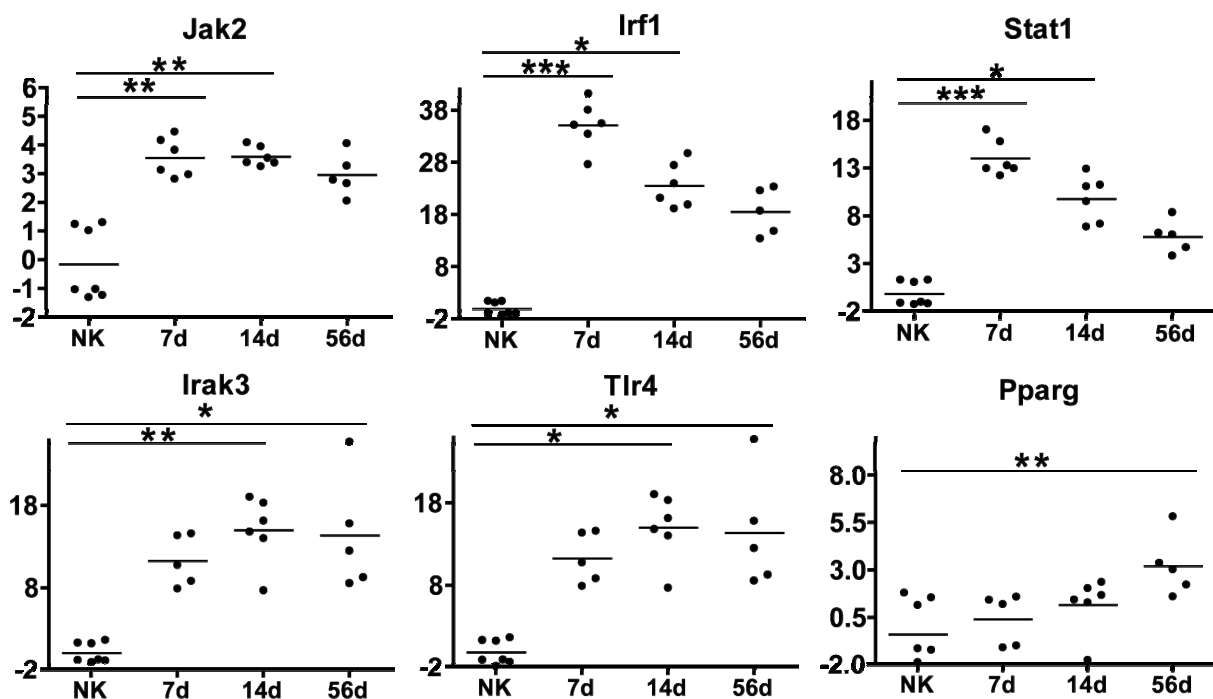


Fig. 15: Inflammation associated signal transduction. Expression data of genes assigned to signal transduction after qPCR analysis. Data was generated employing qPCR, as described in 4.2.4 and displayed fold changes were calculated, as described in 4.2.5. For statistical analysis, the Kruskal-Wallis non-parametric test was applied to analyze the differences between the individual animal groups. Dunn's post test was applied for multiple testing. Significant differences are denoted by an asterisk. * denotes a statistically significant difference with a p value < 0.05, ** denote a statistically significant difference with a p value < 0.01 and *** denote a statistically significant difference with a p value < 0.0001.

This analysis verified that acute inflammation as a reaction to the transplantation insult was reflected in altered gene expression. While inflammation is important to wound healing, persistent inflammation is thought to promote fibrosis and chronic tissue damage which leads to loss of organ function.

5.1.2 EMT and fibrosis associated gene expression in CAD

Renal interstitial fibrosis is the hallmark of progressive kidney disease [80]. During fibrosis, extracellular matrix (ECM) is synthesized in excess by activated fibroblasts. Neither the origin of the activated fibroblasts nor the stimuli that lead to increased ECM production have been completely elucidated. Understanding the biological networks that regulate these processes is central to characterizing the underlying pathogenic events and may help to identify potential targets for therapeutic intervention. In pulmonary fibrosis, as well as in rodent kidney models, the epithelial-to-mesenchymal transition (EMT) is presented as a potential mechanism of fibrogenesis during fibrosis *in vivo* [81, 82]. EMT is characterized by the *de novo* synthesis of alpha smooth muscle actin, upregulation of mesenchymal markers and the loss of E-cadherin.

The expression of a series of marker genes linked to fibrosis and EMT were then evaluated in the progressive rat model by both array and qPCR analysis. Downregulation of E-cadherin (*Cdh1*) is associated with EMT. This is thought to allow the cells to acquire a motile phenotype [83]. Upregulation of the transcription factors connective tissue growth factor (*Ctgf*) and snail homolog 1 (*Snai1*) are thought to play a role in the downregulation of *Cdh1* [17]. While steady state expression of all three genes was seen, no differential regulation of these genes was observed during the progression of tissue damage. Importantly, general markers of fibroblast activation and fibrosis including vimentin (*Vim*), smooth muscle actin (*Actg2*) and fibroblast specific protein 1 (*Fsp1/S100a4*) [7, 82] did show progressive upregulation by microarray and qPCR.

To further characterize the induction and progression of fibrosis, mRNA expression of collagen type I (*Col1a1*) and collagen type III (*Col3a1*), pro-fibrogenic mediators such as tumor growth factor beta 1, 2, 3 (*Tgfb1, 2, 3*) and plasminogen activator inhibitor 1 (*Serpine1/Pai1*) as well as the anti-fibrotic bone morphogenic protein 7 (*Bmp7*) was analyzed [8, 84, 85]. Both collagens were upregulated during disease progression. *Tgfb2* and *Tgfb3* showed no differential regulation. *Tgfb1* expression was increased at all time points while *Serpine1/Pai1* showed significantly increased expression only by day 56. *Bmp7*, a *Tgfb1* antagonist, was coincidentally downregulated with progression of CAD. Discussed in the context of EMT, BMP7 is able to counteract TGF β -associated renal fibrosis, and even reverse it [86-88].

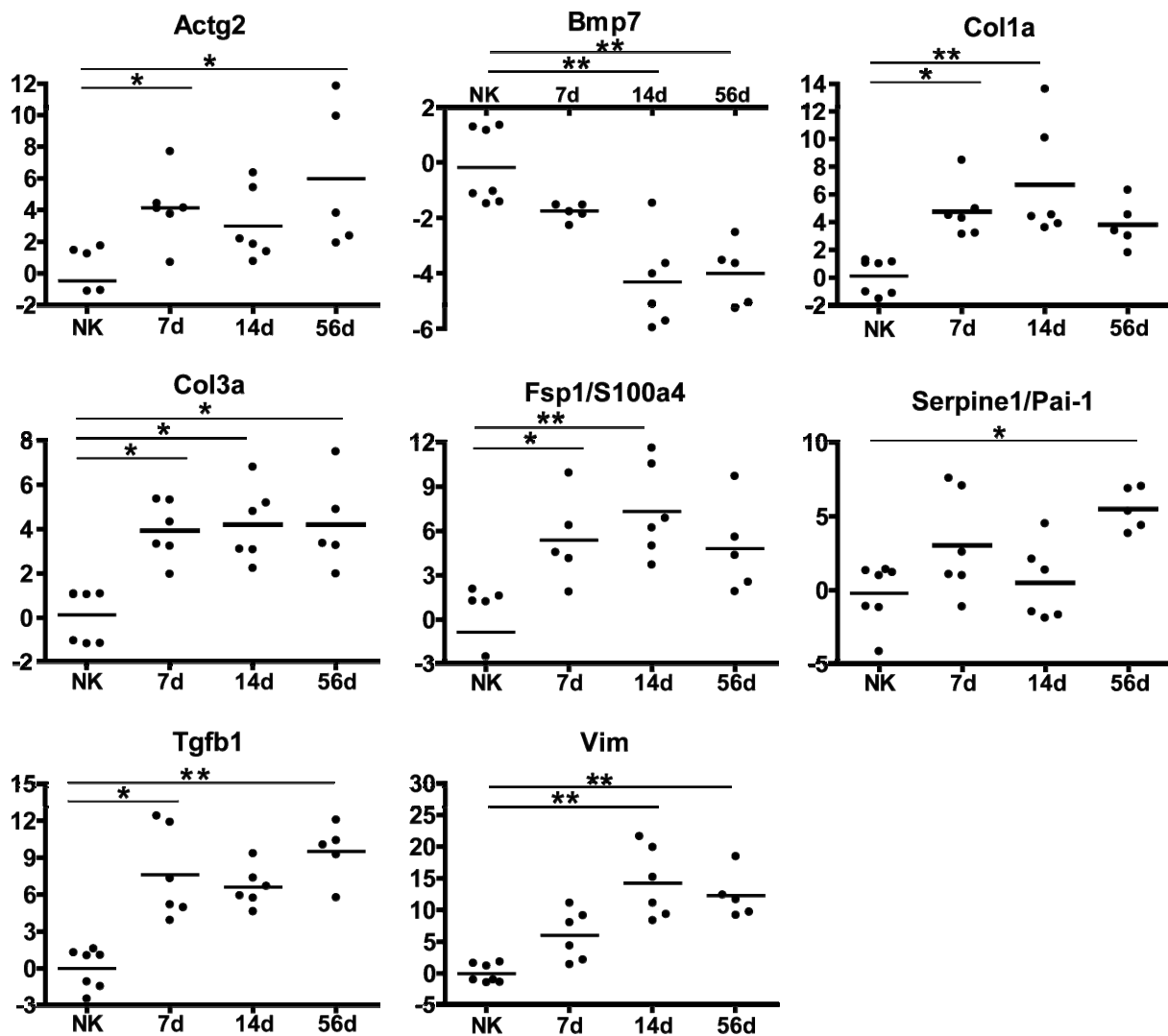


Fig. 16: Fibrosis associated genes. Expression data of fibrosis associated genes after qPCR analysis. Data was generated employing qPCR, as described in 4.2.4 and displayed fold changes were calculated, as described in 4.2.5. For statistical analysis, the Kruskal-Wallis non-parametric test was applied to analyze the differences between the individual animal groups. Dunn's post test was applied for multiple testing. Significant differences are denoted by an asterisk. * denotes a statistically significant difference with a p-value < 0.05, ** denote a statistically significant difference with a p-value < 0.01 and *** denote a statistically significant difference with a p-value < 0.0001.

Results of the analysis of profibrotic genes are summarized in figure 16. The upregulation of collagen mRNA was verified on the protein level using Sirius red staining which stains for total collagen and thereby shows the general level of fibrosis in a tissue sample. The results showed a progressive increase in collagen over time. Immunohistochemical staining for collagen I also showed increasing levels through all time points, as displayed in figure 17.

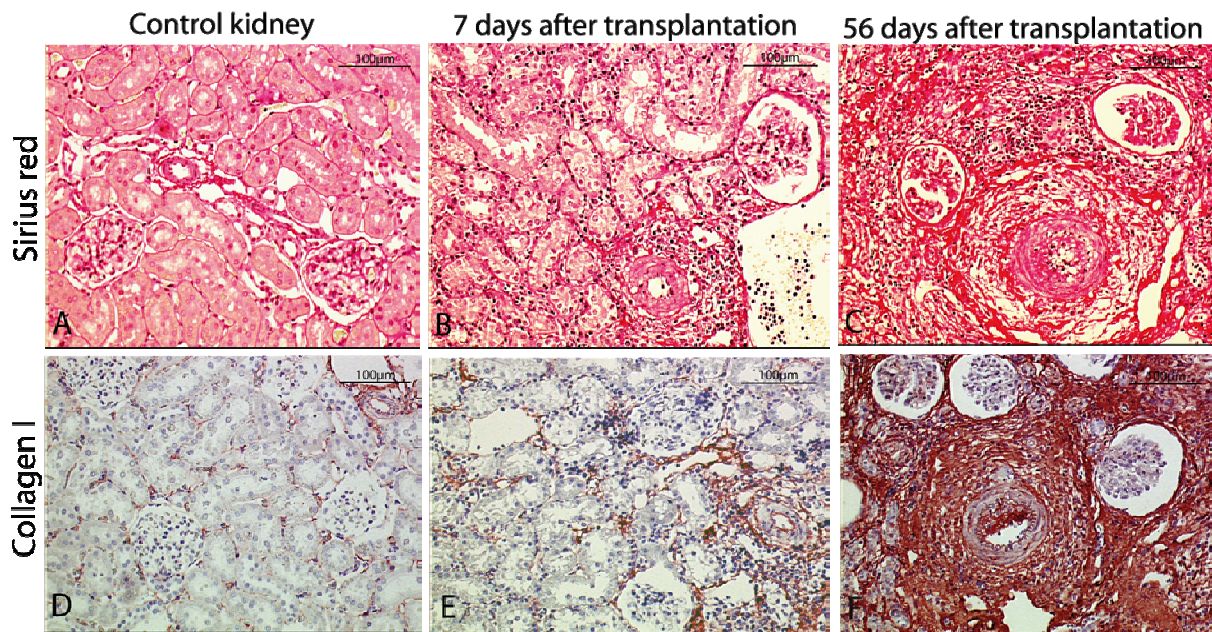


Fig. 17: Sirius red and collagen I staining. Sirius red staining was performed on kidney sections by Ms. Gabrielle Schmidt from the DKFZ, Heidelberg, as described in 4.3.1. Collagen I staining was performed as described in 4.3.2. Figures display extracellular matrix deposition in rat kidney allografts on day 56 after transplantation (C,F) in comparison to allografts on day 7 after transplantation (B,E) and native Fisher rat kidneys (A,D). Sections are positive for Sirius red and collagen I (brown) staining in the tubulointerstitium, as well as in the subendothelial area of a preglomerular artery in the kidney allograft on day 56 after transplantation (C, F). (A-C: Sirius red; D-F: Immunostaining for collagen I (ABC method); 200x).

After demonstrating the induction and progression of fibrosis in the rat model, the goal was then to characterize selective temporal changes in the pathways that are thought to be associated with fibrosis, EMT, and wound healing. Specifically, it was sought to characterize pathways that may help orchestrate the processes underlying fibrosis, and through this, identify potential targets for therapeutic intervention.

5.1.3 Pathways regulated during progression of CAD

Consistent with the hypothesis of a potential recapitulation of developmental programs after tissue injury, many pathways discussed in the context of fibrosis and EMT were originally identified during embryogenesis. By analyzing the temporal activation status of a series of these pathways during progressive tissue damage, the goal was to identify alterations in the networks of pathways responsible for the transition of inflammatory signals into profibrotic stimuli. It was hoped that by specifically focusing on crosstalk and alternative signaling between the distinct pathways, it might be possible to detect major switches and targets for therapeutic intervention. The pathways investigated included the NOTCH pathway, the TGF β pathway, the HH pathway, and the WNT signaling pathways.

Upregulation of the receptor *Notch1* was indicated by the microarray analysis and the expression of *Notch1* and the ligand jagged 1 (*Jag1*) was evaluated by qPCR. No differential regulation of the NOTCH pathway genes was observed via qPCR analysis suggesting that activation of this pathway could not be demonstrated in the context of our study.

TGFB has been implicated as a master switch in the induction of fibrosis in many organs, and is a major mediator of EMT in a number of physiological contexts including tissue fibrosis [89]. Upregulation of *Tgfb1* and the target gene *Serpine/Pai1* were observed. The main signaling pathway activated by TGFB1 acts through the SMAD proteins. The *Smad* genes were not present on the microarray and gene expression was assessed by qPCR. None of the investigated genes *Smad1*, *Smad2*, *Smad3* and *Smad4* demonstrated a significant change in expression during disease progression. It is known that TGFB1 can activate signal transduction in a SMAD-independent manner. The ability of TGFB1 to crosstalk has been implicated for several pathways including RhoA, Ras, MAPK, PI3 kinase, NOTCH, and WNT signaling pathways [89].

5.1.3.1 Specific activation of the hedgehog pathway

Binding of the hedgehog (HH) ligand to the receptor patched (PTCH1) leads to a relief of repression of the downstream receptor smoothed (SMO), followed by inhibition of transcription factor degradation and subsequent target gene expression. The mammalian HH homologues display intricate expression patterns during development, as well as in adult organisms [90]. HH signaling remains active in the adult where it is thought to help maintain tissue homeostasis [91]. HH has been recognized in different types of cancer [92], EMT [17, 93], stem cell biology, and tissue repair during chronic persistent inflammation [31]. The mRNA expression of HH pathway genes, according to the microarray analysis, is summarized in a schematic diagram of the alterations in the pathway during disease progression in figure 18.

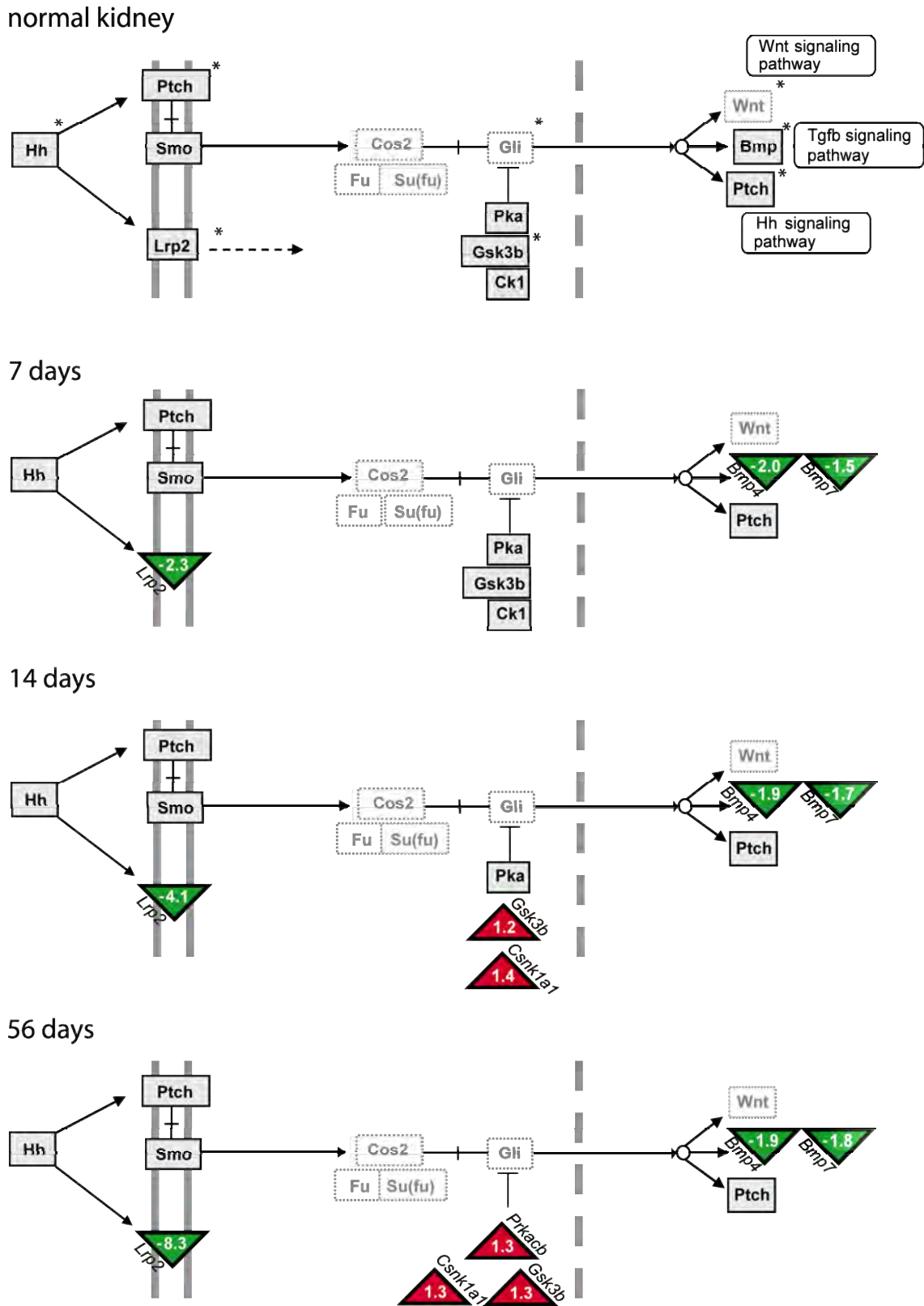


Fig. 18: Microarray analysis of the hedgehog pathway. The scheme displays microarray data integrated into a modified version of the Hh pathway (discussed in 1.1.3.3). A white box marks a gene not annotated to the microarray. Boxes with an asterisk indicate further or additional investigation of the gene by qPCR. The sketch is divided in four parts displaying time points 0 (normal kidney), 7, 14 and 56 days after transplantation. Triangles indicate the up or downregulation of genes in comparison to the control kidney. Red triangles indicate upregulation, green triangles indicate downregulation. Numbers displayed are ChipInspector generated fold changes. Displayed downstream target genes include *Bmp4*, *Bmp7* and *Ptch1*.

Only a few HH genes including bone morphogenic proteins 4 and 7 (*Bmp4,7*), as well as the receptors patched 1 (*Ptch1*) and low-density lipoprotein related protein 2 (*Lrp2/Megalin*) were present on the microarray, and showed differential regulation. To better characterize the activation of the HH pathway, genes assigned to this pathway were analyzed using qPCR. Analyses were performed for receptors *Ptch1* and *Lrp2*, as well as the ligands sonic hedgehog (*Shh*), indian hedgehog (*Ihh*) and desert hedgehog (*Dhh*). *Dhh* is most closely related to the *Drosophila hh*, whereas *Ihh* and *Shh* are more closely related to each other, and represent a recent gene duplication [94]. The three *Hh* genes are expressed in different tissues at different stages of development, suggesting different biological activities [95]. Expression of *Ihh* has been demonstrated in embryonic and adult kidney [96, 97]. Further, the expression of the HH-associated transcription factor Gli-kruppel member 1 (*Gli1*) and target genes secreted frizzled protein 1 (*Sfrp1*), *Bmp4* and *Bmp7* were investigated. The genes of the HH pathway showed very distinct expression patterns.

The receptor *Ptch1*, a reliable indicator for HH signal reception, showed constant upregulation [95]. The receptor *Lrp2* was strongly downregulated with tissue damage. This receptor is expressed on the apical site of the tubular epithelial cells and is thought to help establish the brush border of the kidney tubulus. The brush border is destroyed in the context of disease progression [5].

The HH ligands *Ihh* and *Shh* were downregulated, while *Dhh* demonstrated an increasing upregulation. The target genes *Bmp4* and *Bmp7* also showed a constant downregulation. The family of BMPs belongs to the superfamily of tumor growth factors and provides a connection between the HH pathway, TGFB signaling and fibrosis [98, 99]. The target gene *Sfrp1* showed a minor upregulation that became statistically significant on day 14. It is linked to the WNT pathway, where it acts as an upstream pathway inhibitor [100]. qPCR results of the analysis of HH pathway regulation are summarized in figure 19. Supplementary table 2 summarized microarray results and gene names/symbols, displayed in figure 18.

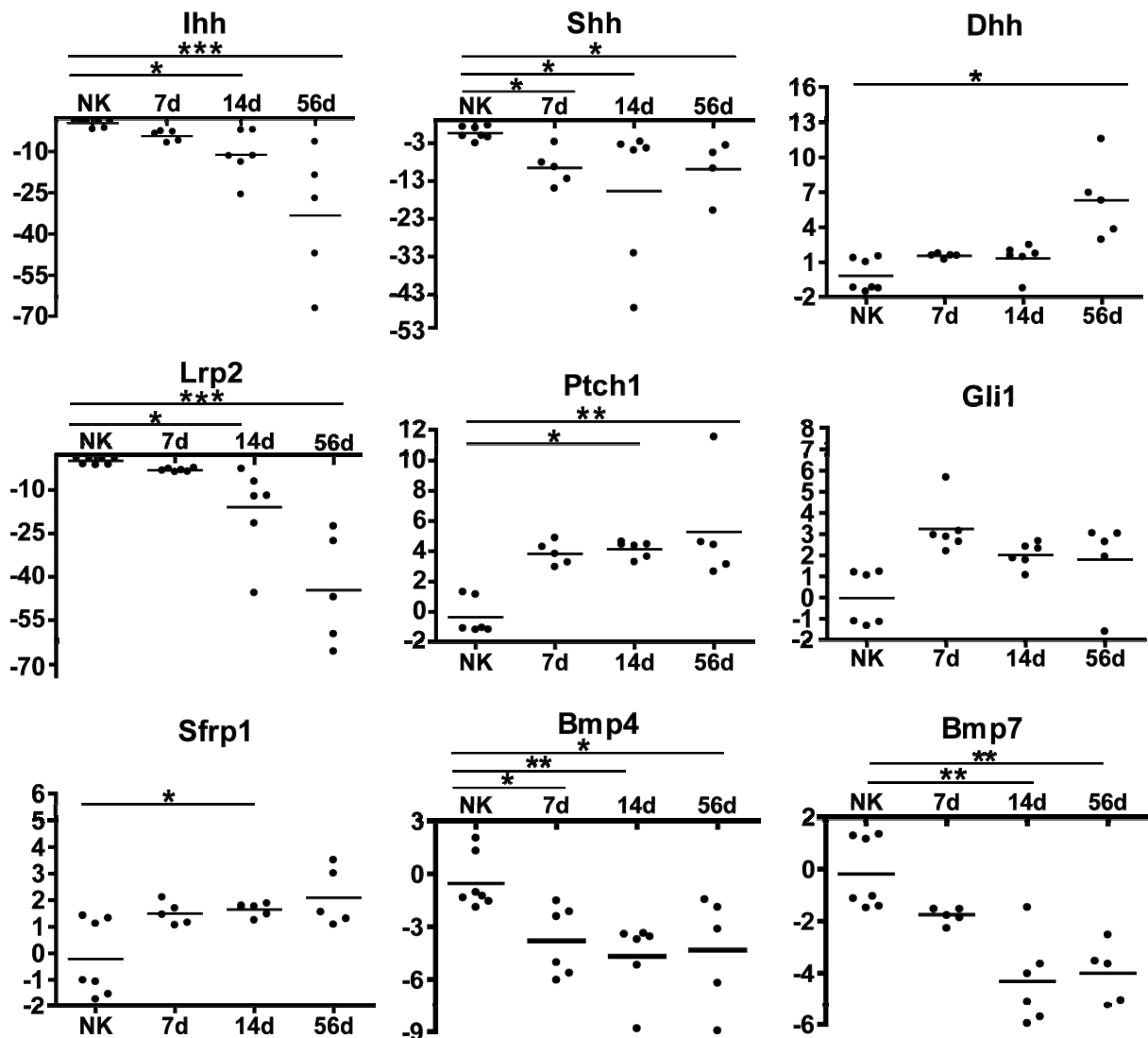


Fig. 19: Hedgehog pathway associated genes. Expression data of hedgehog pathway associated genes after qPCR analysis. Data was generated employing qPCR, as described in 4.2.4 and displayed fold changes were calculated, as described in 4.2.5. For statistical analysis, the Kruskal-Wallis non-parametric test was applied to analyze the differences between the individual animal groups. Dunn's post test was applied for multiple testing. Significant differences are denoted by an asterisk. * denotes a statistically significant difference with a p-value < 0.05, ** denote a statistically significant difference with a p-value < 0.01 and *** denote a statistically significant difference with a p-value < 0.0001.

These results demonstrate activation of a distinct part of the HH pathway. It seems that at least two sub-pathways exist, within the set of genes investigated. This might result from mixed culture effects. The ligand *Dhh*, together with the receptor *Ptch1*, the signaling molecule *Gli1* and target genes such as *Sfrp1*, as well as several WNT pathway ligands (discussed in 5.1.3.2), are upregulated, demonstrating activation of this sub-pathway. In contrast, the ligands *Shh* and *Ihh*, together with the receptor *Lrp2* and target genes such as the *Bmps* (discussed in 5.1.2) and again several, WNT pathway ligands are downregulated.

A close inter-relationship between HH and WNT pathways is evidenced by the fact that the WNT ligands are HH target genes. Crosstalk between the HH and the WNT pathway has been identified in embryonic development and cancer [101-103]. HH and WNT pathways regulate each other. An inhibitory relationship has been described in the context of epithelial cells of the colon and cancer [31, 104]. IHH has been directly addressed as WNT signaling inhibitor [104]. Having analyzed the role of HH pathway, the characteristics of the WNT pathways were further investigated.

5.1.3.2 Specific and progressive changes of WNT genes and pathways

Expression of *WNT* genes is regulated in a coordinated temporal and spatial manner during development [105]. WNT ligands are tightly associated with the extracellular matrix and tend to exert paracrine or endocrine, but not more distant effects [106]. Reactivation of WNT ligand expression and abnormal WNT signaling has been observed in an inflammatory, fibrotic diseases and cancer [40, 107-110].

The expression of individual WNT ligand genes was assessed by qPCR (only *Wnt5a* was present on the Affymetrix array and showed no regulation). Out of the 19 known *Wnt* genes, all but *Wnt1* and *Wnt16* were found to be expressed in rat kidney. However, *Wnt3a*, *Wnt8a* and *Wnt10b* were expressed at levels too low for us to reliably evaluate their regulation. *Wnt3* showed a moderate upregulation. A statistically significant regulation was observed for *Wnt2b*, *Wnt6*, *Wnt7a*, *Wnt7b*, *Wnt8b* and *Wnt10a*. *Wnt6* and *Wnt7a* expression were increased with CAD, while *Wnt7b* was downregulated – with the most pronounced effect seen on day 14. *Wnt2b* showed progressive downregulation during the development of CAD. *Wnt8b* and *Wnt10a* were also both downregulated relative to the normal control kidney. The *Wnt8b* downregulation was most pronounced on day 14 and *Wnt10a* on day 7. Results are summarized in table 1 and figure 20.

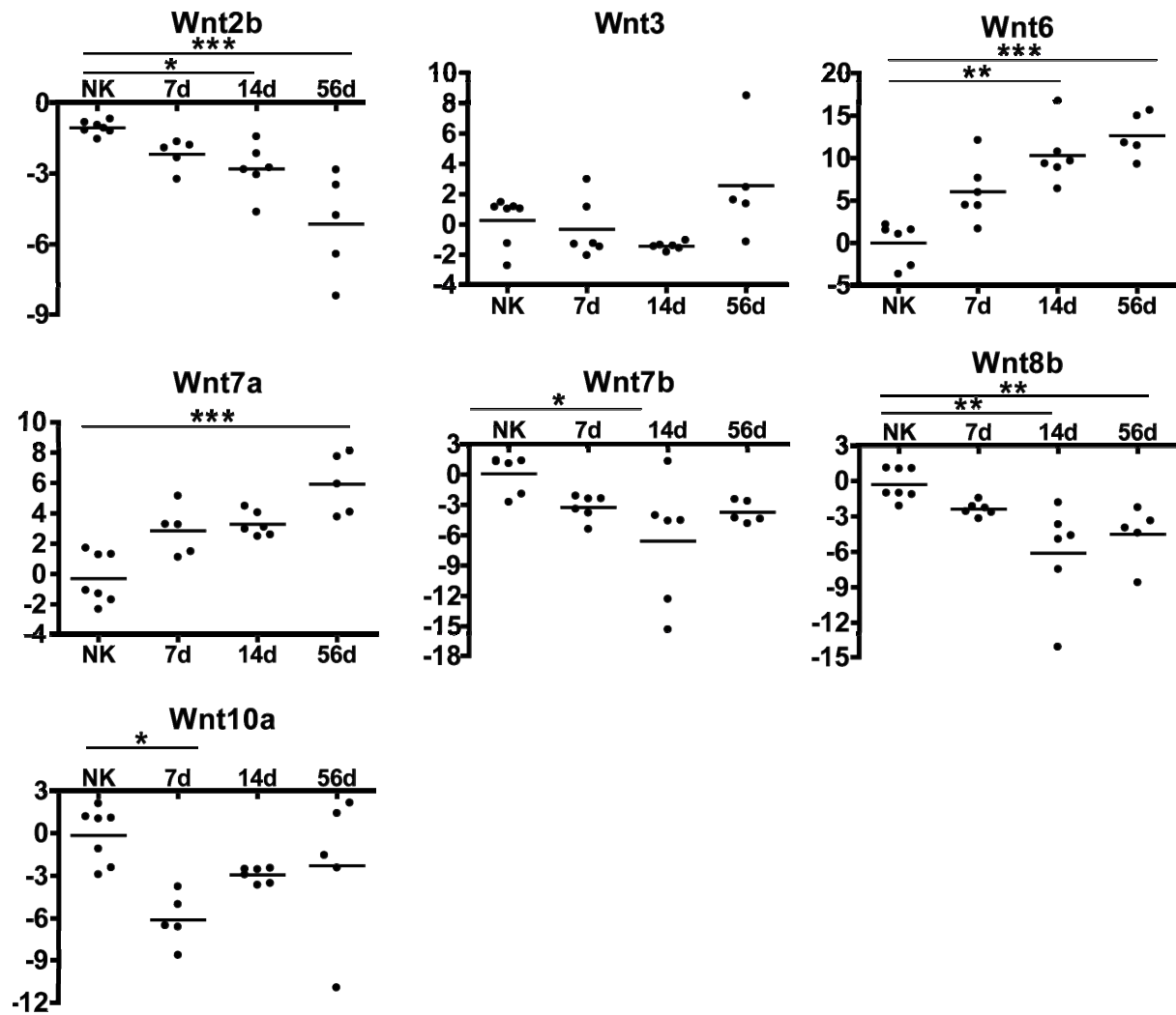


Fig. 20: Expression of Wnt genes. Expression data of Wnt ligands after qPCR analysis is displayed. Only Wnt5a was present on the array, therefore expression of all 19 Wnt ligands had to be evaluated by qPCR. Table 1 summarizes expression and regulation of all 19 Wnt ligands investigated. Data was generated employing qPCR, as described in 4.2.4 and displayed fold changes were calculated, as described in 4.2.5. For statistical analysis, the Kruskal-Wallis non-parametric test was applied to analyze the differences between the individual animal groups. Dunn's post test was applied for multiple testing. Significant differences are denoted by an asterisk. * denotes a statistically significant difference with a p value < 0.05, ** denote a statistically significant difference with a p value < 0.01 and *** denote a statistically significant difference with a p value < 0.0001.

WNT signaling may be directly activated through WNT ligand over-expression, or through alterations downstream in the WNT signaling cascade [111].

In the next step of our analysis, alterations in the different WNT signaling cascades, consisting of the canonical WNT, the WNT-Ca²⁺ and the WNT planar cell polarity pathway were investigated.

Table 1. Wnt gene expression and regulation in the rat kidney

Gene ID	Symbol	Expression	Signaling	Regulation
24881	Wnt1	not expressed in rat kidney	Canonical	
114487	Wnt2	expressed	Canonical	n.s.
116466	Wnt2b	expressed	ND	Downregulation
24882	Wnt3	expressed	Canonical	Upregulation
303181	Wnt3b	expression at detection limits	Canonical	could not be evaluated
84426	Wnt4	expressed	Wnt-Ca2+	n.s.
64566	Wnt5a	expressed	WntCa2+ /PCP	n.s.
282582	Wnt5b	expressed	Wnt-Ca2+	n.s.
316526	Wnt6	expressed	Wnt-Ca2+	Upregulation
114850	Wnt7a	expressed	Wnt-Ca2+	Upregulation
315196	Wnt7b	expressed	Wnt-Ca2+	Downregulation
291678	Wnt8a	expression at detection limits	Canonical	could not be evaluated
293990	Wnt8b	expressed	Canonical	Downregulation
287357	Wnt9a	expressed	ND	n.s.
303586	Wnt9b	expressed	ND	n.s.
316527	Wnt10a	expressed	Canonical	Downregulation
315294	Wnt10b	expression at detection limits	Canonical	could not be evaluated
140584	Wnt11	expressed	Wnt-Ca2+ / PCP+	n.s.
500047	Wnt16	not expressed in rat kidney	ND	

Table 1: n.s. denotes a differential regulation not to be statistically significant. ND: not defined to activate a certain WNT signaling pathway.

5.1.3.2.1 Regulation of the canonical WNT pathway

Beta-catenin is the central regulator of the canonical WNT pathway. The protein is normally rapidly degraded. In WNT pathway activation, ligand binding to the frizzled receptor is followed by inhibition of beta-catenin degradation, allows nuclear beta-catenin accumulation and subsequent effects on target gene transcription. General effects of canonical WNT pathway activation include proliferation, differentiation, and cell fate determination [108].

Transient upregulation of WNT beta-catenin signaling after tubular cell injury was described *in vitro* and *in vivo* [112, 113]. Analysis of microarray data allowed a schematic graph of the pathway and thus, importantly, a dynamic view of the components of the canonical WNT pathway that changed during the development of CAD as displayed in figure 21. Supplementary table 3 summarizes microarray results, gene names and symbols, displayed in figure 21. In addition, potential points of cross talk between the canonical WNT pathway with other regulatory pathways (e.g. HH, MAPK and TGFB) were added to the scheme.

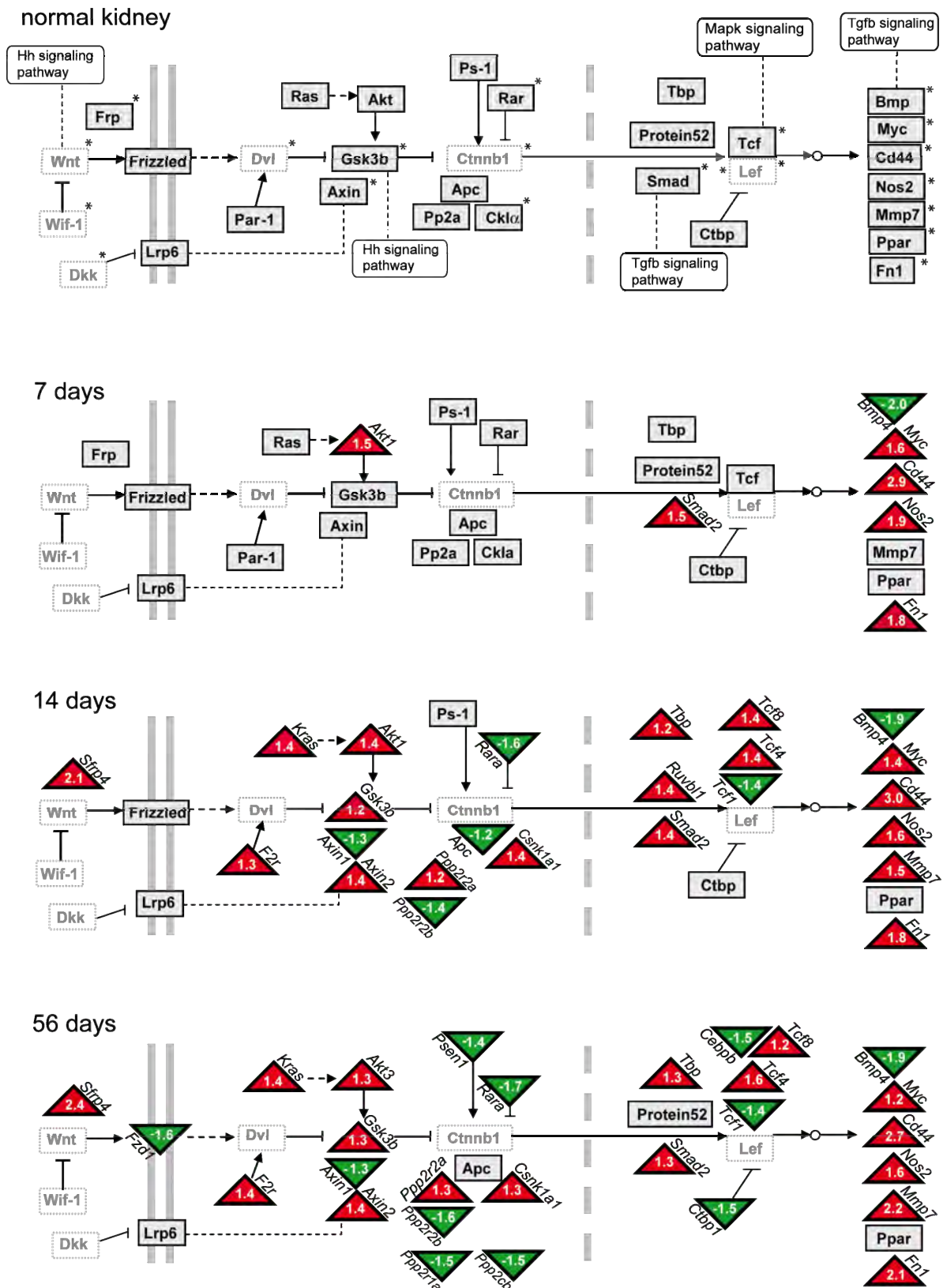


Fig. 21: Microarray analysis of the Wnt canonical pathway. The scheme displays microarray data integrated into a modified version of the Wnt pathway (discussed in 1.1.3.4). A white box marks a gene not annotated to the microarray. Boxes with an asterisk indicate further or additional investigation of the gene by qPCR. The sketch is divided in four parts displaying time points 0 (normal kidney), 7, 14 and 56 days after transplantation. Triangles indicate the up or downregulation of genes in comparison to the control kidney. Red triangles indicate upregulation and green triangles indicate downregulation. The numbers displayed are ChipInspector generated fold changes (native scale, not log transformed). Displayed downstream target genes include *Nos2*, *Cd44*, *Mmp7* and *Fn1*.

While beta-catenin was not found to be regulated at the mRNA level by microarray or qPCR analysis, nuclear accumulation of beta-catenin protein could be verified by immunohistochemistry. Control kidneys demonstrated a strong basolateral staining of epithelial cells of the tubule. During disease progression a shift from a predominantly basolateral to a cytoplasmic localization and starting nuclear localization in endothelial cells was observed. Interestingly, expression was localized in nuclei preferentially in the endothelium of peritubular capillaries and in some tubular epithelia. This expression increased with fibrosis, as displayed in figure 22.

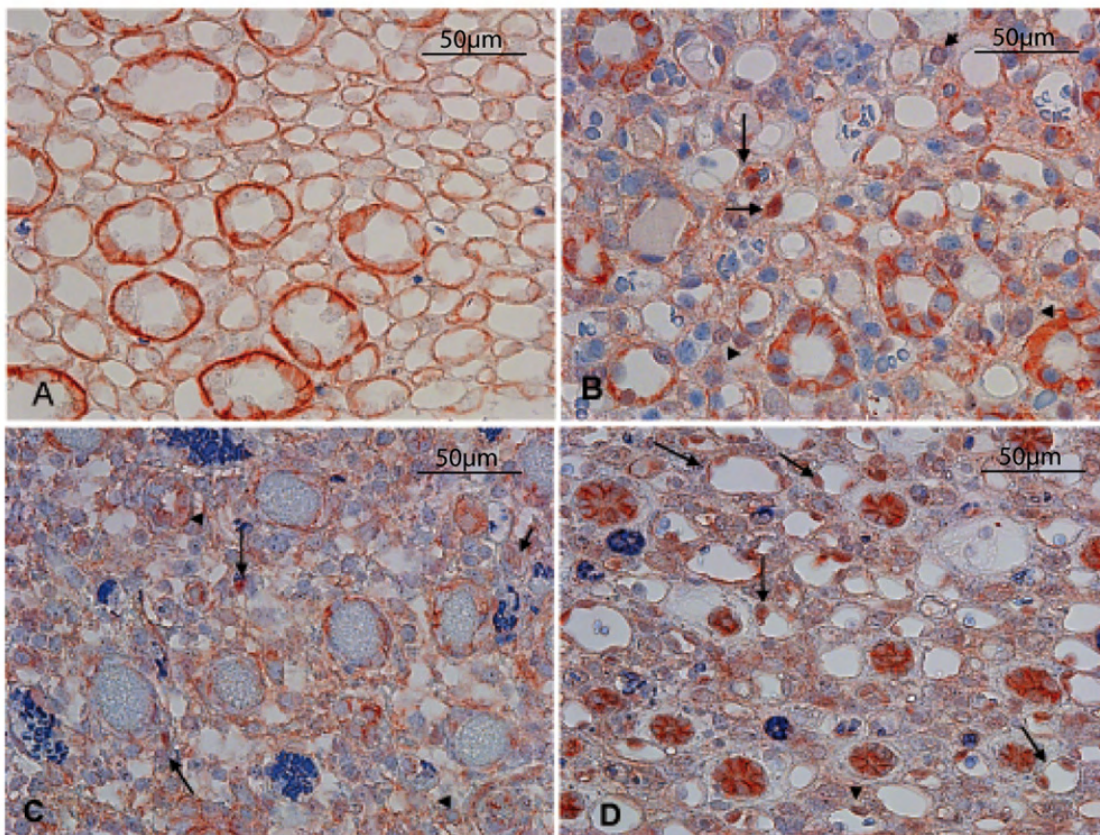


Fig. 22: Beta-catenin nuclear localization. **A:** Control kidney, non-transplanted with strong basolateral positivity for beta-catenin in collecting ducts and distal tubules, staining in red. **B:** Kidney 7 days after transplantation with a shift from a predominantly basolateral to a cytoplasmic localization and an increase in nuclear positivity in capillary endothelia (\rightarrow). Weak but clear cut label is detectable in nuclei of some epithelial-, and interstitial cells (\blacktriangleright) (lower left). **C:** 14 days post transplantation pre-collapsed tubules become noticeable in the kidney. Staining for nuclear beta-catenin in endothelial cells (\rightarrow) and with less pronounced nuclear label in some tubular epithelia (\blacktriangleright) can be demonstrated. **D:** 56 days after transplantation, there are many endothelial cells with nuclear positivity with different intensities (\rightarrow : strong; \blacktriangleright : weak). Collapsed tubules show strong beta-catenin positivity in epithelia, without clear distinction between cytoplasm and nucleus.(400x).

The expression of genes assigned to the canonical WNT pathway by KEGG, showing differential regulation on the microarray, as well as pathway genes not included on the microarray, was further examined by qPCR over the course of the experiment.

The Wnt pathway genes investigated during CAD included the upstream Wnt pathway inhibitors secreted frizzled-related proteins 1, 4, 5 (*Sfrp1,4,5*), Wnt inhibitory factor 1 (*Wif1*) and Dickkopf homolog 3 (*Dkk3*). Additionally, gene expression of the WNT pathway genes glycogen synthase kinase 3 beta (*Gsk3b*), dishevelled 3 (*Dvl3_pred*), *Axin2*, casein kinase 1 (*Csnk1a1*), transcription factors 1, 4, 5 (*Tcf1, 4, 5*) and lymphoid enhancer binding factor 1 (*Lef1*) was examined. WNT pathway inhibitors showed no uniform expression pattern. No significant regulation of *Sfrp4* and *Wif1* was observed. *Sfrp1* and *Dkk3*, which is also a WNT target gene [100], showed a minor upregulation on day 14 and day 56, respectively. *Sfrp5* showed an attenuated downregulation during all time points. Of the known WNT pathway genes, no differential expression was observed for *Gsk3b*, *Dvl3_pred*, *Csnk1a1*, *Tcf4* and 5. However, a minor but not significant upregulation of *Axin2* was observed on day 56. The canonical WNT pathway associated transcription factors *Lef1* and *Tcf1* displayed significant regulation during CAD. *Lef1* upregulation was highest on day 7, but remained elevated throughout all the time points tested, while *Tcf1* mRNA showed progressive downregulation in comparison to controls throughout all points, displayed in figure 23.

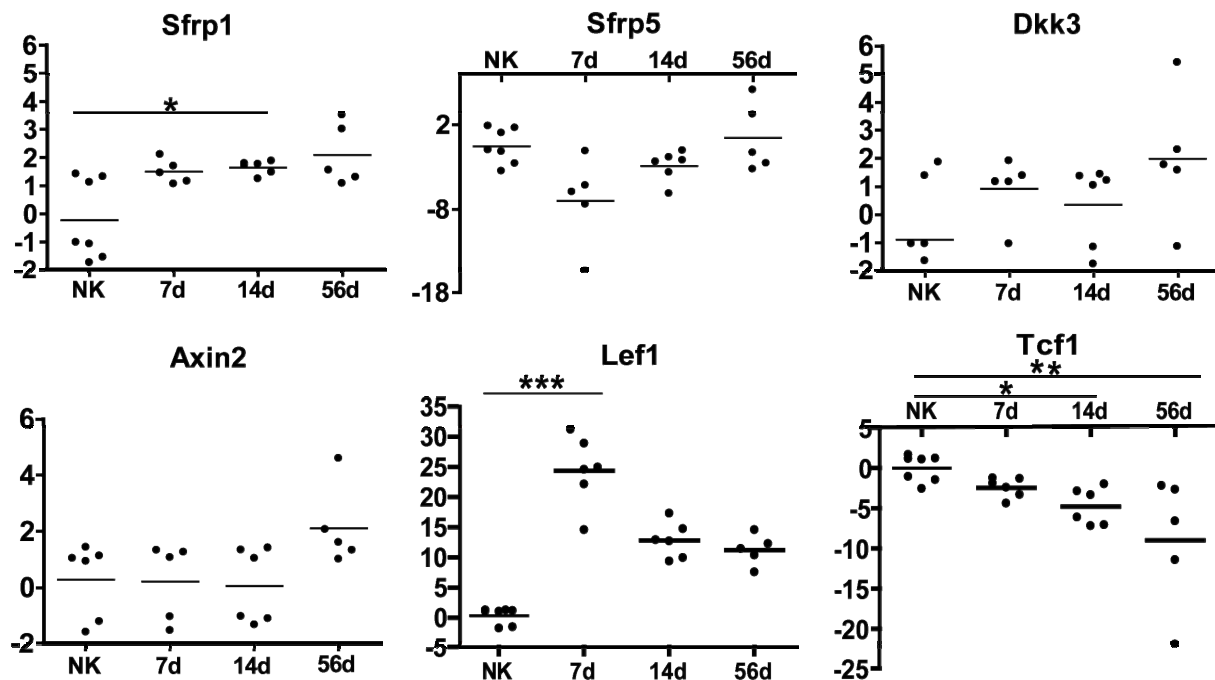


Fig. 23: Expression of WNT canonical pathway genes Expression data of Wnt pathway genes after qPCR analysis is displayed. Data was generated employing qPCR, as described in 4.2.4 and displayed fold changes were calculated, as described in 4.2.5. For statistical analysis, the Kruskal-Wallis non-parametric test was applied to analyze the differences between the individual animal groups. Dunn's post test was applied for multiple testing. Significant differences are denoted by an asterisk. * denotes a statistically significant difference with a p value < 0.05, ** denote a statistically significant difference with a p value < 0.01 and *** denote a statistically significant difference with a p value < 0.0001.

These results suggest a progressive change in the pathway occurring during CAD with the initial changes seen by day 7 and pronounced changes evidenced by day 56. The effect of these changes on the canonical WNT pathway can be evidenced by the expression of downstream target genes. Canonical WNT target genes investigated included fibronectin 1 (*Fn1*), Cd44 molecule (*Cd44*), matrix metalloproteinase 7 (*Mmp7*), nitric oxide synthase 2 (*Nos2*), myelocytomatosis oncogene (*Myc*) and bone morphogenic protein 4 (*Bmp4*) [110, 111, 114]. *Fn1* and *Cd44* showed upregulation over all points. Of all the genes investigated, *Mmp7* and *Nos2* were amongst the most drastically upregulated genes. The *Myc* gene, the first Wnt target gene to be identified [115], was found to be significantly upregulated on day 7 and expression remained elevated above normal kidney levels. *Bmp4* was downregulated during progression of CAD, summarized in figure 24.

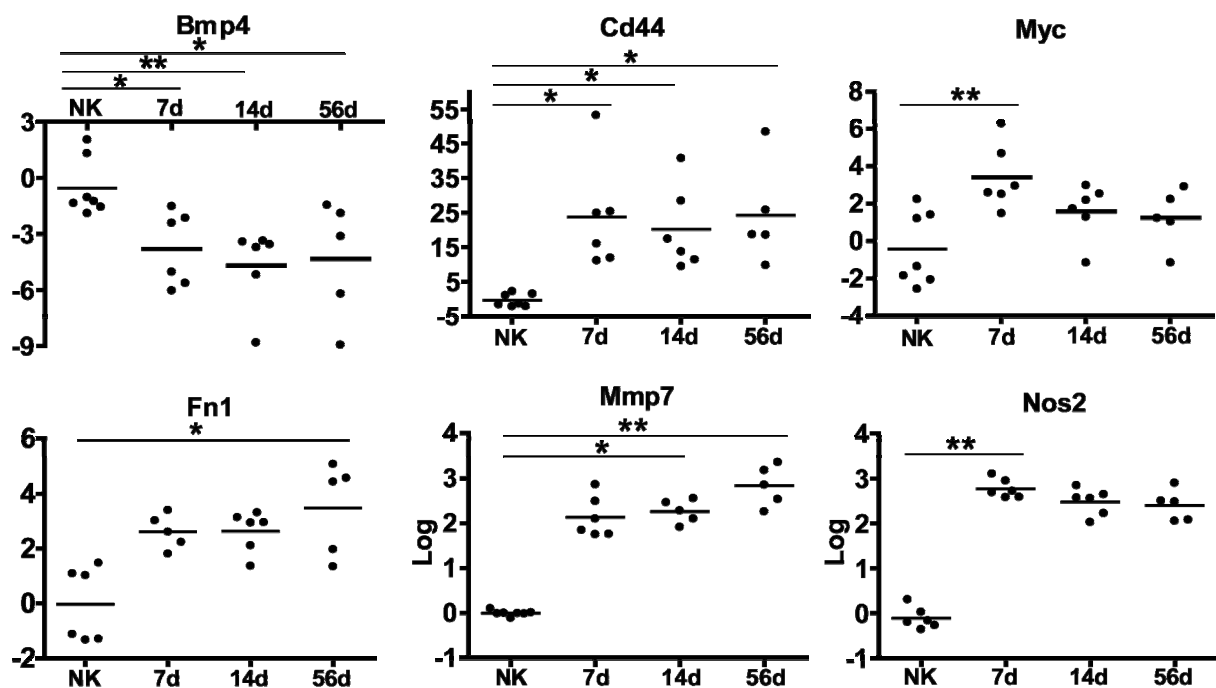


Fig. 24: Expression of Wnt canonical target genes. Expression data of Wnt canonical target genes, after qPCR analysis. Data was generated employing qPCR, as described in 4.2.4 and displayed fold changes were calculated, as described in 4.2.5. “Log” denotes a logarithmic scale, if not noted otherwise the scale is linear. For statistical analysis, the Kruskal-Wallis non-parametric test was applied to analyze the differences between the individual animal groups. Dunn’s post test was applied for multiple testing. Significant differences are denoted by an asterisk. * denotes a statistically significant difference with a p value < 0.05, ** denote a statistically significant difference with a p value < 0.01 and *** denote a statistically significant difference with a p value < 0.0001.

An increase in nuclear Lef1 within target cells could be demonstrated at the protein level (see figure 25), as well as the upregulation of Cd44 and fibronectin protein in the tubulointerstitial region was, by immunohistochemistry, using specific antibody

reagents. The general results observed closely paralleled those seen in the qPCR data, see figures 22 and 25.

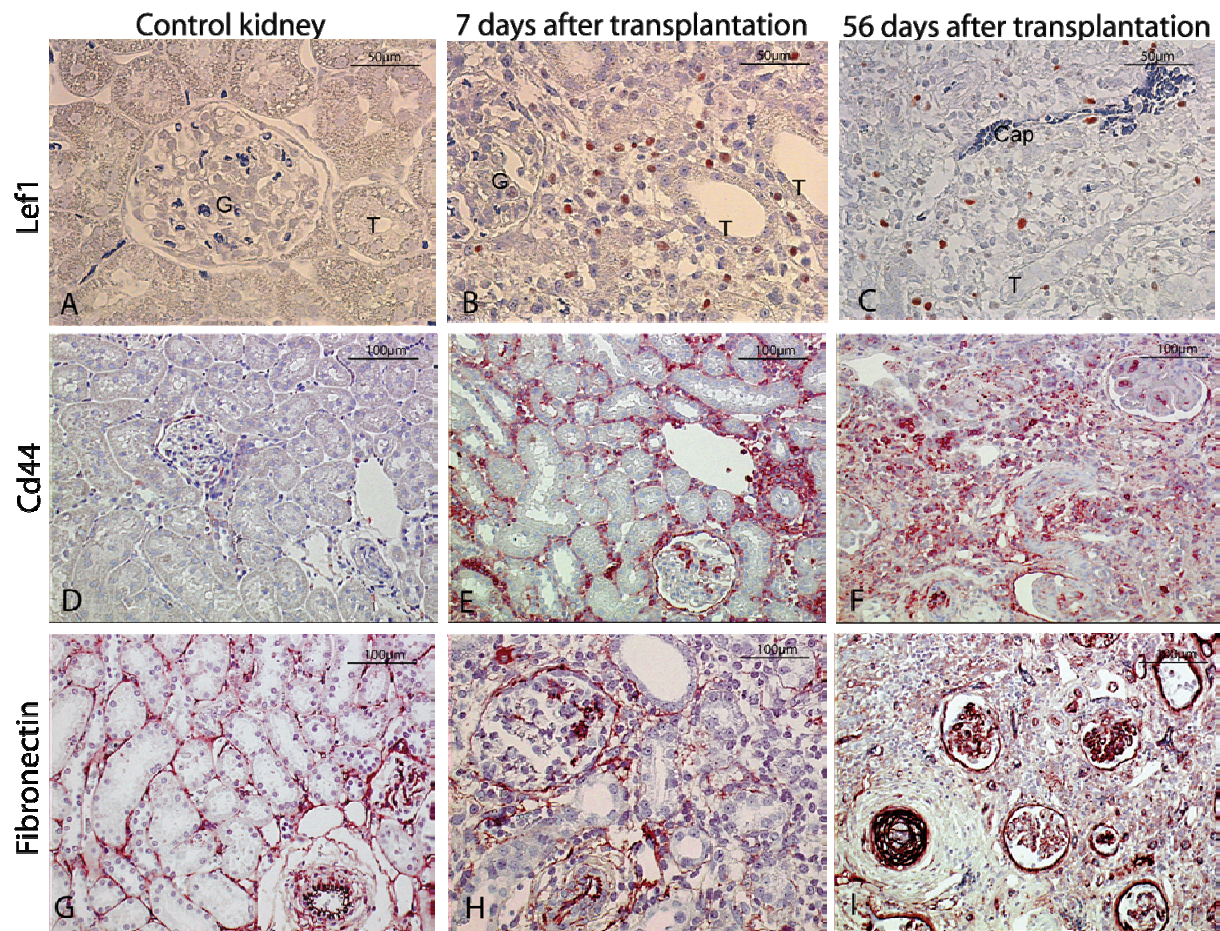


Fig. 25: Protein expression of the Wnt target genes. Lef1 (A-C), Cd44 (D-F) and fibronectin (G-I) in Fisher-Lewis rat kidney allografts. **A:** Control kidney non-transplanted: regular glomerular structure and typically differentiated tubules without nuclear Lef1 positivity, stained in blue. **B:** Kidney 7 days after transplantation with several interstitial mononuclear cells with strong Lef1 nuclear label. T: tubule; G: glomerulus. **C:** 56 days after transplantation kidney with collapsed tubule (T), ectatic capillary (Cap) and with nuclear Lef1 stain in mononuclear cells in the interstitium and focally in the tubule. (A-C, 400x) **D:** Only a few Cd44+ cells can be observed in the native Fisher kidney; **E:** A high number of Cd44+ cells in the interstitium and glomeruli of kidney allografts were detected on day 7 as well as on day 56 (**F**) after transplantation; **I:** Tubulointerstitial fibrosis, transplant glomerulopathy and vasculopathy in rat kidney allografts on day 56 after transplantation are associated with strong expression of fibronectin, in comparison to acute rejection on day 7 after transplantation (**H**) or native Fisher rat kidneys (**G**). (Cd44: D-F; Fibronectin: G-I; 200x)

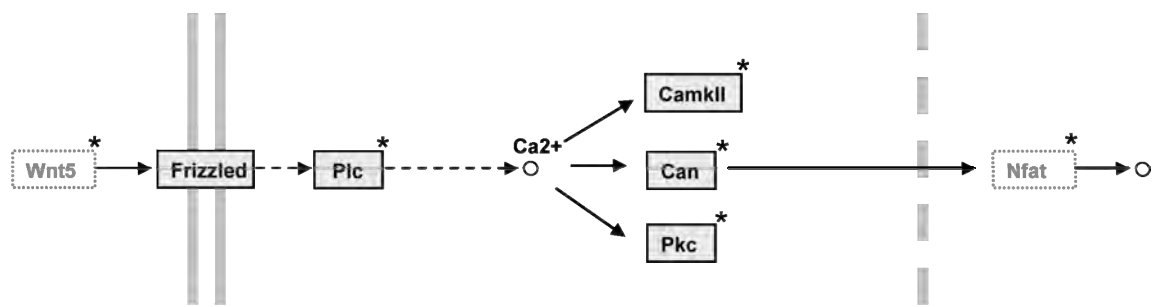
These results suggest that WNT regulation and activation of the canonical WNT pathway occurs during progression of CAD. Strong upregulation could be demonstrated for most pathway genes, including transcription factors and target genes. Furthermore, the canonical WNT pathway displays downregulation of at least one transcription factor and one target gene, similar to the observation made in the regulation of the hedgehog pathway.

5.1.3.2.2 Changes in the WNT-Ca²⁺ pathway

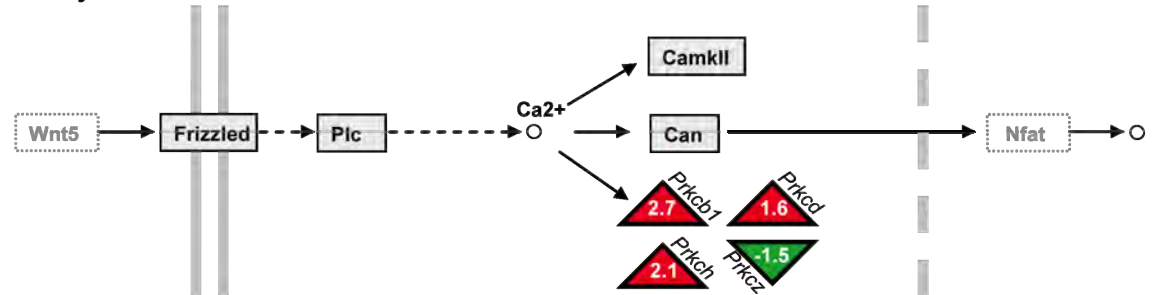
Following binding of WNTs to the frizzled receptors, WNT-Ca²⁺ pathway activation results in an increase in intracellular calcium. In contrast to the canonical WNT pathway, the downstream effects are beta-catenin independent. The WNT-Ca²⁺ pathway was shown to play a role in cell fate and morphogenesis [108].

The microarray analysis showed regulation of protein kinase C (*Pkc*), calcium/calmodulin-dependent protein kinase (*Camk*), protein phosphatase and phospholipase C (*Plc*), with progression of damage. All of these genes are associated with the WNT-Ca²⁺ pathway as displayed in figure 26. Supplementary table 4 summarizes microarray results and gene names/symbols, displayed in figure 26.

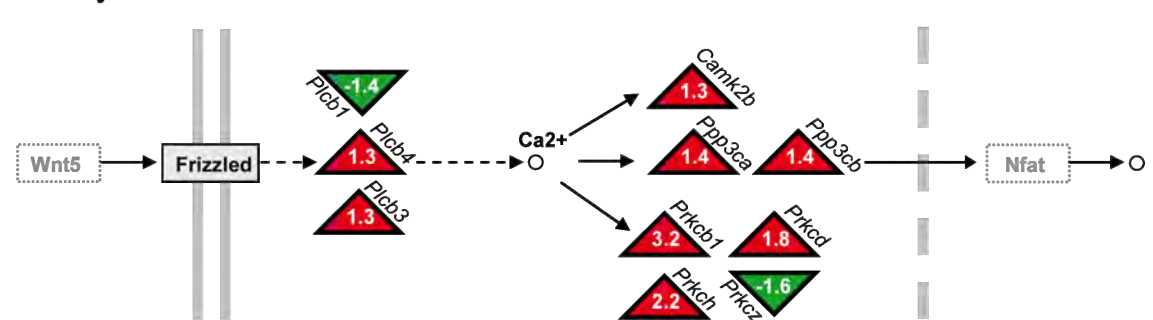
normal kidney



7 days



14 days



56 days

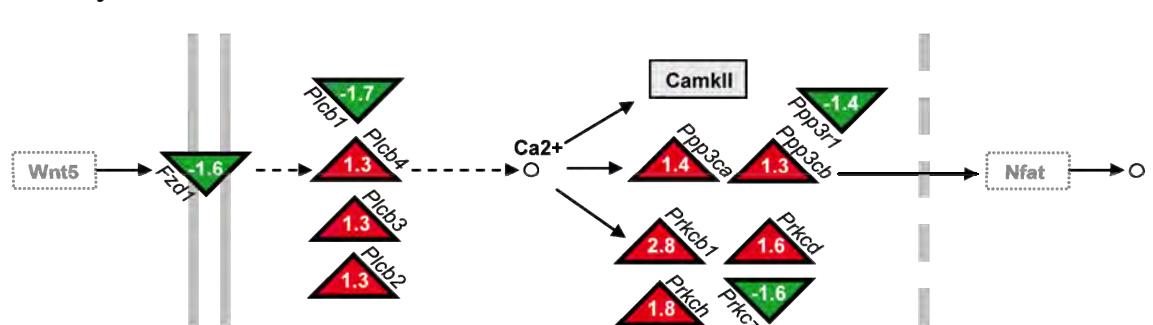


Fig. 26: Microarray analysis of the Wnt-Ca²⁺ pathway. The scheme is a modified version of the Wnt-Ca²⁺ pathway displayed on the KEGG database for rat (discussed in 1.1.3.4). A white box marks a gene not annotated to the microarray. Boxes with an asterisk indicate investigation of the gene by qPCR. The sketch is divided in four parts displaying time points 0 (normal kidney), 7, 14 and 56 days after transplantation. Triangles indicate the up or downregulation of genes in comparison to the control kidney. Numbers displayed are ChipInspector generated fold changes (native scale, not log transformed).

To study the activation status of this WNT pathway, mRNA expression of protein kinase C beta 1 and protein kinase C eta (*Prkcb1*, *Prkch*), calcium/calmodulin-dependent protein kinase II beta and delta (*Camk2b*, *Camk2d*), protein phosphatase 3, catalytic subunit, alpha isoform (*Ppp3ca*) and phospholipase C, beta 1 (*Plcb1*) was investigated by qPCR. Additionally, the expression of the transcription factors nuclear factor of activated T-cells 1, 2, 3, 4 and 5 (*Nfatc1_pred*, *Nfatc2*, *Nfatc3*, *Nfatc4* and *Nfat5*) was determined, see figure 27.

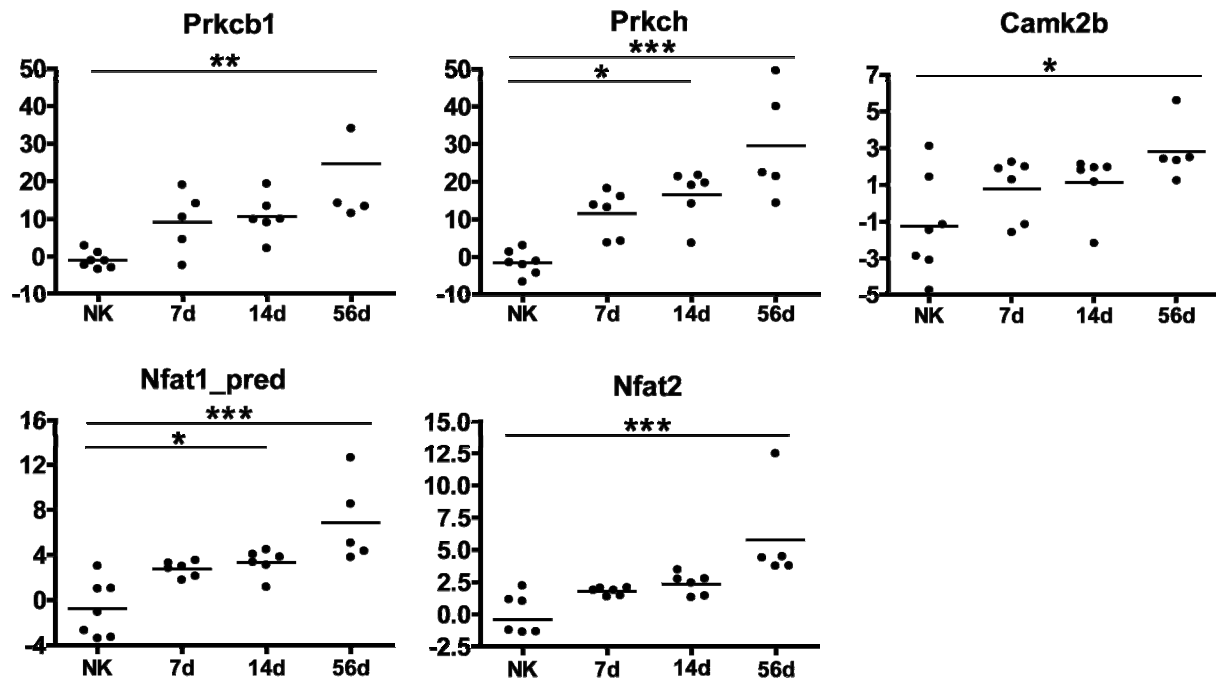


Fig. 27: Expression of Wnt-Ca²⁺ genes. Expression data of Wnt-Ca²⁺ genes after qPCR analysis. Data was generated employing qPCR, as described in 4.2.4 and displayed fold changes were calculated, as described in 4.2.5. For statistical analysis, the Kruskal-Wallis non-parametric test was applied to analyze the differences between the individual animal groups. Dunn's post test was applied for multiple testing. Significant differences are denoted by an asterisk. * denotes a statistically significant difference with a p value < 0.05, ** denote a statistically significant difference with a p value < 0.01 and *** denote a statistically significant difference with a p value < 0.0001.

Prkcb1 and *Prkch* were found to be strongly increased with CAD. *Ppp3ca*, *Plcb1* and *Camk2d* regulation at the mRNA level could not be confirmed, but upregulation of *Camk2b* was seen on day 56. While *Nfatc3*, *Nfatc4* and *Nfat5* showed no differential regulation, expression of *Nfatc1_pred* and *Nfatc2* was progressively increased over time. Supplementary tables 3 and 4 summarize the expression data from the microarrays, and genes verified by qPCR for Wnt canonical and Wnt-Ca²⁺ pathways.

5.1.3.2.3 The WNT planar cell polarity pathway

The Wnt planar cell polarity pathway is associated with cell movement, morphogenesis and metastasis [108]. As in the WNT-Ca²⁺ pathway, signals are transduced without the involvement of beta-catenin.

The regulation of genes linked to the WNT-associated planar cell polarity pathway, include mitogen-activated protein kinase 9 (*Mapk9*), Rho-associated, coiled-coil containing protein kinase 1 (*Rock1*), and dishevelled 3 predicted (*Dvl3_pred*). While each of these genes was found to be expressed in normal rat kidney, none showed regulation of basal mRNA expression in the context of progressive tissue damage in our model. In summary, these results demonstrate a reflection of inflammation and fibrosis in the transcription. No direct indication of the involvement of EMT during progression of CAD could be demonstrated in our animal model. Regarding the pathways analyzed, regulation of the HH and various WNT signal transduction pathways was identified.

5.2 13cRA is a master regulator of CAD induced transcriptomic alterations

5.2.1 Cluster analysis of overall gene expression

A direct effect of 13cRA treatment on the development of CAD in this model was previously demonstrated [5]. Animals treated with 13cRA showed excellent preservation of renal function and statistically significant reduced fibrosis. The transcriptomic profiling results of animals treated with 13cRA were compared and contrasted with the results of the placebo treated animals, as discussed in 5.1.

Interestingly, despite the histological findings showing good preservation of kidney morphology by 13cRA treatment, transcriptomic profiling of these largely “normal” tissues still showed a dramatic regulation of genes as compared to the control kidneys.

Employing hierarchical clustering with euclidean distance on all arrays, a grouping of the normal kidneys together with the treatment group on day 56 could be observed. The linkage of the normal kidney group with the 56 days treatment group is in contrast to the other time points and the 56 day placebo group, whose branching shows the largest distance, as seen in figure 28.

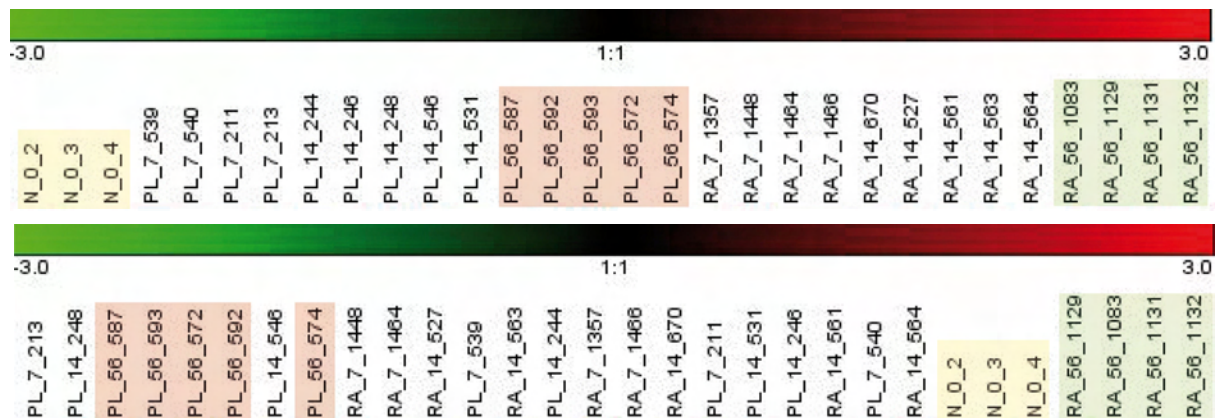


Fig. 28: Clustering of samples. Employing the Genesis program (see 4.1.5) to expression data, normalized by RMAExpress (see 4.1.4), the upper part of the figure displays unprocessed data and the order of all 30 arrays (upper row starting with N_0_3), as loaded into the program. After hierarchical clustering, the sequence of arrays changed. On the right side of the tree, the three normal kidney controls cluster in close proximity to the 56 day treatment group arrays.

Although the day 56 treatment group showed similarities to non-grafted organs, a lack of concordance of the gene-expression profiles is apparent. Differences in expression are expected, due to an infiltrate in the transplanted organs that is not present in the control kidneys. Nevertheless, the allografts from the treated animals appear to have an overall gene-expression profile resembling that of normal kidneys.

Figure 29 demonstrates in two exemplary clusters how well the control group and the 56 days treatment group are distinguishable from the other groups in their expression pattern.

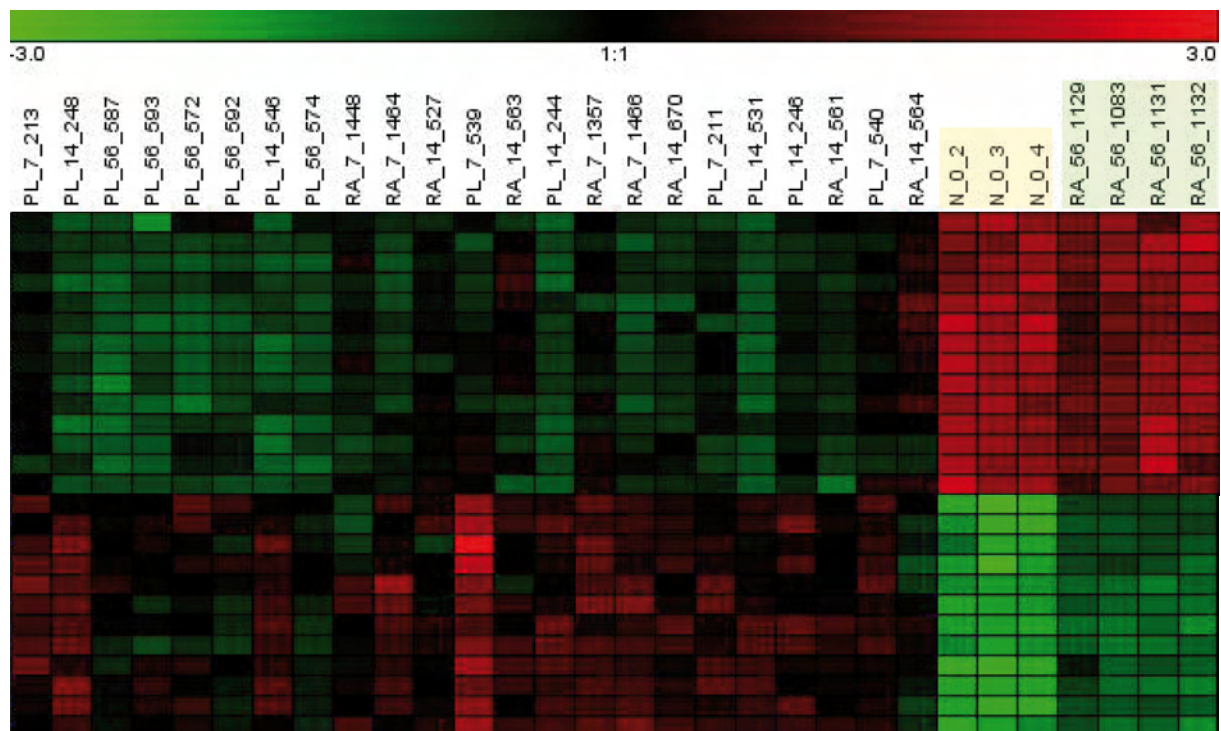


Fig. 29: Clustering of genes Employing the Genesis program (see 4.1.5) to expression data, normalized by RMAExpress (see 4.1.4). The diagram displays expression data after hierarchical clustering. Both exemplary clusters demonstrate uniform expression patterns of the normal, control kidney arrays and 56 days treatment arrays, in contrast to the other experimental groups. The red color indicates relative upregulation of genes and the green color indicates downregulation of genes, in comparison to the average expression level.

This observation reflects the changes observed in histology after treatment with 13cRA for the period of 56 days [5].

The goal of the second part of the study was to identify potential therapeutic mechanisms of 13cRA function by analysis of potential alterations in the regulatory pathways linked to disease progression identified earlier (5.1.3.1 and 5.1.3.2).

As in the first part of the study, the expression values of all time points of the treatment group were compared to the control kidneys serving as time point zero. For the second part of the analysis, these differences in gene expression were then compared, between the placebo and treatment group and contrasted for each time point.

5.2.2 The retinoic acid – HH – WNT axis

Retinoic acid (RA) has complex and pleiotropic functions during vertebrate development [116]. RA is recognized as an important signaling molecule, which can influence developmental pathways including hedgehog [116]. *In vitro* SHH and RA exert synergistic effects on the differentiation of mesenchymal stem cells [117].

A link between retinoids or members of the steroid family with the WNT pathway is well defined [111]. Nuclear receptors including PPAR γ and the RAR receptor bind beta-catenin and/or regulate activation of WNT target genes [118]. RAR can form a complex with beta-catenin competing with TCF/LEF1 for the binding to the DNA, thus suppressing its activity [111] (the inhibitory relation between the HH and WNT pathway has already been addressed in 5.1.3.1).

5.2.2.1 HH pathway

Genes associated with the HH pathway underwent changes during CAD (5.1.3.1) and treatment with 13cRA modulated expression of genes assigned to this pathway. The results from microarrays of the treatment group were integrated into the schematic diagram of the pathway and are displayed in supplementary figure 1. Comparing microarray results of the placebo and treatment groups revealed increased numbers of genes to be regulated in both groups. In addition, qPCR was performed for *Ptch1*, *Lrp2*, *Shh*, *Ihh*, *Dhh*, *Gli1*, *Bmp4*, *Bmp7* and *Sfrp1*.

The receptor *Ptch1* demonstrated an attenuated upregulation in the treatment group which was significant by day 56. The downregulation of the receptor *Lrp2* seen during CAD could be prevented by 13cRA treatment, returning its expression close to that seen in normal kidneys on day 56.

13cRA treatment resulted in modulation of mRNA expression of the HH ligands *Ihh*, *Shh* and *Dhh* on day 56. In the case of *Ihh*, the expression pattern was almost identical to that seen with *Lrp2* expression. The downregulation of *Ihh*, *Shh* and *Lrp2* observed during CAD could be prevented by 13cRA treatment. No effects were observed on the expression of the transcription factor *Gli1*. The downregulation of *Bmp4* and *Bmp7* was limited, and the difference between placebo and treatment group became significant on day 56 for *Bmp7*. The target gene *Sfrp1*, upregulated in the placebo group, was significantly downregulated during all time points in the treatment groups (figure 30). The 13cRA treatment was found to reverse many of the

progressive changes seen in the HH pathway during CAD and potentially to induce a switch in sub-pathway regulation.

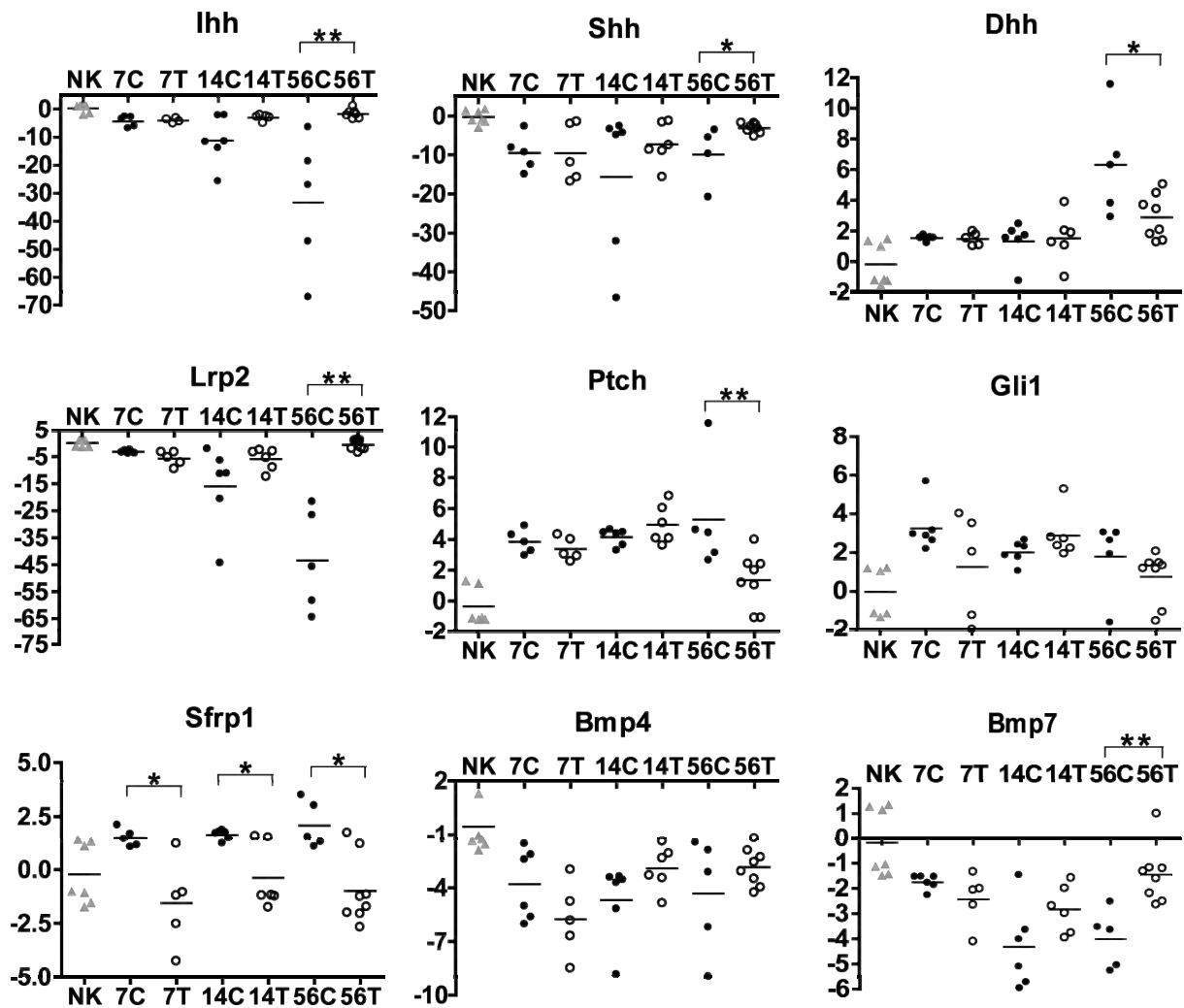


Fig. 30: Expression of hedgehog pathway genes. Through qPCR, expression of genes was assessed for all experimental groups. “C” denoting the Placebo/ untreated control group and “T” denoting the Treatment/13cRA group. Data was generated employing qPCR, as described in 4.2.4 and displayed fold changes were calculated, as described in 4.2.5. “Log” denotes a logarithmic scale, if not noted otherwise the scale is linear. For statistical analysis, the Mann-Whitney-U non-parametric test was applied to analyze the differences between the placebo and treatment groups, comparing individual time points. Significant differences are denoted by an asterisk. * denotes a statistically significant difference with a p value < 0.05, ** denote a statistically significant difference with a p value < 0.01.

5.2.2.2 WNT pathway

The WNTs are target genes of the HH pathway. Analysis of the CAD transcriptome showed the modulation of expression of seven Wnt genes in our rat model. Treatment with 13cRA exerted significant effects on the expression of *Wnt2b*, *Wnt3*, *Wnt6*, *Wnt8b* and *Wnt10a*. The downregulation of gene expression for *Wnt2b* and *Wnt10a* was attenuated. qPCR detected that downregulation of *Wnt7b* and *Wnt8b* was even more pronounced than in the placebo group. While *Wnt3* and *Wnt7a*

showed an attenuated upregulation, *Wnt6* demonstrated a significant upregulation on days 7 and 14 and a significant downregulation compared to the placebo group, see figure 31.

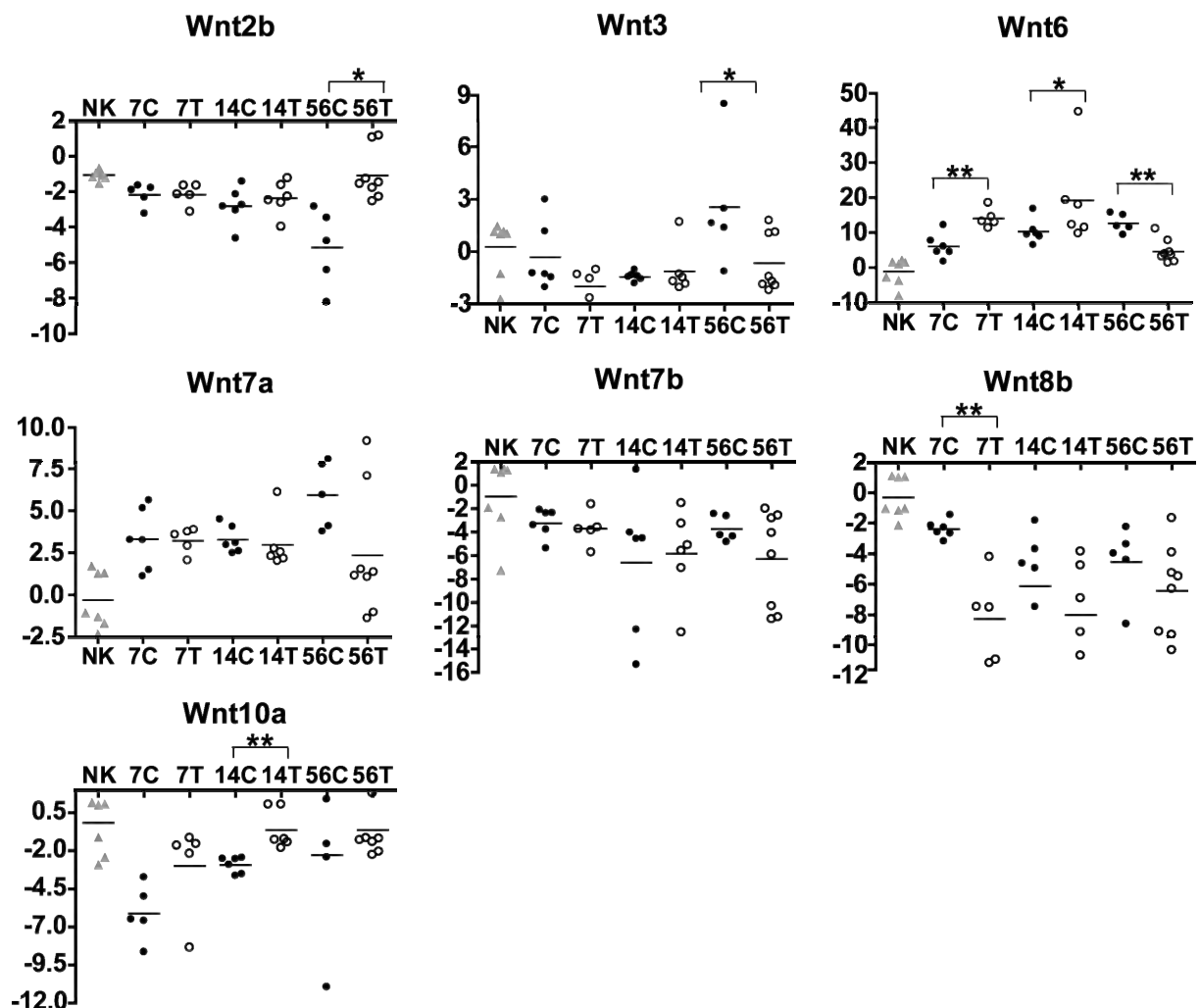


Fig. 31: Expression of Wnt ligands. Through qPCR, expression of genes was assessed for all experimental groups. “C” denoting the Placebo/ untreated control group and “T” denoting the Treatment/13cRA group. Data was generated employing qPCR, as described in 4.2.4 and displayed fold changes were calculated, as described in 4.2.5. “Log” denotes a logarithmic scale, if not noted otherwise the scale is linear. For statistical analysis, the Mann-Whitney-U non-parametric test was applied to analyze the differences between the placebo and treatment groups, comparing individual time points. Significant differences are denoted by an asterisk. * denotes a statistically significant difference with a p value < 0.05, ** denote a statistically significant difference with a p value < 0.01.

Along with disease progression, the microarray analysis of the WNT canonical pathway revealed regulation of increasing numbers of pathway genes, in both experimental groups. Supplementary table 3 and figure 2 summarize the results and display the microarray results for the WNT pathway, visually comparing data of the placebo group to data of the treatment group, for each time point of the analysis qPCR revealed a significant difference in the expression of most genes of this pathway investigated on day 56 after transplantation. The HH target gene and WNT

inhibitor *Sfrp1*, upregulated in the placebo group, was downregulated in the treatment group (5.2.2.1). 13cRA treatment had no effect on the inhibitor *Sfrp5* and caused a significant downregulation of the inhibitor *Dkk3*, which is also a WNT target gene. *Axin2* was downregulated compared to control kidney on days 7 and 56. The transcription factors *Lef1* and *Tcf1* showed attenuation of the up and downregulation, respectively seen in progressive CAD. All target genes, with the exception of *Bmp4*, showed significant differences in the mRNA levels between the placebo and the treatment group on day 56 after transplantation. On day 56 the previously elevated levels of *Cd44* and *Fn1* were found to return to control kidney levels, as did *Myc* levels. Interestingly, while the mRNA levels of *Nos2* and *Mmp7* remained elevated above normal kidney levels, they were significantly decreased on day 56, in comparison to the placebo group. Results are summarized in figure 32 and 33.

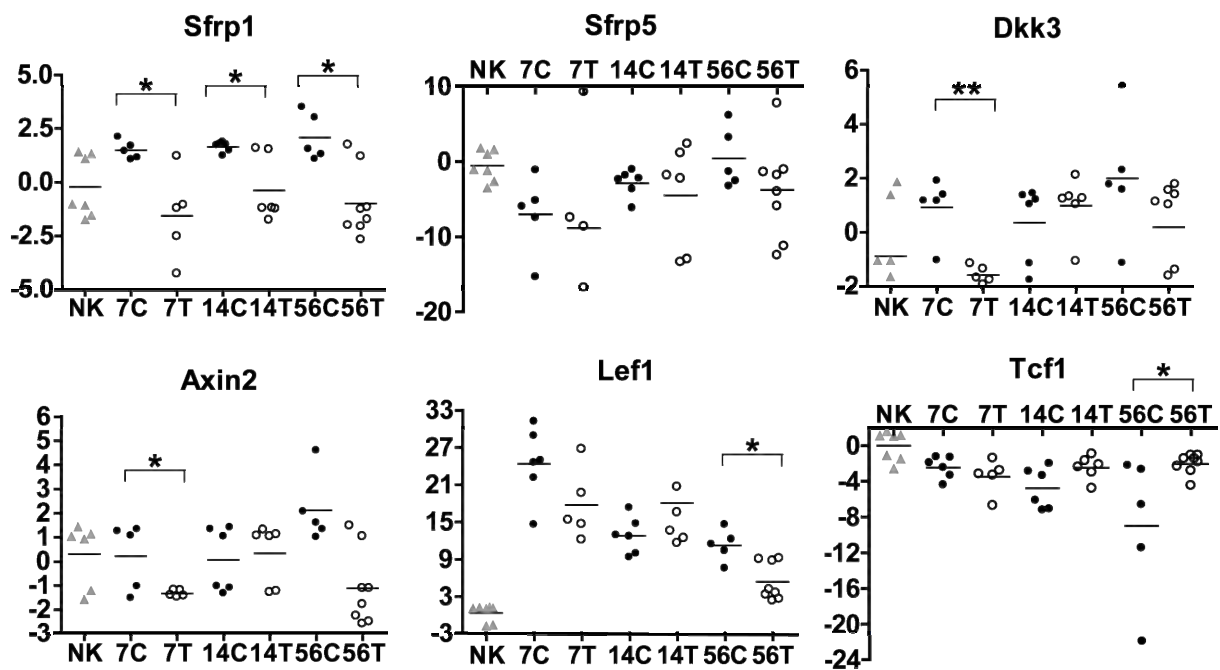


Fig. 32: Expression of Wnt canonical pathway genes. Through qPCR, expression of genes was assessed for all experimental groups. “C” denoting the Placebo/ untreated control group and “T” denoting the Treatment/13cRA group. Data was generated employing qPCR, as described in 4.2.4 and displayed fold changes were calculated, as described in 4.2.5. “Log” denotes a logarithmic scale, if not noted otherwise the scale is linear. For statistical analysis, the Mann-Whitney-U non-parametric test was applied to analyze the differences between the placebo and treatment groups, comparing individual time points. Significant differences are denoted by an asterisk. * denotes a statistically significant difference with a p value < 0.05, ** denote a statistically significant difference with a p value < 0.01.

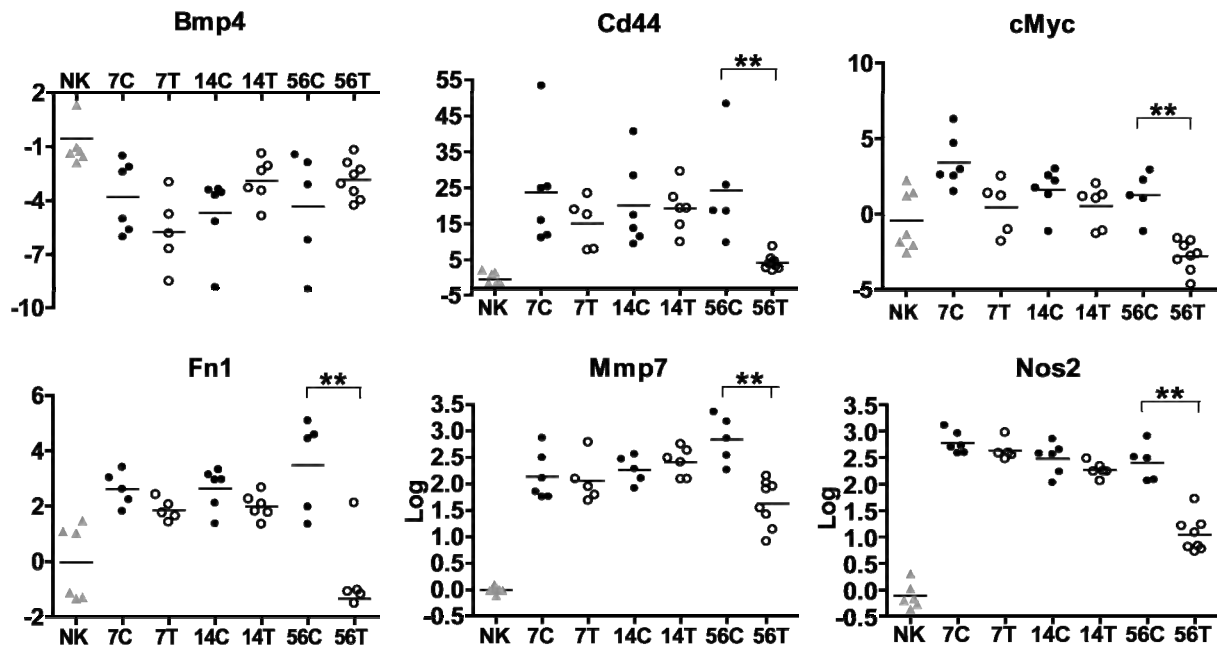


Fig. 33: Expression of Wnt canonical target genes. Through qPCR, expression of genes was assessed for all experimental groups. “C” denoting the Placebo/ untreated control group and “T” denoting the Treatment/13cRA group. Data was generated employing qPCR, as described in 4.2.4 and displayed fold changes were calculated, as described in 4.2.5. “Log” denotes a logarithmic scale, if not noted otherwise the scale is linear. For statistical analysis, the Mann-Whitney-U non-parametric test was applied to analyze the differences between the placebo and treatment groups, comparing individual time points. Significant differences are denoted by an asterisk. * denotes a statistically significant difference with a p value < 0.05, ** denote a statistically significant difference with a p value < 0.01.

In the WNT-Ca²⁺ pathway, alterations in gene expression could be observed by microarray analysis. Supplementary figure 3 summarizes alterations observed over time, and compares the microarray results of the placebo and to that of the treatment groups.

By qPCR analysis, no effect was observed on the expression of *Camk2b*, following 13cRA treatment. However, all other genes investigated in this context showed reduced upregulation on day 56 through treatment. Differences in expression levels were found to be significant for *Prkcb1*, *Prkch1*, *Nfat1_pred* and *Nfat2*, as summarized in figure 34. No differential gene regulation was observed either with or without 13cRA treatment in the WNT-PCP pathway (data not shown).

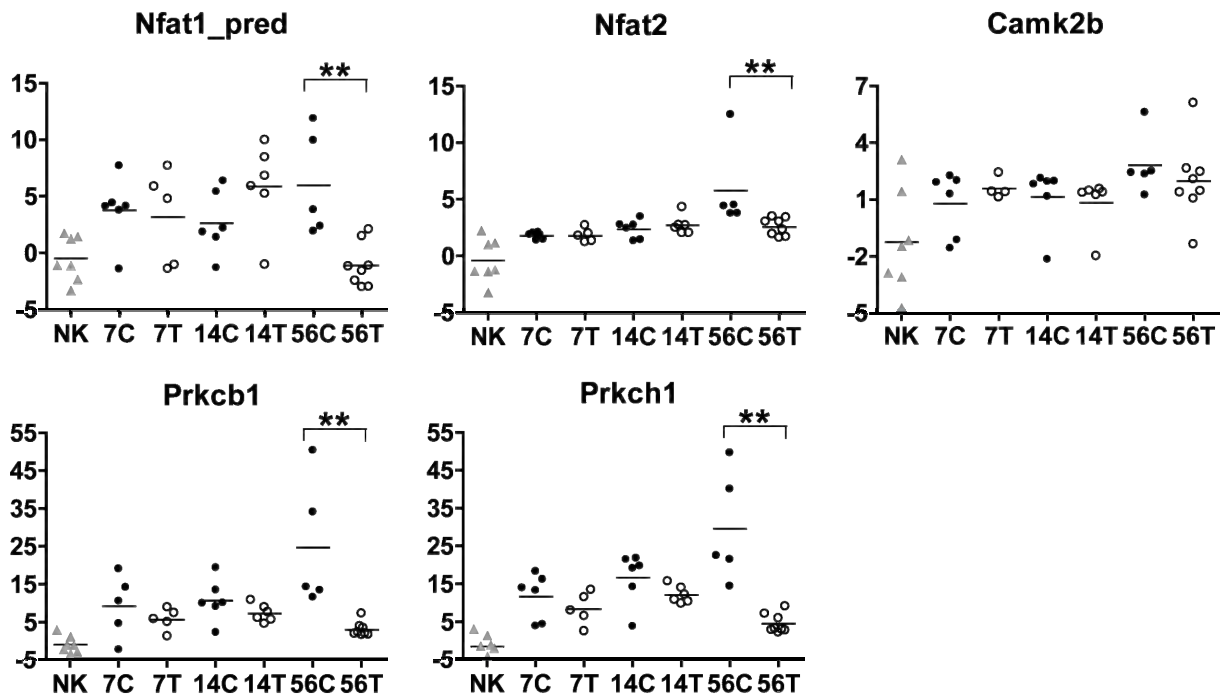


Fig. 34: Expression of Wnt-Ca²⁺ pathway genes. Through qPCR, expression of genes was assessed for all experimental groups. “C” denoting the Placebo/ untreated control group and “T” denoting the Treatment/13cRA group. Data was generated employing qPCR, as described in 4.2.4 and displayed fold changes were calculated, as described in 4.2.5. “Log” denotes a logarithmic scale, if not noted otherwise the scale is linear. For statistical analysis, the Mann-Whitney-U non-parametric test was applied to analyze the differences between the placebo and treatment groups, comparing individual time points. Significant differences are denoted by an asterisk. * denotes a statistically significant difference with a p value < 0.05, ** denote a statistically significant difference with a p value < 0.01.

Taken together, the results suggest that 13cRA may act as a regulator of HH and WNT signaling and that these effects may help explain the therapeutic effects seen during renal allograft damage.

In addition to the specific effects on these pathways, potential effects of 13cRA treatment, on the general immune and micro-milieu within the treated kidneys, were further investigated.

5.2.3 13cRA influences the proinflammatory and profibrotic milieu

Retinoids can have anti-inflammatory as well as anti-proliferative effects in diverse biologic systems [52]. The oral treatment of the rats with 13cRA within this study would have systemic effects, as well as local effects. Alterations in the inflammatory and profibrotic milieu observed in the kidneys after transplantation could help limit damage and preserve organ structure and function. Treatment with 13cRA decreased mRNA levels of almost all the inflammatory genes investigated. With the exception of Jak2, 13cRA had a significant effect on the expression of all genes

analyzed, during at least one point. Figures 35 and 36 summarize the results of the effect of 13cRA on inflammation-associated genes.

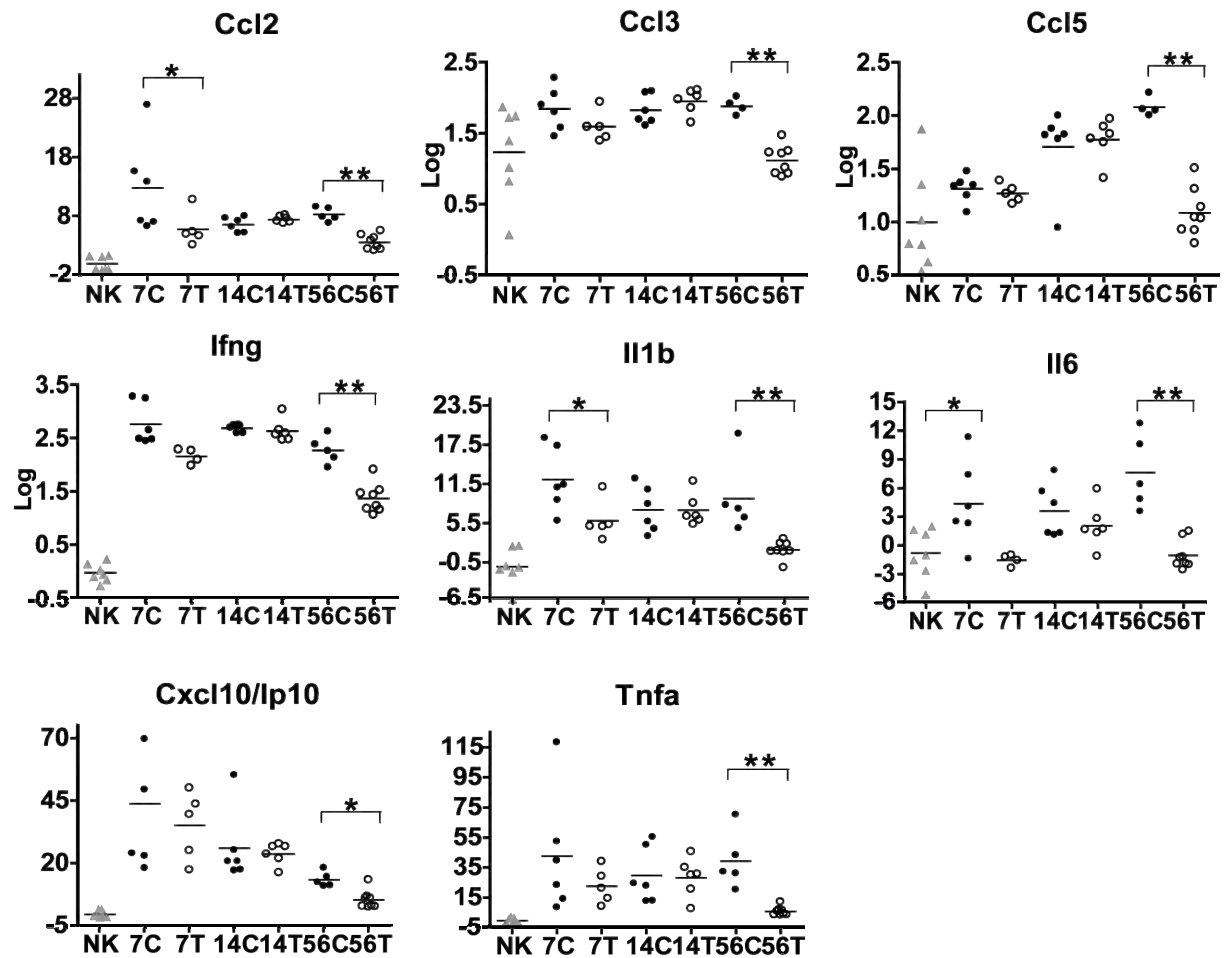


Fig. 35: Expression of inflammation associated genes. Through qPCR, expression of genes was assessed for all experimental groups. “C” denoting the Placebo/ untreated control group and “T” denoting the Treatment/13cRA group. Data was generated employing qPCR, as described in 4.2.4 and displayed fold changes were calculated, as described in 4.2.5. “Log” denotes a logarithmic scale, if not noted otherwise the scale is linear. For statistical analysis, the Mann-Whitney-U non-parametric test was applied to analyze the differences between the placebo and treatment groups, comparing individual time points. Significant differences are denoted by an asterisk. * denotes a statistically significant difference with a p value < 0.05, ** denote a statistically significant difference with a p value < 0.01.

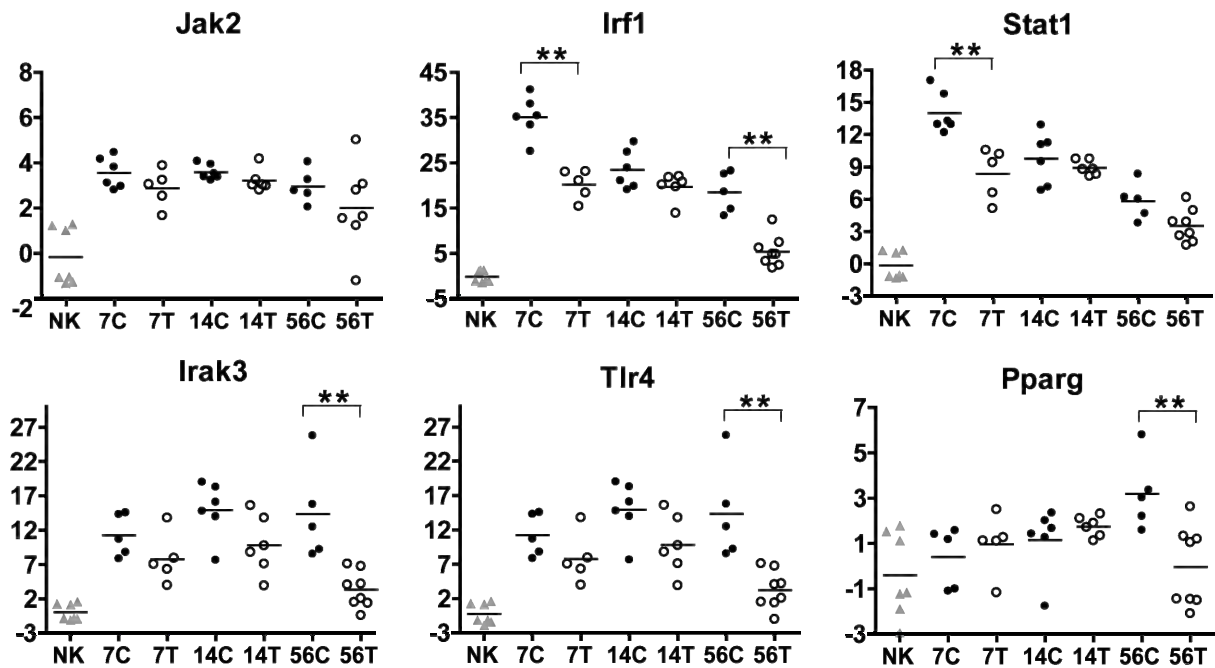


Fig. 36: Expression of inflammatory signal transduction associated genes. Through qPCR, expression of genes was assessed for all experimental groups. “C” denoting the Placebo/ untreated control group and “T” denoting the Treatment/13cRA group. Data was generated employing qPCR, as described in 4.2.4 and displayed fold changes were calculated, as described in 4.2.5. “Log” denotes a logarithmic scale, if not noted otherwise the scale is linear. For statistical analysis, the Mann-Whitney-U non-parametric test was applied to analyze the differences between the placebo and treatment groups, comparing individual time points. Significant differences are denoted by an asterisk. * denotes a statistically significant difference with a p value < 0.05, ** denote a statistically significant difference with a p value < 0.01.

A potential regulatory role of retinoic acid in immune tolerance and development of regulatory T cells has been proposed [119-121]. The expression of marker genes associated with different T cell populations was investigated to analyze possible effects of 13cRA treatment on the T cell and immune milieu. These markers included *Foxp3*, *Il10*, interleukin 4 receptor (*Il4r*), interleukin 6 receptor (*Il6r*), *Il17*, *Il21* and interleukin 23 (*Il23*). Neither during disease progression, nor in the treatment groups was a change in expression of *IL23* or *IL17* detectable (data not shown). On day 7, the *Foxp3* expression level of the placebo group equaled that of the treatment group. On day 14, *Foxp3* was more upregulated in the treatment group and on day 56 it was downregulated. *Il10* and *Tgfb1* were upregulated. *Il21* was most strongly upregulated in the non-treated group on day 7. The *Il6r* and its ligand *Il6* were upregulated in the placebo group. This upregulation was significantly reduced for *Il6* by 13cRA treatment on day 56. *Il4r* showed only minor upregulation at all time points - with no significant differences in expression seen following treatment. This suggests that even though a milieu that could stimulate the generation of Th17 cells is present in the kidney, no upregulation of *Il17* on the gene expression level was observed. The

presence of cells expressing *Foxp3*, in the kidneys investigated was observed. A stimulatory effect of retinoic acid on the *Foxp3* expression could not be demonstrated. Results are summarized in figure 37.

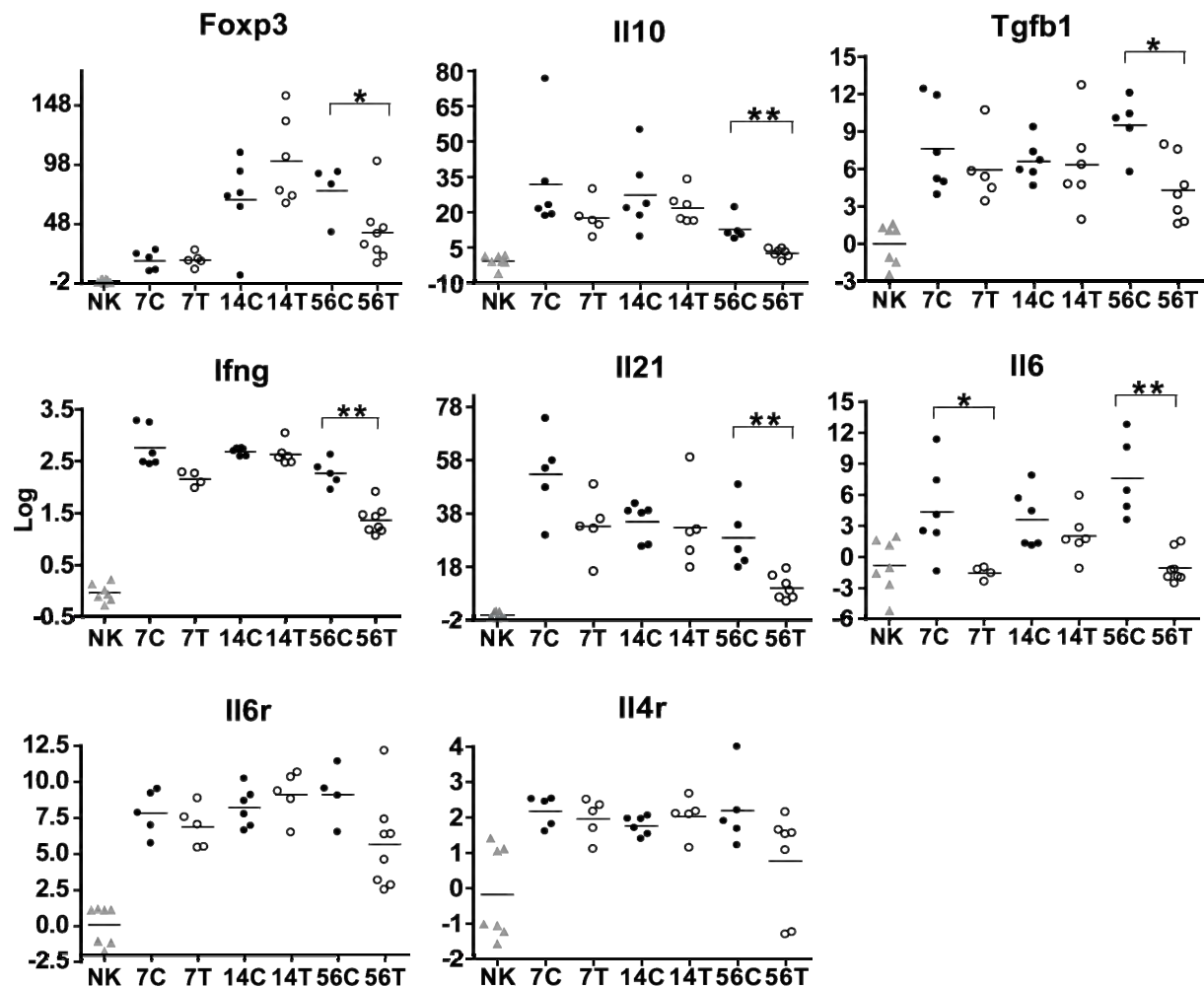


Fig. 37: Expression of genes associated with a T cell development. Through qPCR, expression of genes was assessed for all experimental groups. “C” denoting the Placebo/ untreated control group and “T” denoting the Treatment/13cRA group. Data was generated employing qPCR, as described in 4.2.4 and displayed fold changes were calculated, as described in 4.2.5. “Log” denotes a logarithmic scale, if not noted otherwise the scale is linear. For statistical analysis, the Mann-Whitney-U non-parametric test was applied to analyze the differences between the placebo and treatment groups, comparing individual time points. Significant differences are denoted by an asterisk. * denotes a statistically significant difference with a p value < 0.05, ** denote a statistically significant difference with a p value < 0.01.

Morphometric analysis of kidneys showed inhibition of subendothelial fibrosis in 13cRA treated animals [5]. This was reflected in the transcriptomic studies where 13cRA treated animals showed reduced upregulation of markers of fibroblast activation including *Vim*, *Actg2* and *Fsp1/S100a4*. Similar effects were observed for *Col1a1* and *Col3a1* following treatment (figure 38).

The effect of 13cRA treatment was significant with respect to elevated *Tgfb1* levels on day 56.

The TGFB1 target gene *Serpine1/Pai*, which was increased at late stages of CAD, was not increased following treatment, suggesting a direct effect on the TGFB1 pathway. The TGFB1 antagonist *Bmp7* showed less pronounced downregulation during treatment as compared to the placebo-treated animals.

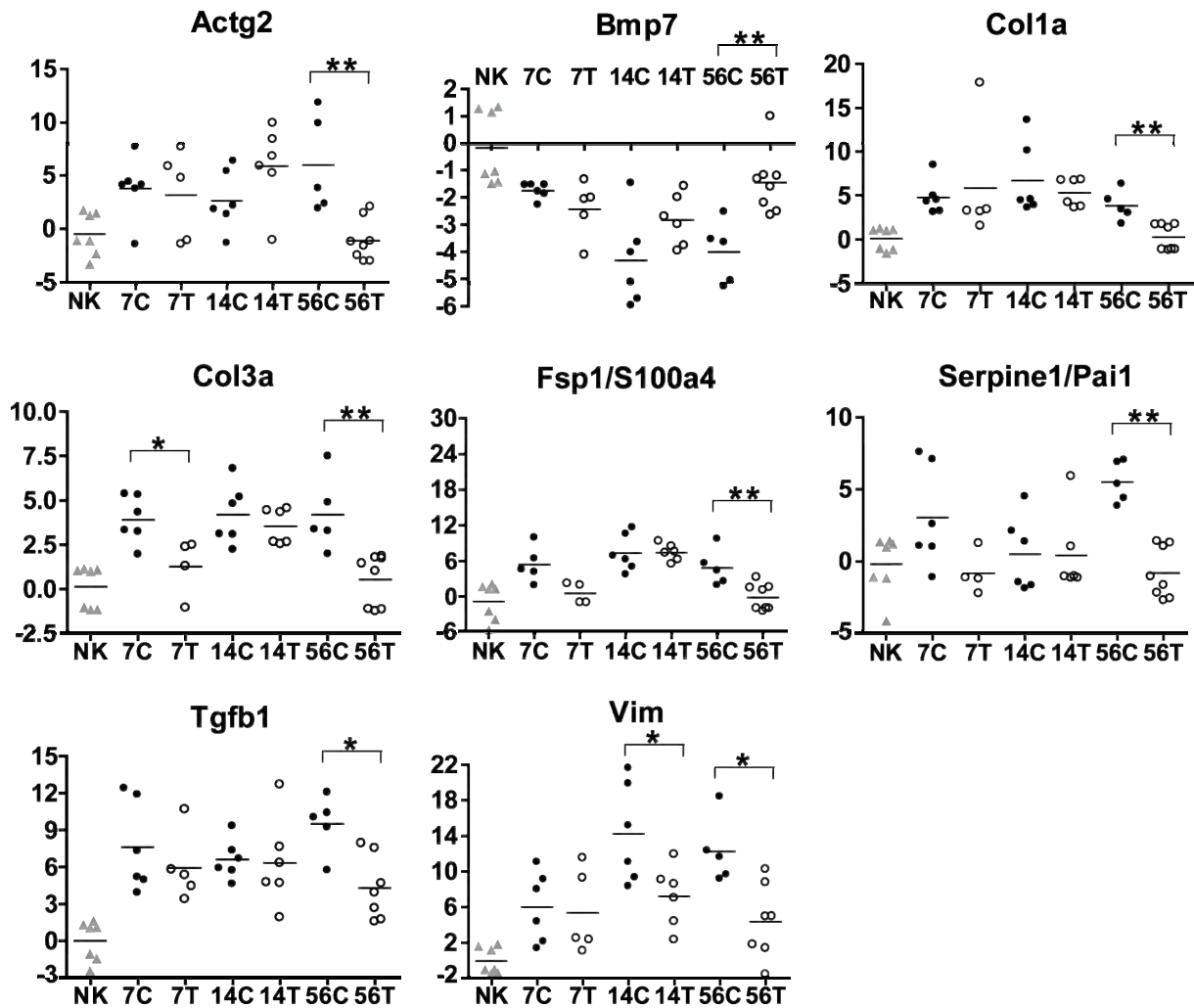


Fig. 38: Expression of marker genes of fibrosis. Through qPCR, expression of genes was assessed for all experimental groups. “C” denoting the Placebo/ untreated control group and “T” denoting the Treatment/13cRA group. Data was generated employing qPCR, as described in 4.2.4 and displayed fold changes were calculated, as described in 4.2.5. “Log” denotes a logarithmic scale, if not noted otherwise the scale is linear. For statistical analysis, the Mann-Whitney-U non-parametric test was applied to analyze the differences between the placebo and treatment groups, comparing individual time points. Significant differences are denoted by an asterisk. * denotes a statistically significant difference with a p value < 0.05, ** denote a statistically significant difference with a p value < 0.01.

Figure 40 summarizes the alterations in gene expression observed during disease progression or after 13cRA treatment focusing on the roles of the HH and the WNT canonical pathways. Transcriptomic profiling revealed changes in gene expression levels of genes associated with inflammation and fibrosis during progression of CAD.

5.2.4 Working mechanism of 13cRA at the promoter level

5.2.4.1 13cRA mediates inhibition of TNFA stimulated *CCL5* promoter activation

The potential working mechanism of 13cRA was previously investigated at the promoter level. TNFA-induced activation of the exemplary gene - *CCL5*, is inhibited by 13cRA. Promoter analysis suggested that the effect of 13cRA did not appear to be mediated through direct binding of RXR/RAR complexes to the *CCL5* promoter, since deletion of the relevant consensus sequences did not influence 13cRA suppression of *CCL5* promoter activity [5]. The results suggested an indirect effect of 13cRA, potentially acting through other transcriptional regulators. To this end, modulation of binding of the nuclear corepressor (NCOR) to the *CCL5* promoter was investigated as a potential mode of action of 13cRA.

5.2.4.2 Nuclear corepressor (NCOR) binding to promoters

Chromatin immunoprecipitation (ChIP) experiments were performed to investigate whether 13cRA utilizes the same mechanism for the transrepression of *CCL5* promoter activation as identified by Pascual et al. [59] for a PPARG-dependent repression of the *Nos2* promoter. If this mechanism was also active in the control of *CCL5* transcription by 13cRA, then binding of the NCOR to the *CCL5* promoter under non- stimulated or transrepressed conditions should be observed.

5.2.4.2.1 Establishing the ChIP

Chromatin immunoprecipitation was tested and a protocol established in our lab. Formaldehyde fixation is critical for later detection of protein binding sites on the chromatin. Formaldehyde concentrations in the range of 0.5% to 2% formaldehyde have been tested. Fixation using 0.5% led to problems with immune precipitation, the fixation with 2% formaldehyde was found to inhibit the lysis of cells and nuclei, and thereby to limit access of the antibody to the target proteins. A concentration of 1% appeared to be appropriate and was employed for subsequent experiments. After fixation, shearing of the chromatin is the next step of the protocol which is a critical

issue for the specificity of these experiments. Shearing conditions were found to depend on the volume of the sample, the origin of the chromatin and the total amount of chromatin. Extended sonication resulted in foaming, overheating and denaturation of the chromatin, and therefore loss of the sample. Insufficient shearing produced chromatin fragments that were too large for the examined DNA binding protein to be assigned to a specific promoter region. Sonication of chromatin was optimized to render an average fragment length of 500 bp [122], within the range of 200 bp to 1000 bp (data not shown). For antibodies, it had to be ensured that they could recognize the respective protein following denaturation with formaldehyde. To establish the protocol, test-samples (K4IM, HUT78 - a T-cell tumor celline, and YT - a natural killer cell line [123], data not shown) in combination with an antibody that detects active chromatin (acetylated Histone H3 (Lys9/18)) and primers for the glyceraldehyde-3-phosphate dehydrogenase (GAPDH) promoter were used. The specific enrichment of active chromatin is measured in a PCR and validated against the unspecific background. The different controls performed define for DNA contamination of the reagents (Mock control), unspecific reactions of the StaphA cells (no AB control), and the specificity of the antibody (isotype control). The parameters were later adapted for the NCOR antibody. For precipitation, different methods were tested and evaluated based on binding capacity, visibility during washing steps, and cost. Precipitation systems tested included agarose beads, sepharose beads, paramagnetic beads and Staphylococcus aureus cells. Agarose, sepharose or paramagnetic beads were eliminated based on their poor binding capacity and visibility problems. Protein A-bearing Staphylococcus aureus cells were found to be best-working approach for the experiments. StaphA cells are commercially available, show high affinity to IgG, are visible during pipetting, and allow stringent washing steps. Visibility is very helpful for the complete removal of wash buffers without aspirating the samples. DNA purification using commercially available columns was tested, but due to the minimal amount of precipitated chromatin and its short length the approach was not successful. DNA was extracted using phenol-chloroform protocols and glycogen as inert carrier, to minimize loss of sample. Due to low amounts of starting material the total amount of precipitated chromatin could be expected to be close to detection limits. Different amounts of eluted DNA were tested as PCR inputs. Against prior expectations, high PCR inputs contained, despite extended washing and extracting steps, contaminants interfering with the enzymatic

reaction resulted in poor efficiency of PCR reactions. To minimize inhibitory effects the sample input size for the PCR was reduced to the minimum level so that it could be reliably pipetted. For PCR, 35 amplification cycles were necessary to sufficiently amplify the enriched DNA in the sample. We came to the conclusion that the ChIP method is only advisable to use if the proper controls are employed and the question asked can explicitly be answered by this method. The established protocol was successfully employed to investigate the binding of the transcription factor SP1 to the CCL5 promoter in a natural killer cell line as described in [123].

5.2.4.2.2 NCOR binding to the CCL5 promoter

Based on our hypothesis, it was proposed that the NCOR could be bound to the CCL5 promoter, as long as the cells were not treated with an activating stimulus. With activation, the inhibitory complex would be replaced, allowing the formation of a transcriptional activation complex. This hypothesis, extended to the “indirect” effect of 13cRA previously demonstrated, was evaluated using immortalized human dermal fibroblast cells (K4IM) under different stimulation conditions for NCOR modulation by 13cRA, as described in 4.4.2. The method allowed preliminary exploration of the hypothesis. Based on the limited experiments that could be conducted in this regard, no direct binding of NCOR to the inactive CCL5 promoter could be demonstrated. Thus, we were unable to generate data to support the hypothesis. This hypothesis extended to the “indirect” effect of 13cRA previously demonstrated was evaluated using immortalized human dermal fibroblast cells (K4IM) under different stimulation conditions for NCOR modulation by 13cRA, as described in 4.4.2. The method allowed preliminary exploration of the hypothesis. Based on the limited experiments that could be conducted in this regard, no direct binding of NCOR to the inactive CCL5 promoter could be demonstrated. Thus, we were unable to generate data to support the hypothesis.

While the mock (see supplementary figure 4) and the isotype controls (figure 39 and supplementary figure 4) demonstrated no signals after a PCR with 35 cycles, employing the *CCL5* primers, a signal was detected in the no-antibody control suggesting potential contamination.

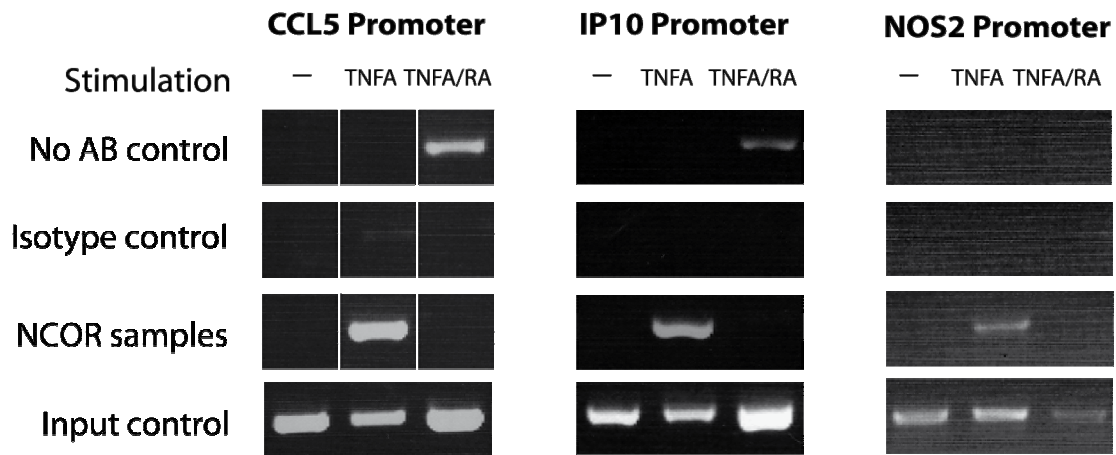


Fig. 39: Chromatin immunoprecipitation results for CCL5, CXCL10/IP10 and NOS2. ChIP was performed as described in 4.4.4. Using 1×10^6 K4IM cells per condition, unstimulated, TNFA and TNFA/RA treated cells were precipitated using an NCOR antibody. After chromatin purification PCR was performed using primer pairs amplifying the CCL5, IP10 and NOS2 promoter. This figure displays a compilation of parts of the original agarose gels (supplementary figure 4) of the ChIP experiment discussed. Due to problems with the colour assignment after scanning the original photographs the colour information has been recalculated to a grey scale. CCL5 results are represented as composite, since the lanes of the original gel were in a different order than presented here (supplementary figure 4).

In addition, a strong signal was found only after an inflammatory stimulus was applied, and no signal was seen with 13cRA-treatment. To exclude that this contradictory effect was solely *CCL5* dependent, we further investigated the promoters of two additional pro-inflammatory genes. Microarray and qPCR experiments demonstrated upregulation of *CXCL10/IP10* and the *NOS2* promoter after transplantation. Treatment with 13cRA decreased the expression at the mRNA level. Primers for both promoters were designed and evaluated in ChIP. With the exception of the signal in the isotype control of the *NOS2* PCR, the results for the *CXCL10/IP10* and *NOS2* primers showed the same effect, as observed at the *CCL5* promoter (figure 39). Based on these contrary results it was not possible to draw a definitive conclusion regarding the transrepression mechanism of the 13cRA in our cell system. However, the preliminary results in these studies (even in the absence of adequate controls) could not support the original hypothesis.

6 Discussion

The changes that characterize CAD include inflammation, interstitial fibrosis, tubular atrophy, glomerular sclerosis with basement membrane abnormalities, and chronic lesions. Histological examination demonstrated an accumulation of damage and subsequent deterioration of organ function in the transplanted rat kidneys that mirrored, to a significant degree, that which was seen in human disease [5, 47]. The goal of this study was to correlate alterations, observed in histology during the rejection process, with alterations in the transcriptome and select regulatory pathways.

Orally applied 13cRA treatment starting just after organ transplantation had been previously shown to limit damage and preserve organ function [5]. By the end of the study (56 days after transplantation), the morphometry of the treated kidneys resembled that of the non-transplanted control kidneys. The second goal of this study was to characterize transcriptomic alterations in relevant regulatory pathways, induced by the treatment with 13cRA.

6.1 *Transcriptomic analysis*

Microarray analysis showed over one thousand different genes to be differentially regulated between the mRNA of the control kidneys and the mRNA of the transplanted kidneys on time points 7 days, 14 days, and 56 days after transplantation. To evaluate the transcriptome of the experimental kidneys, three major problems linked to the general method had to be considered.

First, changes on the RNA level may not be reflected in changes on the protein level. To help address this protein verification was performed.

Second, microarrays are tools for large scale investigations of gene expression, but the output of the analysis has to be regarded as a ratio between a control and a treatment group. Statistical parameters and evaluation of the output is necessary to define thresholds of regulation. The calculation of thresholds is also relative to the total number of genes present on the array, and to the number of differentially regulated genes. Therefore, depending on the number of genes observed to be regulated, the thresholds of significance will adjust. Hence, the comparison of two groups, with differing numbers of regulated genes is based on a different statistic, and therefore can be problematic. This problem could be limited by regarding the

microarray analysis as only a preliminary indicator of regulation, where important genes were later verified by qPCR before conclusions are drawn.

Third, the microarray design only allowed evaluation of part of the transcriptome. The U34A microarray used here has 8000 annotated genes on the array. Hence, data is parital e.g. neglecting some genes and splice variants. It was necessary to investigate missing genes directly by qPCR to complete the picture. New generations of whole-genome arrays will facilitate further investigation of signal transduction. Most of the pathways identified to be dysregulated in this study did not demonstrate a significant differential regulation after the microarray analysis, due in part to incomplete annotation of pathway genes.

One further challenge is the nature of the samples investigated. Samples were generated from whole kidney lysates. Normal kidneys consist of a variety of different cell types. In addition to the diverse cell types, a varying degree of infiltrating immune cells, in accordance to immune responses within the allograft, defines the total mRNA pool which is being analyzed. The origin of a specific mRNA could not be easily determined by this study. Some genes are uniquely transcribed by special cell types allowing for an estimation of relative numbers of these cells within different samples. By epigenetic analyses, it is also possible to differentiate the source of a specific mRNA. Through monitoring the epigenetic status of a control sample it becomes possible to evaluate whether a specific mRNA is really regulated at the transcriptional level, or if the number of cells producing this mRNA varies. For this kind of analysis genomic DNA material is required. Visualizing RNA co-localization is a method that makes use of frozen or paraffin embedded sections. In this approach, through *in situ* hybridization, an RNA signal can be multiplied and detected by fluorescence microscopy. Using different dyes for the different RNAs, it would be possible to identify possible co-localization of RNAs, which would give further insight into possible co-regulation. Unfortunately, these methods could not be used in this study, since they first had to be established in the rat, as to the availability of genomic sequences and hybridization probes.

Employing qPCR was an important tool to investigate alterations in mRNA levels of genes not annotated to the microarray. qPCR allowed a verification of microarray results. Based in large part, on the method used for analysis of the array data (ChipInspector), a good correlation between microarray and qPCR data was observed, in general.

6.2 Alterations in gene expression during disease progression

An upregulation of inflammatory effector molecules and signal transducers in combination with the infiltration of the organ by leukocytes were used to demonstrate an inflammatory milieu within the test kidneys. Inflammation that occurs in the acute phase of an immune response can often heal with complete functional and morphologic restitution. In smoldering, chronic active inflammation, not only “classical” inflammatory cell elements, but also activation of endothelial cells, epithelial cells or fibroblasts has been reported [124]. A role for inflammation in developing fibrosis and tissue remodeling had been well established [124].

CAD is associated with increased TGFB1 expression [125]. In the transplanted kidneys of the placebo group, upregulation of profibrotic mediators, such as *Tgfb1* and *Serpine1/Pai-1* was observed. The immunosuppressive effects of TGFB1 are contradictory to its proinflammatory role in tissues [125]. Consistent with its function in wound healing and repair, it is chemoattractive for leukocytes [126]. A correlation between intragraft TGFB1 expression and interstitial fibrosis was demonstrated in human renal allografts [126]. In human fibroblasts of the lung, TGFB1 was identified as a strong transcriptional activator of plasminogen activator inhibitor 1 (PAI-1) [127]. The deposition of *Serpine1/Pai1* is associated with ECM expansion and fibrosis [84], and could be observed on day 56 in animals of the placebo group. Regulation of *Serpine1/Pai1* is dependent on the expression of inflammatory cytokines, such as *IL1b*, *Il6*, *Tnfa* and *Ifng*, all of which were observed to be upregulated in our model. BMP7, a member of the TGFB family, can suppress the expression of many proinflammatory cytokines and growth factors and is also a biomarker for progressive chronic renal disease [85, 128, 129]. BMP7 is thought to act as a counter regulator of TGFB1 and therefore, *Bmp7* downregulation can be interpreted to enhance progression of CAD in this model. Tyler et al. showed in an *in vitro* study that the addition of BMP7 to TGFB-stimulated cells reduced *Fsp1/S1004a* expression, a marker of fibroblast activation [85]. The *Bmps* are downstream target genes of the WNT canonical pathway, demonstrating potential crosstalk between the TGFB and WNT pathways during CAD. The differentially regulated markers of fibrosis, verified by qPCR, are summarized in table 2.

Table 2. Summary of qPCR results of inflammation and fibrosis associated genes

Gene ID	Gene Symbol	CAD Regulation	Significant effect of treatment
Inflammation associated genes			
24770	Ccl2	↑	+
25542	Ccl3	↑	+
81780	Ccl5	↑	+
245920	Cxcl10/lp10	↑	+
25712	Ifng	↑	+
24494	Il1b	↑	+
24498	Il6	↑	+
24508	Irf1	↑	+
314870	Irak3	↑	+
24514	Jak2	↑	-
25664	Pparg	↑	+
25124	Stat1	↑	+
24835	Tnfa	↑	+
29260	Tlr4	↑	+
Fibrosis related genes			
25365	Actg2	↑	+
85272	Bmp7	↓	+
29393	Col1a1	↑	+
84032	Col3a1	↑	+
24615	Fsp1/S100a4	↑	+
59086	Tgfb1	↑	+
24617	Pai-1	↑	+
81818	Vim	↑	+

Table 2: Arrows indicate up or downregulation of gene expression in relation to the normal control kidneys. Further, statistically significant effects of the treatment, on the expression of genes are denoted.

Fibrosis in basal membranes and interstitial tissues results from an excessive synthesis of interstitial collagens, such as type I and III [81, 84]. Epithelial to mesenchymal transition (EMT) has been proposed to underlie renal fibrosis [130]. EMT is linked to the assembly of nuclear beta-catenin and activation of transcription factors such as SNAIL (*Snai1* in the rat), which are necessary to downregulate the expression of E-cadherin and thereby moderate cell motility. While stabilization of protein expression and nuclear enrichment of beta-catenin could be determined in our study by immunohistochemistry, no changes were observed in the expression of beta-catenin at the mRNA level. Importantly, we did not detect the upregulation of *Snai1* or the downregulation of E-cadherin expression, thought to be mandatory for EMT. In this regard, evidence of “complete” EMT could not be detected.

Progressive upregulation of *Fsp1/S100a4* was found in the model. The expression of this gene has been implicated as a marker for the generation of fibroblasts through

EMT [80, 131]. However, the notion that FSP1/S100A4 is specific for fibroblasts has been put to question by the observation that FSP1/S100A4 is also expressed by lymphocytes, macrophages and granulocytes [132-135]. Indeed, Le Hir et al. demonstrated that a large fraction of FSP1/S100A4 positive cells in models of peritubular inflammation were leukocytes [132]. Thus, the increase in *Fsp1/S100a4* mRNA could be explained, to a significant degree, by the mononuclear infiltrate present in our model. The same may apply for the “mesenchymal” marker vimentin, whose upregulation is accepted as an indication of the change of an epithelial phenotype towards a mesenchymal or fibroblastoid phenotype. Despite the broadly discussed EMT context, Gröne et al. discuss this filament protein as a marker for mitosis, observed during nephrogenic repair [136]. This is supported by the results of Nakatsuji et al. [137], stating vimentin to be an upregulated marker of regenerating epithelial cells, further suggesting an important role for vimentin-positive tubule cells in promoting proliferation of myofibroblasts, without putting vimentin in any EMT context. The notion of Katoh [138], that vimentin is a target of WNT non-canonical signaling in stem cells, puts vimentin and its possible role in CAD into a whole new context.

Despite the fact that EMT could not be demonstrated to occur in our renal allograft model, evidence could be found for the dysregulation of a series of EMT-associated signal transduction pathways. It is thought that the TGFB, NOTCH, hedgehog, and WNT pathway contribute to EMT (and fibrosis).

The NOTCH pathway plays a crucial role in kidney development, while in the mature kidney, only very little active NOTCH1 receptor can be detected [28]. The NOTCH pathway has been discussed in the context of EMT [17], and has been proposed to play a role in the pathogenesis of glomerular kidney disease [28]. No differential regulation of the NOTCH pathway genes was observed by qPCR analysis, suggesting that transcriptional activation of this pathway could not be demonstrated in the context of our study.

Hedgehog (HH) signaling remains active in the adult where it helps maintain tissue homeostasis [91]. HH has been recognized in different types of cancer [92], stem cell biology, and tissue repair during chronic persistent inflammation [31]. Moreover, Le et al. could demonstrate, in an *in vivo* mouse model of wound healing, that cyclopamine-induced HH signaling-disruption impaired normal wound healing [32].

Microarray and subsequent qPCR analyses revealed alterations in the expression of hedgehog pathway genes.

The mRNA of desert hedgehog (Dhh), one of the three vertebrate HH ligands, the receptor and target *Ptch1*, the target gene *Sfrp1*, and several WNT ligands was found to be upregulated during CAD. This suggested pathway activation. Target genes of the HH pathway exert stimulatory signals, including WNT ligand expression, as well as upregulation of WNT inhibitors (*Sfrp1*). In contrast, the HH pathway ligands indian hedgehog (*Ihh*), *sonic hedgehog* (*Shh*), the receptor *Lrp2*, and target genes *Bmp4* and *Bmp7* were downregulated with CAD. The receptor LRP2, also called megalin, is an endocytotic scavenger receptor expressed in the adult kidney in the brush border of the renal proximal tubule [36]. Receptor-mediated endocytosis facilitates the clearing of substances – such as nutrients, lipoproteins, hormones, vitamins, and enzymes by tubulus cells – and also moderates signaling through direct activation of signaling cascades [36]. Decreased renal *LRP2* expression has been demonstrated in diseases characterized by proteinuria and defective tubular re-uptake of filtered proteins [36]. In an *in vitro* system of proximal-tubule-derived cells, TGFB1-induced reduction of *LRP2* expression could be observed in a time and dose-dependent manner [37]. Caruso-Neves et al. further identified LRP2 as a sensor of albumin that determines whether tubule cells are protected or injured by albumin which would result in apoptosis [38]. Alterations in *Lrp2* expression, as observed in our model, fit into a model that integrates non-specific protein uptake, HH signaling and fibrosis-mediated apoptosis of renal tubule structures, all induced by the general insult to the organ.

HH and TGFB signaling are further connected by the expression of BMPs which are antifibrotic HH target genes. HH pathway genes such as *Lrp2*, that are known to be influenced by TGFB1, as well as TGFB1 antagonists, such as BMP7, were downregulated during progression of CAD.

While a central role for the biology of TGFB1 in human and experimental models of renal fibrosis has been well documented [139, 140], the potential role of the WNT pathway is less clear. There are several points at which potential crosstalk or cross-regulation between the canonical WNT and TGFB1 signaling pathways may occur.

A role for the WNT canonical pathway in renal interstitial fibrosis has been evaluated in an *in vivo* mouse model [141]. In our model of progressive CAD, a dynamic modulation of specific elements of the WNT signaling pathway was observed.

The *Wnt* gene expression profile suggested activation of the canonical and WNT-Ca²⁺ pathways, but did not support activation of the PCP pathway during CAD [41]. Seven *Wnt* genes were found to be differentially regulated at the mRNA level in our rat model (Table 1). The subcategorization of WNT action can be difficult as individual WNTs may influence several WNT pathways. For example, WNT6 has been assigned to the canonical WNT pathway by Kirikoshi et al. [142], whereas Nishizuka et al. [143] report WNT6 to be a part of the WNT-Ca²⁺ pathway. During development, restricted zones of intense canonical WNT signaling drive nephrogenesis in fetal kidney [144]. WNT7b has been shown to be a key regulator of the ductal architecture that establishes a functional physiologically active mammalian kidney [145]. Here a progressive loss of expression of *Wnt7b* was associated with CAD. The modulation of select WNT genes during progressive CAD suggests a fine control of distinct pathway branches associated with these pathophysiologic events. While macrophages play a prominent role in the development of renal fibrosis and *Wnt2*, *Wnt5a* and *Wnt7b* expression have been linked to macrophage infiltration in various contexts [146, 147], these *WNT* genes were not increased in expression during CAD. Since expression of 17 *WNT* ligands was seen in the control kidneys, resident kidney cells appear to represent the principal source of *WNT* ligands during CAD. The ability to further dissect WNT-ligand specific pathway regulation will help to devise potential programs to modulate this pathway. In the adult, WNT signaling plays an important role in the control of tissue self-renewal [148]. Canonical WNT signaling promotes cell proliferation, tissue expansion and the control of cell fate determination and terminal differentiation [110].

Table 3. Summary of qPCR results of hedgehog and WNT pathway genes

Gene ID	Gene Symbol	CAD Regulation	Significant effect of treatment
Hedgehog pathway			
29499	Shh	↓	+
16147	Ihh	↓	+
620711	Dhh	↑	+
29216	Lrp2	↓	+
89830	Ptch1	↑	+
140589	Gli1	↑	-
84402	Sfrp1	↑	+
25296	Bmp4	↓	-
85272	Bmp7	↓	+
Canonical WNT pathway			
24882	Wnt3	↑	-
293990	Wnt8b	↓	+
316527	Wnt10a	↓	+
161452	Lef1	↑	+
24817	Tcf1	↓	+
25296	Bmp4	↓	-
25406	Cd44	↑	+
25661	Fn1	↑	+
24577	Myc	↑	+
25335	Mmp7	↑	+
24599	Nos2	↑	+
WNT-Ca2+ pathway			
316526	Wnt6	↑	+
114850	Wnt7a	↑	+
315196	Wnt7b	↓	+
25023	Prkcb1	↑	+
81749	Prkch	↑	+
307231	Nfatc1_pred	↑	+
311658	Nfatc2	↑	+

Table 3: Arrows indicate up or downregulation of gene expression in relation to the normal control kidneys. Further, statistically significant effects of the treatment, on the expression of genes are denoted.

Transient upregulation of WNT canonical pathway has been described in the context of wound healing [112, 113]. Abnormal WNT signaling has been associated with many diseases including pulmonary fibrosis [40]. In the experiments detailed here the activation of each sub-pathway appeared to be guided through the selective modulation of specific transcription factors associated with the individual pathway and downstream target genes. The transcription factors LEF1 and Tcf1 are associated with activation of the canonical pathway. Lef1 target genes, including *Nos2*, *Fn1*, *Mmp7* and *Cd44* [114], showed pronounced upregulation in the model. In contrast, *Tcf1* was progressively downregulated.

Upregulation of the canonical WNT target gene *Fn1* links the observed fibrosis directly to activation of this pathway. The expression of *Nos2*, a canonical WNT target associated with inflammation and macrophage activation [149] was increased with CAD. *Mmp7* showed the strongest regulation of any WNT target gene studied (over 1000-fold). *Mmp7* is linked with ECM remodeling and the posttranslational modification of growth factors. These actions are thought to facilitate tissue milieu-dependent “sensing” of pathways (e.g. TNF and TNFRI & II) [150]. The canonical WNT target gene *Cd44* plays a role in leukocyte infiltration and has been linked to chronic inflammatory disease [151]. CD44 is a receptor for hyaluronan and moderates cell-cell/cell-matrix interactions [152]. CD44 has also been shown to promote the activation of TGFB1 in fibroblasts via an MMP-dependent mechanism [153].

Activation of the canonical WNT pathway resulting in the upregulation of *Cd44* and *Mmp7*, and the effects seen on TGFB1 biology highlight the potential interplay between the WNT and TGFB pathways during CAD and suggests a direct role for these pathways in the generation of a profibrotic tissue milieu. Rouschop et al. have suggested that *de novo* expression of CD44 in an injured kidney contributes to the development of fibrosis, at least in part, through enhanced TGFB signaling [152].

Our analysis also suggests a parallel activation of the WNT-Ca²⁺ pathway during the development of CAD. The WNT-Ca²⁺ pathway is unique to vertebrates and plays critical roles in orchestrating the cellular events that characterize vertebrate development and morphogenesis. In contrast to the canonical WNT pathway, target genes for the WNT-Ca²⁺ pathway are not well defined, but are generally thought to be targets of the NFAT family of transcription factors. Increased expression of the WNT-Ca²⁺ pathway genes *Prkcb1* and *Prkch* and the transcription factors *Nfact1_pred* and *Nfact2* were associated with CAD. In this setting, the transcriptional regulators of the NFAT family function as molecular integrators of calcium signals with other signaling pathways, including MAPK, WNT or NOTCH [154]. Bourajjaj et al. [155] recently demonstrated the importance of the WNT-Ca²⁺ pathway in myocyte hypertrophy and pathological cardiac remodeling during heart failure. Similar regulatory events may help dictate the pathophysiology seen in renal fibrosis and CAD. While WNT signaling is essential for renal development, select components of the WNT signaling pathway were found here to be modulated during progression of CAD. The dysregulation of these components during CAD suggests that these

pathways may be potential targets for therapeutic intervention in CAD and other progressive renal diseases.

6.3 Therapeutic intervention of disease progression by 13cRA

The therapeutic effect of 13cRA on transcriptomic profiles and regulatory pathways was further evaluated with the treated kidneys appeared essentially “normal” following treatment by morphometry. The transcriptomic analysis did reveal significantly altered expression of genes. Hierarchical clustering revealed that with time, the overall gene expression profiles of the 56 day-treatment group regained a similar expression pattern, as compared to the normal kidney controls. The treatment could not prevent alterations in gene-expression altogether, as observed by numerous alterations at early time points in the treatment group. The changes were rather reversed by the prolonged treatment, as observed on day 56 after transplantation. The kidneys of the placebo group, as well as kidneys from the treatment group, differ from the control kidney in the amount of immune cells. Treatment could not eliminate infiltration completely, but may have induced tolerance. This assumption is based on the similarity of expression patterns 56 days after treatment, despite a detectable infiltrate.

Analysis of gene expression of kidney tissue does not allow us to draw conclusions about potential events occurring systemically. A reduction in proinflammatory stimuli could result form a systemic effect on leukocyte priming or homing. Previous studies have shown a reduction in mononuclear infiltration with treatment in the same model [5]. In addition, effects of 13cRA on the infiltrate present in the kidney are also possible. The overall effect may thus result from a combination of effects [5]. Since inflammation is thought to help trigger the development of fibrosis, changes in the nature or quantity of the infiltrate will influence the outcome of the disease. A significantly-attenuated upregulation could be observed in all inflammation and inflammatory signal transduction-associated genes, with the exception of *Jak2* (5.2.3). These effects on gene expression reflect our observations in morphometry [5]. Since many of the genes discussed in the context of inflammation are mainly transcribed by immune cells, it has to be noted that a reduction of mRNA measured in the 13cRA treated animals is probably partially due to the decrease of leukocyte infiltrates in these organs. Therefore, the overall effects result from the combination of regulation of gene expression and decreased infiltrate of immune cells.

To gain further insight into the potential mechanism of 13cRA on the promoter level, experiments investigating an indirect repression mechanism were performed. Adams et al. [5] excluded a transrepression mechanism involving direct binding of the RAR/RXR receptors to the response elements of the promoter of the exemplary gene *CCL5*. Pascual et al. [59] showed that posttranslational modification of a nuclear receptor (PPARG) led to the adherence of a nuclear corepressor (NCOR) at the promoter, preventing transcriptional activation of an inflammatory gene. We hypothesized that a NCOR-dependent mechanism might be similarly involved in the indirect transrepression mechanism described for *CCL5* transcription (i.e. that NCOR would normally be found bound to the promoter and blocking expression). Stimulation would result in loss of NCOR, thus allowing transcription from the promoter.

The experiments were difficult to perform in part due to problems with generating sufficient cell numbers. Thus only preliminary data could be presented. Problems with the method included compromising signals in the isotype control allowed no definitive conclusion to be drawn of the ChIP experiment. The signal in the no-antibody control suggests an unspecific binding of the preblocked StaphA cells to the chromatin. A potential explanation for the signal seen in these controls, and not in the PCR samples using *NOS2* primers, is a combination of insufficient washing with a higher abundance of *CCL5* and *CXCL10/IP10* chromatin as compared to *NOS2*. Taking the differences of the input controls into consideration normalization against total input would have reduced the no antibody control signal compared to the NCOR sample signal. Evaluation of this experiment by quantitative PCR was not performed, but could help to interpret future experiments. For a definitive answer to these questions a new cell system should be employed that allows for larger amounts of starting material. Problems such as the ratio of background to enriched chromatin, non-uniform loss of sample during washing and purification and high numbers of PCR cycles are often found when only small sample sizes can be used and should therefore be avoided.

In parallel experiments out side the focus of this thesis, where large numbers of cells could be used, the general method was efficiently applied to assess the binding of the transcription factor SP1 to the *CCL5* promoter in a natural killer cell line [123]. Retinoic acid has been reported to modulate the generation of helper T cell populations from an inflammatory towards an anti-inflammatory, self tolerant phenotype through various mechanisms. For example, by promoting FOXP3-positive

regulatory T cells (Tregs) [119, 156]. *In vitro*, TGF β -induced *FOXP3* expression in T cells was found to be unstable [119], but the protein could be stabilized by retinoic acid treatment [157]. Despite the upregulation of *FOXP3 in vitro*, treatment of experimental autoimmune encephalomyelitis (EAE) with retinoids was found to suppress Th17 cell function without promoting *Foxp3* expression [158]. In an *in vivo* mouse model, mice infected with *Listeria monocytogenes*, a reduction in Th17 cells was observed following retinoic acid administration which acted through a reduction in the transcription factor “RAR-related” orphan receptor gamma t (ROR γ t). This factor is important for Th17 development [157]. We also looked at the expression of genes specific for Tregs and Th17 cells to investigate whether 13cRA might induce tolerance through influencing the T cell milieu. Upregulation of *Foxp3* was observed in all groups. Differences in *Foxp3* expression were statistically significant between the placebo and the treatment group on day 56, with reduced expression observed in the treatment group. Genes involved in the development of the Th17 cell lineage including *Il6*, *Il6r*, *Il21*, and *Tgfb1* were upregulated, but none of the groups demonstrated a regulation in *Il17* expression. This suggested that while a Th17-promoting regulatory milieu was present in the kidney, no upregulation at the gene expression level of *Il17* was observed. This may be due to a strong allo-Th1 response that suppresses the Th17 lineage, as represented by upregulated *Ifng*. With regards to the Tregs, even though a stimulatory effect of retinoic acid on the *Foxp3* expression has been described, our data could not demonstrate this effect at the mRNA level. On the other hand, there is a clear downregulation of inflammation in the kidneys of 13cRA-treated rats, as shown by a decrease of inflammatory as well as suppressive cytokines on day 56, reflecting a decrease in kidney inflammation and, concomitantly, the need for counter-regulation. Further studies investigating T cell lineages by using *in vitro* systems will have to be employed to better characterize the effect of 13cRA on the immune milieu. In summary, we found a reduction in inflammation and fibrosis by morphology and downregulation on the gene expression level (see 5.2.3). In addition to alterations of the kidney tissue itself, effects might be due to a shift in amount and effector type of infiltrating cells of the immune system.

The roles of the HH and the various WNT pathways during the progression of CAD were discussed in 6.2. Having established that a well defined regulation of these

pathways was observed during CAD, we investigated the potential influence of 13cRA treatment on the activation status of these pathways.

Retinoic acid (RA) has complex and pleiotropic functions during vertebrate development [116]. RA is recognized as an important signaling molecule which can influence developmental pathways including HH [116]. *In vitro*, SHH and RA have been shown to exert synergistic effects on the differentiation of mesenchymal stem cells [117].

13cRA treatment appeared to reverse the CAD associated effects on the HH pathway. Steady state levels of mRNA for HH pathway genes were reversely regulated. Genes, observed to be upregulated during CAD, were downregulated in the treatment group and genes initially found to be downregulated during CAD, were observed to be upregulated by treatment. 13cRA treatment appeared to alter gene expression of HH pathway genes more in line with the control normal kidney and thus potentially, to re-establish normal tissue homeostasis. For example, the extreme downregulation of the receptor *Lrp2* observed during CAD was prevented by 13cRA treatment. In an *in vitro* system, upregulation of megalin (*Lpr2*) mRNA and protein expression after retinoic acid treatment could be demonstrated [159, 160]. The decreasing *Lrp2* mRNA levels, measured in our study, could also reflect apoptosis of the main *Lrp2* expressing cells. Hence, the minor changes in expression observed after treatment could indicate better survival of the cells that express *Lrp2*. A direct stimulation of *Lrp2* transcription by retinoic acid, as described in the literature [160], could also explain the effect observed.

To address this question, we investigated the effect of 13cRA on different cell systems *in vitro* (data not shown). Unfortunately, all of the cell types tested including a human proximal tubule cell line, a mouse tubule cell line, and primary rat tubule cells did not show stable expression of the *Lrp2* gene. Thus, neither stable *Lrp2* expression, nor a reproducible stimulation of *Lrp2* expression could be demonstrated *in vitro*. With a better cell culture system, it may be possible to better address this question. Of all HH pathway genes investigated, *Lrp2* and the ligand *Ihh* demonstrated almost equal regulation. Although in the literature only SHH is discussed to be an LRP2 ligand, this closely linked expression suggests potential interplay between SHH and LRP2.

The HH target genes *Bmp4* and *Bmp7*, initially downregulated in CAD, returned to normal levels after 13cRA treatment. A direct stimulatory effect of retinoic acid on

Bmp7 expression had been previously demonstrated *in vitro* [161]. Upregulation of the anti-fibrotic *Bmp7* expression may represent an important means by which RA exerts its anti-fibrotic effects. Katoh et al. reported that mesenchymal BMP can induce the indian hedgehog gene (*IHH*) in gastrointestinal epithelial cells which led to the induction of WNT2B and BMP4 through activation of epithelial hedgehog [162]. A similar effect in regulation of *Ihh*, *Bmp4* and *Wnt2b* gene expression was observed in the 13cRA treated rat kidneys, further suggesting a close connection between HH and WNT signaling pathways.

Four of the 17 WNT ligands expressed in the kidney tissue were downregulated during CAD. 13cRA treatment resulted in the upregulation of *Wnt2b* and *Wnt10a*, and at the same time, in an increased downregulation of *Wnt7b* and *Wnt8b*. In the same manner that specific activation of WNT signaling could be observed during CAD progression, a specific regulation could be seen in response to 13cRA treatment. More information concerning the effect of the individual WNT ligands on downstream target gene activation will help clarify the consequences of dysregulation.

A link between retinoids or members of the steroid family with the canonical WNT pathway is well defined [111]. Nuclear receptors including PPAR γ and the RAR receptor bind beta-catenin and/or regulate activation of WNT target genes [118]. RAR can form a complex with beta-catenin competing with TCF/LEF1 for the binding to DNA and thus suppressing activity [111] (the inhibitory relationship between the HH and WNT pathway has already been addressed in 5.1.3.1). In response to RA, beta-catenin protein levels of tumor cell lines increased significantly at the membrane, although mRNA levels remained constant [163].

Similar effects were observed for the WNT canonical and Ca²⁺ pathways. Upregulation of the transcription factor *Lef1* and the WNT canonical target genes *Cd44*, *Fn1*, *Nos2*, *Mmp7*, and *Myc* seen with CAD were diminished in comparison to the placebo group. In contrast, the observed downregulation of the transcription factor *Tcf1*, as well as the target gene *Bmp4* was attenuated by treatment. Treatment appeared to specifically reduce the activation of the fibrosis-promoting part of the WNT canonical pathway as evidenced by the effects seen on fibronectin, *Cd44* and *Mmp7*.

Increased expression of the WNT-Ca²⁺ pathway genes *Prkcb1* and *Prkch* and the transcription factors *Nfact1_pred* and *Nfact2* was observed to be attenuated through treatment. As already discussed in 6.2, vimentin is a target of the non-canonical WNT

pathway, moreover, CD44 was discussed as also acting as a non-canonical WNT target in stem cells [138]. This links not only the intermediate filament protein vimentin to fibrosis and the WNT-Ca²⁺ pathway, but also demonstrates the strong context-dependency of the determination of the WNT signaling cascades in general.

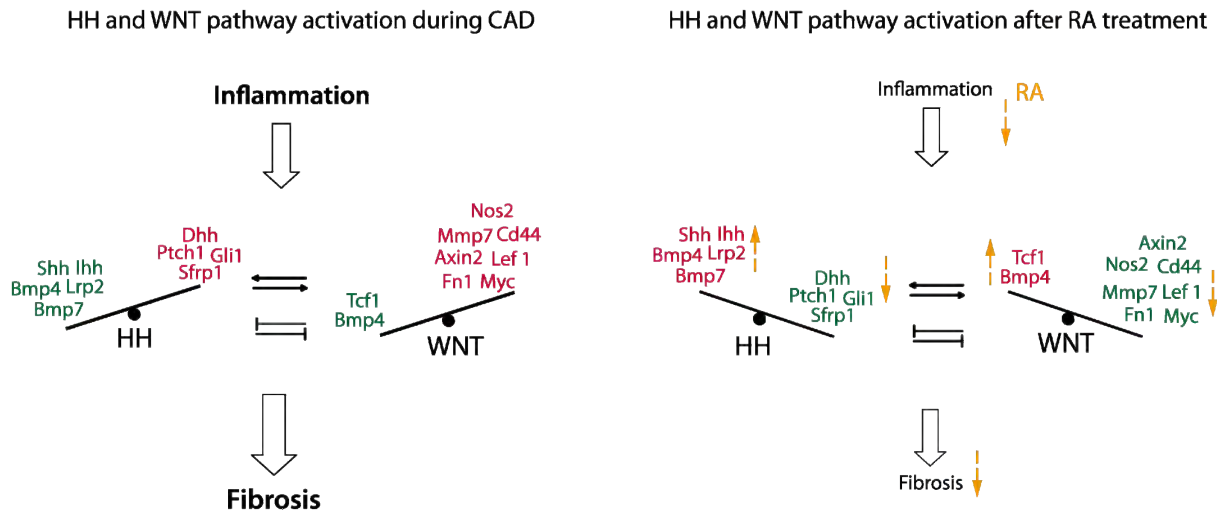


Fig. 40: The roles of HH and WNT canonical pathway in transplantation-induced fibrosis. Figure 40 summarizes up or downregulation of HH and WNT canonical pathway genes, as observed by qPCR analysis. Green indicates downregulation of gene expression, while red indicates upregulation. Symbols denote a positive, as well as a negative regulatory relationship between both pathways. The left diagram displays a model of inflammation-induced dysregulation of pathway activation, resulting in fibrosis, as observed in the rat model. The right diagram displays possible influence of RA treatment and a shift observed in pathway regulation.

From studies of embryonic development, RA has been shown to act as a major integrator of signaling pathways that control apoptosis, proliferation and differentiation [116]. Similar actions may help explain the positive effects seen in our CAD model. Aside from transcriptional regulation, 13cRA might influence the stability of RNA or Protein, RNA turnover or the regulation of microRNAs (miRNA). Direct effects of RA treatment on pathway activation could not be easily investigated in our system, but overall transcriptomic effects suggest a predominant induction of hedgehog pathway genes, and a reduction in the activation of the WNT pathway. The indian hedgehog gene *Ihh* is also discussed as an antagonist of WNT signaling in colonic epithelial cell differentiation [104]. The hedgehog pathway target gene secreted frizzled protein 1 (*Sfrp1*) which is a WNT inhibitor [100]. Both genes were upregulated after treatment. A tight and complex relationship between signal transduction and treatment is suggested.

In conclusion, we propose a model that integrates effects generated by the transplantation-process. Inflammation factors induce an imbalance in the wound-

healing and homeostatic processes, marked by dysregulation of hedgehog and Wnt pathway activation (see figure 40). The combined effects of chronic inflammation and dysregulation of these central regulator pathways lead to fibrosis and organ deterioration. Treatment with 13cRA, not only attenuated disease progression, but even reversed early effects of CAD. The overall effects of the treatment consist of potentially direct effects on fibrosis and inflammation associated gene expression, as well as a specific modulation, observed in hedgehog and WNT pathways activation.

7 Abbreviations

13cRA	13-cis retinoic acid
CAD	Chronic allograft dysfunction
CCL	CC- Chemokine ligand
CD	Cluster of differentiation
CEL	Cell intensity file
ChIP	Chromatin immunoprecipitation
CTNNB1	Beta-catenin
CT	Cycle Threshold
DAVID	Database for Annotation, Visualization, and Integrated Discovery
ECM	Extra cellular matrix
EMT	Epithelial to mesenchymal transition
FC	Fold change
GO	Gene ontology
HH	Hedgehog
IFN	Interferon
IHC	Immunohistochemistry
IL	Interleukin
K4IM	Immortalized synoviocyte line K4WT
KEGG	Kyoto Encyclopedia of Genes and Genomes
LEF1	Lymphoid enhancer binding factor 1
NCOR	Nuclear Corepressor
NFAT	Nuclear factor of activated T-cells
PPAR	Peroxisome proliferator-activated receptor
StaphA	Staphylococcus aureus
TGFB	Tumor growth factor beta
WNT	Combination of “wingless” and “ <i>INT</i> ”

Symbols:



Molecular interaction or relation of gene products



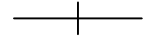
Indirect effect of regulation



Inhibition of expression



Molecule, mostly chemical compound



Dissociation of proteins



Gene product or protein

8 References

1. Mas, V., et al., Establishing the molecular pathways involved in chronic allograft nephropathy for testing new noninvasive diagnostic markers. *Transplantation*, 2007. **83**(4): p. 448-57.
2. Hayry, P., *Chronic rejection: new potential venues of therapy*. *Transplant Proc*, 1999. **31**(4): p. 1799-800.
3. Ewout A. Kouwenhoven, J.N.M.I., Ron W. F. Bruin,, *Etiology and pathophysiology of chronic transplant dysfunction*. *Transplant International*, 2000. **13**(6): p. 385-401.
4. Libby, P. and J.S. Pober, *Chronic rejection*. *Immunity*, 2001. **14**(4): p. 387-97.
5. Adams, J., et al., 13-cis Retinoic Acid Inhibits Development and Progression of Chronic Allograft Nephropathy. *Am J Pathol*, 2005. **167**(1): p. 285-298.
6. Sobotta, J., Welsch, U., *Atlas Histologie, 7. Auflage*. 2005.
7. Chai, Q., et al., Localisation and phenotypical characterisation of collagen-producing cells in TGF-beta 1-induced renal interstitial fibrosis. *Histochem Cell Biol*, 2003. **119**(4): p. 267-80.
8. Huang, Y. and N.A. Noble, *PAI-1 as a target in kidney disease*. *Curr Drug Targets*, 2007. **8**(9): p. 1007-15.
9. Hewitson, T.D., Renal Tubulointerstitial Fibrosis: Common but Never Simple. *Am J Physiol Renal Physiol*, 2009.
10. Wain, H.M., et al., *Guidelines for human gene nomenclature*. *Genomics*, 2002. **79**(4): p. 464-70.
11. Haskell, C.A., S. Ribeiro, and R. Horuk, *Chemokines in transplant rejection*. *Curr Opin Investig Drugs*, 2002. **3**(3): p. 399-405.
12. Hewitson, T.D. and G.J. Becker, *Interstitial myofibroblasts in IgA glomerulonephritis*. *Am J Nephrol*, 1995. **15**(2): p. 111-7.
13. Wiggins, R., et al., Vascular adventitial cell expression of collagen I messenger ribonucleic acid in anti-glomerular basement membrane antibody-induced crescentic nephritis in the rabbit. A cellular source for interstitial collagen synthesis in inflammatory renal disease. *Lab Invest*, 1993. **68**(5): p. 557-65.
14. Grimm, P.C., et al., Neointimal and tubulointerstitial infiltration by recipient mesenchymal cells in chronic renal-allograft rejection. *N Engl J Med*, 2001. **345**(2): p. 93-7.
15. Liu, Y., Epithelial to mesenchymal transition in renal fibrogenesis: pathologic significance, molecular mechanism, and therapeutic intervention. *J Am Soc Nephrol*, 2004. **15**(1): p. 1-12.
16. Picard, N., et al., Origin of renal myofibroblasts in the model of unilateral ureter obstruction in the rat. *Histochem Cell Biol*, 2008.
17. Huber, M.A., N. Kraut, and H. Beug, Molecular requirements for epithelial-mesenchymal transition during tumor progression. *Current Opinion in Cell Biology* Cell-to-cell contact and extracellular matrix, 2005. **17**(5): p. 548-558.
18. Piek, E., C.H. Heldin, and P. Ten Dijke, *Specificity, diversity, and regulation in TGF-beta superfamily signaling*. *FASEB J*, 1999. **13**(15): p. 2105-24.
19. Feng, X.H. and R. Derynck, *Specificity and versatility in tgf-beta signaling through Smads*. *Annu Rev Cell Dev Biol*, 2005. **21**: p. 659-93.
20. Moustakas, A. and C.H. Heldin, *Non-Smad TGF-beta signals*. *J Cell Sci*, 2005. **118**(Pt 16): p. 3573-84.

21. Border, W.A. and N.A. Noble, *Transforming growth factor beta in tissue fibrosis*. N Engl J Med, 1994. **331**(19): p. 1286-92.
22. Yamamoto, T., et al., Sustained expression of TGF-beta 1 underlies development of progressive kidney fibrosis. Kidney Int, 1994. **45**(3): p. 916-27.
23. Zeisberg, M., et al., Renal fibrosis. Extracellular matrix microenvironment regulates migratory behavior of activated tubular epithelial cells. Am J Pathol, 2002. **160**(6): p. 2001-8.
24. Gal, A., et al., Sustained TGF beta exposure suppresses Smad and non-Smad signalling in mammary epithelial cells, leading to EMT and inhibition of growth arrest and apoptosis. Oncogene, 2008. **27**(9): p. 1218-30.
25. Borggrefe, T. and F. Oswald, *The Notch signaling pathway: Transcriptional regulation at Notch target genes*. Cellular and Molecular Life Sciences (CMLS).
26. Iso, T., L. Kedes, and Y. Hamamori, *HES and HERP families: multiple effectors of the Notch signaling pathway*. J Cell Physiol, 2003. **194**(3): p. 237-55.
27. Fischer, A. and M. Gessler, Delta-Notch--and then? Protein interactions and proposed modes of repression by Hes and Hey bHLH factors. Nucleic Acids Res, 2007. **35**(14): p. 4583-96.
28. Niranjana, T., et al., The Notch pathway in podocytes plays a role in the development of glomerular disease. Nat Med, 2008. **14**(3): p. 290-8.
29. Timmerman, L.A., et al., Notch promotes epithelial-mesenchymal transition during cardiac development and oncogenic transformation. Genes Dev, 2004. **18**(1): p. 99-115.
30. Zavadil, J., et al., Integration of TGF-beta/Smad and Jagged1/Notch signalling in epithelial-to-mesenchymal transition. Embo J, 2004. **23**(5): p. 1155-65.
31. Katoh, Y. and M. Katoh, Hedgehog signaling pathway and gastrointestinal stem cell signaling network (review). Int J Mol Med, 2006. **18**(6): p. 1019-23.
32. Le, H., et al., *Hedgehog signaling is essential for normal wound healing*. Wound Repair Regen, 2008. **16**(6): p. 768-73.
33. McCarthy, R.A., et al., *Megalin functions as an endocytic sonic hedgehog receptor*. J Biol Chem, 2002. **277**(28): p. 25660-7.
34. Morales, C.R., et al., *Epithelial trafficking of Sonic hedgehog by megalin*. J Histochem Cytochem, 2006. **54**(10): p. 1115-27.
35. McCarthy, R.A. and W.S. Argraves, *Megalin and the neurodevelopmental biology of sonic hedgehog and retinol*. J Cell Sci, 2003. **116**(Pt 6): p. 955-60.
36. Christensen, E.I. and H. Birn, *Megalin and cubilin: multifunctional endocytic receptors*. Nat Rev Mol Cell Biol, 2002. **3**(4): p. 256-66.
37. Gekle, M., et al., Transforming growth factor-beta1 reduces megalin- and cubilin-mediated endocytosis of albumin in proximal-tubule-derived opossum kidney cells. J Physiol, 2003. **552**(Pt 2): p. 471-81.
38. Caruso-Neves, C., et al., *PKB and megalin determine the survival or death of renal proximal tubule cells*. Proc Natl Acad Sci U S A, 2006. **103**(49): p. 18810-5.
39. Theilig, F., et al., Abrogation of protein uptake through megalin-deficient proximal tubules does not safeguard against tubulointerstitial injury. J Am Soc Nephrol, 2007. **18**(6): p. 1824-34.
40. Königshoff, M., et al., Functional Wnt Signaling Is Increased in Idiopathic Pulmonary Fibrosis. PLoS ONE, 2008. **3**(5): p. e2142.
41. Staal, F.J., T.C. Luis, and M.M. Tiemessen, *WNT signalling in the immune system: WNT is spreading its wings*. Nat Rev Immunol, 2008. **8**(8): p. 581-93.

42. Endo, Y., et al., Wnt-3a-dependent cell motility involves RhoA activation and is specifically regulated by dishevelled-2. *J Biol Chem*, 2005. **280**(1): p. 777-86.
43. Liang, H., et al., Noncanonical Wnt signaling promotes apoptosis in thymocyte development. *J Exp Med*, 2007. **204**(13): p. 3077-84.
44. Lee, S., An improved technique of renal transplantation in the rat. *Surgery*, 1967. **61**(5): p. 771-3.
45. Dressel, R., L. Walter, and E. Gunther, *Genomic and functional aspects of the rat MHC, the RT1 complex*. *Immunol Rev*, 2001. **184**: p. 82-95.
46. Gunther, E. and L. Walter, *The major histocompatibility complex of the rat (Rattus norvegicus)*. *Immunogenetics*, 2001. **53**(7): p. 520-42.
47. Bedke, J., et al., Beneficial effects of CCR1 blockade on the progression of chronic renal allograft damage. *Am J Transplant*, 2007. **7**(3): p. 527-37.
48. Kunter, U., et al., Expression of A20 in the vessel wall of rat-kidney allografts correlates with protection from transplant arteriosclerosis. *Transplantation*, 2003. **75**(1): p. 3-9.
49. GRONE, H.-J., et al., Met-RANTES reduces vascular and tubular damage during acute renal transplant rejection: blocking monocyte arrest and recruitment. *FASEB J.*, 1999. **13**(11): p. 1371-1383.
50. Lehrke, I., et al., *Retinoid receptor-specific agonists alleviate experimental glomerulonephritis*. *Am J Physiol Renal Physiol*, 2002. **282**(4): p. F741-51.
51. Kreutz, M., et al., Retinoic acid inhibits monocyte to macrophage survival and differentiation. *Blood*, 1998. **91**(12): p. 4796-802.
52. Chambon, P., A decade of molecular biology of retinoic acid receptors. *FASEB J*, 1996. **10**(9): p. 940-54.
53. Mulholland, D.J., et al., Interaction of nuclear receptors with the Wnt/beta-catenin/Tcf signaling axis: Wnt you like to know? *Endocr Rev*, 2005. **26**(7): p. 898-915.
54. Orosz, C.G., et al., Analysis of retinoid-mediated immunosuppression in vivo. Effects of Ro23-6457 on cellular alloimmune responses. *Immunopharmacology*, 1991. **22**(1): p. 49-58.
55. Yang, T., et al., Expression of peroxisomal proliferator-activated receptors and retinoid X receptors in the kidney. *Am J Physiol*, 1999. **277**(6 Pt 2): p. F966-73.
56. Simonson, M.S., Anti-AP-1 activity of all-trans retinoic acid in glomerular mesangial cells. *Am J Physiol*, 1994. **267**(5 Pt 2): p. F805-15.
57. Na, S.-Y., et al., Retinoids Inhibit Interleukin-12 Production in Macrophages through Physical Associations of Retinoid X Receptor and NFkappa B. *J. Biol. Chem.*, 1999. **274**(12): p. 7674-7680.
58. Schaier, M., et al., Isotretinoin alleviates renal damage in rat chronic glomerulonephritis. *Kidney Int*, 2001. **60**(6): p. 2222-34.
59. Pascual, G., et al., A SUMOylation-dependent pathway mediates transrepression of inflammatory response genes by PPAR-[gamma]. 2005. **437**(7059): p. 759-763.
60. Schug, T.T., et al., Opposing effects of retinoic acid on cell growth result from alternate activation of two different nuclear receptors. *Cell*, 2007. **129**(4): p. 723-33.
61. Chomczynski, P. and N. Sacchi, Single-step method of RNA isolation by acid guanidinium thiocyanate-phenol-chloroform extraction. *Anal Biochem*, 1987. **162**(1): p. 156-9.

62. Haas, C., et al., Characterization of SV40T antigen immortalized human synovial fibroblasts: maintained expression patterns of EGR-1, HLA-DR and some surface receptors. *Rheumatol Int*, 1997. **16**(6): p. 241-7.
63. Cohen, C.D., et al., Improved elucidation of biological processes linked to diabetic nephropathy by single probe-based microarray data analysis. *PLoS ONE*, 2008. **3**(8): p. e2937.
64. Tusher, V.G., R. Tibshirani, and G. Chu, *Significance analysis of microarrays applied to the ionizing radiation response*. *Proc Natl Acad Sci U S A*, 2001. **98**(9): p. 5116-21.
65. Ashburner, M., et al., Gene ontology: tool for the unification of biology. The Gene Ontology Consortium. *Nat Genet*, 2000. **25**(1): p. 25-9.
66. Dennis, G., Jr., et al., DAVID: Database for Annotation, Visualization, and Integrated Discovery. *Genome Biol*, 2003. **4**(5): p. P3.
67. Hosack, D.A., et al., Identifying biological themes within lists of genes with EASE. *Genome Biol*, 2003. **4**(10): p. R70.
68. Kanehisa, M. and S. Goto, *KEGG: kyoto encyclopedia of genes and genomes*. *Nucleic Acids Res*, 2000. **28**(1): p. 27-30.
69. Kanehisa, M., et al., *From genomics to chemical genomics: new developments in KEGG*. *Nucleic Acids Res*, 2006. **34**(Database issue): p. D354-7.
70. Kanehisa, M., et al., *KEGG for linking genomes to life and the environment*. *Nucleic Acids Res*, 2008. **36**(Database issue): p. D480-4.
71. Irizarry, R.A., et al., Use of mixture models in a microarray-based screening procedure for detecting differentially represented yeast mutants. *Stat Appl Genet Mol Biol*, 2003. **2**: p. Article1.
72. Irizarry, R.A., et al., Exploration, normalization, and summaries of high density oligonucleotide array probe level data. *Biostatistics*, 2003. **4**(2): p. 249-64.
73. Irizarry, R.A., et al., *Summaries of Affymetrix GeneChip probe level data*. *Nucleic Acids Res*, 2003. **31**(4): p. e15.
74. Bolstad, B.M., et al., A comparison of normalization methods for high density oligonucleotide array data based on variance and bias. *Bioinformatics*, 2003. **19**(2): p. 185-93.
75. Sturn, A., J. Quackenbush, and Z. Trajanoski, *Genesis: cluster analysis of microarray data*. *Bioinformatics*, 2002. **18**(1): p. 207-8.
76. Schmid, H., et al., Validation of endogenous controls for gene expression analysis in microdissected human renal biopsies. 2003. **64**(1): p. 356-360.
77. Pfaffl, M.W., A new mathematical model for relative quantification in real-time RT-PCR. *Nucleic Acids Res*, 2001. **29**(9): p. e45.
78. Dai, M., et al., Evolving gene/transcript definitions significantly alter the interpretation of GeneChip data. *Nucleic Acids Res*, 2005. **33**(20): p. e175.
79. Elo, L.L., et al., Integrating probe-level expression changes across generations of Affymetrix arrays. *Nucleic Acids Res*, 2005. **33**(22): p. e193.
80. Strutz, F. and M. Zeisberg, *Renal fibroblasts and myofibroblasts in chronic kidney disease*. *J Am Soc Nephrol*, 2006. **17**(11): p. 2992-8.
81. Djamali, A., et al., Epithelial-to-Mesenchymal Transition and Oxidative Stress in Chronic Allograft Nephropathy
doi:10.1111/j.1600-6143.2004.00713.x. *American Journal of Transplantation*, 2005. **5**(3): p. 500-509.
82. Iwano, M., et al., Evidence that fibroblasts derive from epithelium during tissue fibrosis
10.1172/JCI200215518. *J. Clin. Invest.*, 2002. **110**(3): p. 341-350.

83. Acloque, H., J.P. Thiery, and M.A. Nieto, The physiology and pathology of the EMT. Meeting on the epithelial-mesenchymal transition. *EMBO Rep*, 2008. **9**(4): p. 322-6.
84. Rerolle, J.P., et al., Plasminogen activator inhibitor type 1 is a potential target in renal fibrogenesis. *Kidney Int*, 2000. **58**(5): p. 1841-50.
85. Tyler, J.R., et al., Chronic Allograft Nephropathy: Intraepithelial Signals Generated by Transforming Growth Factor- β ; and Bone Morphogenetic Protein-7
doi:10.1111/j.1600-6143.2006.01339.x. *American Journal of Transplantation*, 2006. **6**(6): p. 1367-1376.
86. Zeisberg, M., et al., Bone morphogenetic protein-7 inhibits progression of chronic renal fibrosis associated with two genetic mouse models. *Am J Physiol Renal Physiol*, 2003. **285**(6): p. F1060-7.
87. Kalluri, R. and M. Zeisberg, Exploring the connection between chronic renal fibrosis and bone morphogenetic protein-7. *Histol Histopathol*, 2003. **18**(1): p. 217-24.
88. Zeisberg, M., et al., BMP-7 counteracts TGF- β 1-induced epithelial-to-mesenchymal transition and reverses chronic renal injury. *Nat Med*, 2003. **9**(7): p. 964-8.
89. Willis, B.C. and Z. Borok, *TGF- β -induced EMT: mechanisms and implications for fibrotic lung disease*. *Am J Physiol Lung Cell Mol Physiol*, 2007. **293**(3): p. L525-34.
90. Bijlsma, M.F., C.A. Spek, and M.P. Peppelenbosch, *Hedgehog: an unusual signal transducer*. *Bioessays*, 2004. **26**(4): p. 387-94.
91. Lum, L. and P.A. Beachy, *The Hedgehog response network: sensors, switches, and routers*. *Science*, 2004. **304**(5678): p. 1755-9.
92. Rubin, L.L. and F.J. de Sauvage, *Targeting the Hedgehog pathway in cancer*. *Nat Rev Drug Discov*, 2006. **5**(12): p. 1026-33.
93. Katoh, Y. and M. Katoh, Hedgehog signaling, epithelial-to-mesenchymal transition and miRNA (review). *Int J Mol Med*, 2008. **22**(3): p. 271-5.
94. Cohen, M.M., Jr., *The hedgehog signaling network*. *Am J Med Genet A*, 2003. **123**(1): p. 5-28.
95. Hooper, J.E. and M.P. Scott, *Communicating with Hedgehogs*. *Nat Rev Mol Cell Biol*, 2005. **6**(4): p. 306-17.
96. Valentini, R.P., et al., Post-translational processing and renal expression of mouse Indian hedgehog. *J Biol Chem*, 1997. **272**(13): p. 8466-73.
97. Marigo, V., et al., Cloning, expression, and chromosomal location of SHH and IHH: two human homologues of the *Drosophila* segment polarity gene hedgehog. *Genomics*, 1995. **28**(1): p. 44-51.
98. Yoshikawa, M., et al., Inhibition of histone deacetylase activity suppresses epithelial-to-mesenchymal transition induced by TGF- β 1 in human renal epithelial cells. *J Am Soc Nephrol*, 2007. **18**(1): p. 58-65.
99. Zeisberg, M. and R. Kalluri, *The role of epithelial-to-mesenchymal transition in renal fibrosis*. *J Mol Med*, 2004. **82**(3): p. 175-81.
100. Katoh, Y. and M. Katoh, *WNT antagonist, SFRP1, is Hedgehog signaling target*. *Int J Mol Med*, 2006. **17**(1): p. 171-5.
101. Baroni, T., et al., Retinoic acid, GABA-ergic, and TGF- β signaling systems are involved in human cleft palate fibroblast phenotype. *Mol Med*, 2006. **12**(9-10): p. 237-45.
102. Roop, D. and R. Toftgard, *Hedgehog in Wnterland*. *Nat Genet*, 2008. **40**(9): p. 1040-1.

103. Yang, S.H., et al., Pathological responses to oncogenic Hedgehog signaling in skin are dependent on canonical Wnt/beta3-catenin signaling. *Nat Genet*, 2008. **40**(9): p. 1130-5.
104. van den Brink, G.R., et al., Indian Hedgehog is an antagonist of Wnt signaling in colonic epithelial cell differentiation. *Nat Genet*, 2004. **36**(3): p. 277-82.
105. Wodarz, A. and R. Nusse, *Mechanisms of Wnt signaling in development*. *Annu Rev Cell Dev Biol*, 1998. **14**: p. 59-88.
106. Kleber, M. and L. Sommer, *Wnt signaling and the regulation of stem cell function*. *Curr Opin Cell Biol*, 2004. **16**(6): p. 681-7.
107. You, J., et al., Wnt pathway-related gene expression in inflammatory bowel disease. *Dig Dis Sci*, 2008. **53**(4): p. 1013-9.
108. Coombs, G.S., T.M. Covey, and D.M. Virshup, *Wnt signaling in development, disease and translational medicine*. *Curr Drug Targets*, 2008. **9**(7): p. 513-31.
109. Zhou, B.P. and M.C. Hung, Wnt, hedgehog and snail: sister pathways that control by GSK-3beta and beta-Trcp in the regulation of metastasis. *Cell Cycle*, 2005. **4**(6): p. 772-6.
110. Luo, J., et al., Wnt signaling and human diseases: what are the therapeutic implications? *Lab Invest*, 2007. **87**(2): p. 97-103.
111. Pishvaian, M.J. and S.W. Byers, *Biomarkers of WNT signaling*. *Cancer Biomark*, 2007. **3**(4-5): p. 263-74.
112. Surendran, K. and T.C. Simon, CNP gene expression is activated by Wnt signaling and correlates with Wnt4 expression during renal injury. *Am J Physiol Renal Physiol*, 2003. **284**(4): p. F653-62.
113. Imgrund, M., et al., Re-expression of the developmental gene Pax-2 during experimental acute tubular necrosis in mice 1. *Kidney Int*, 1999. **56**(4): p. 1423-31.
114. Vlad, A., et al., *The first five years of the Wnt targetome*. *Cell Signal*, 2008. **20**(5): p. 795-802.
115. He, T.C., et al., *Identification of c-MYC as a target of the APC pathway*. *Science*, 1998. **281**(5382): p. 1509-12.
116. Niederreither, K. and P. Dolle, *Retinoic acid in development: towards an integrated view*. *Nat Rev Genet*, 2008. **9**(7): p. 541-53.
117. Kondo, T., et al., Sonic hedgehog and retinoic acid synergistically promote sensory fate specification from bone marrow-derived pluripotent stem cells. *Proc Natl Acad Sci U S A*, 2005. **102**(13): p. 4789-94.
118. Easwaran, V., et al., Cross-regulation of beta-catenin-LEF/TCF and retinoid signaling pathways. *Curr Biol*, 1999. **9**(23): p. 1415-8.
119. Hill, J.A., et al., Retinoic acid enhances Foxp3 induction indirectly by relieving inhibition from CD4+CD44hi Cells. *Immunity*, 2008. **29**(5): p. 758-70.
120. Xiao, S., et al., Retinoic acid increases Foxp3+ regulatory T cells and inhibits development of Th17 cells by enhancing TGF-beta-driven Smad3 signaling and inhibiting IL-6 and IL-23 receptor expression. *J Immunol*, 2008. **181**(4): p. 2277-84.
121. Elias, K.M., et al., Retinoic acid inhibits Th17 polarization and enhances FoxP3 expression through a Stat-3/Stat-5 independent signaling pathway. *Blood*, 2008. **111**(3): p. 1013-20.
122. Aparicio, O., J.V. Geisberg, and K. Struhl, Chromatin immunoprecipitation for determining the association of proteins with specific genomic sequences in vivo. *Curr Protoc Cell Biol*, 2004. **Chapter 17**: p. Unit 17 7.
123. Kumar, D., et al., JNK MAPK pathway regulates constitutive transcription of CCL5 by human NK cells through SP1. *J Immunol*, 2009. **182**(2): p. 1011-20.

-
124. Nickeleit, V. and K. Andreoni, *Inflammatory cells in renal allografts*. Front Biosci, 2008. **13**: p. 6202-13.
 125. Pribylova-Hribova, P., et al., TGF-beta1 mRNA upregulation influences chronic renal allograft dysfunction. Kidney Int, 2006. **69**(10): p. 1872-9.
 126. Hutchinson, I.V., The role of transforming growth factor-beta in transplant rejection. Transplant Proc, 1999. **31**(7A): p. 9S-13S.
 127. Lund, L.R., et al., Transforming growth factor-beta is a strong and fast acting positive regulator of the level of type-1 plasminogen activator inhibitor mRNA in WI-38 human lung fibroblasts. Embo J, 1987. **6**(5): p. 1281-6.
 128. Zeisberg, M., Bone morphogenic protein-7 and the kidney: current concepts and open questions *10.1093/ndt/gfk010*. Nephrol. Dial. Transplant., 2006. **21**(3): p. 568-573.
 129. Ducy, P. and G. Karsenty, *The family of bone morphogenetic proteins*. Kidney Int, 2000. **57**(6): p. 2207-14.
 130. Inoue, T., et al., A case report suggesting the occurrence of epithelial-mesenchymal transition in obstructive nephropathy. Clin Exp Nephrol, 2009.
 131. Okada, H., et al., Identification of a novel cis-acting element for fibroblast-specific transcription of the FSP1 gene. Am J Physiol, 1998. **275**(2 Pt 2): p. F306-14.
 132. Le Hir, M. and B. Kaissling, *Antibodies against macrophages that overlap in specificity with fibroblasts*. Kidney Int, 2005. **68**(5): p. author reply 2400-2401.
 133. Barraclough, R., *Calcium-binding protein S100A4 in health and disease*. Biochim Biophys Acta, 1998. **1448**(2): p. 190-9.
 134. Mazzucchelli, L., *Protein S100A4: too long overlooked by pathologists?* Am J Pathol, 2002. **160**(1): p. 7-13.
 135. Taylor, S., et al., S100A4 (p9Ka) protein in colon carcinoma and liver metastases: association with carcinoma cells and T-lymphocytes. Br J Cancer, 2002. **86**(3): p. 409-16.
 136. Grone, H.J., et al., Coexpression of keratin and vimentin in damaged and regenerating tubular epithelia of the kidney. Am J Pathol, 1987. **129**(1): p. 1-8.
 137. Nakatsuji, S., J. Yamate, and S. Sakuma, Relationship between vimentin expressing renal tubules and interstitial fibrosis in chronic progressive nephropathy in aged rats. Virchows Arch, 1998. **433**(4): p. 359-67.
 138. Katoh, M., WNT signaling in stem cell biology and regenerative medicine. Curr Drug Targets, 2008. **9**(7): p. 565-70.
 139. Shihab, F.S., et al., Expression of TGF-beta 1 and matrix proteins is elevated in rats with chronic rejection. Kidney Int, 1996. **50**(6): p. 1904-13.
 140. Fan, J.M., et al., Transforming growth factor-beta regulates tubular epithelial-myofibroblast transdifferentiation in vitro. Kidney Int, 1999. **56**(4): p. 1455-67.
 141. He, W., et al., Wnt/beta-catenin signaling promotes renal interstitial fibrosis. J Am Soc Nephrol, 2009. **20**(4): p. 765-76.
 142. Kirikoshi, H., H. Sekihara, and M. Katoh, WNT10A and WNT6, clustered in human chromosome 2q35 region with head-to-tail manner, are strongly coexpressed in SW480 cells. Biochem Biophys Res Commun, 2001. **283**(4): p. 798-805.
 143. Nishizuka, M., et al., Wnt4 and Wnt5a promote adipocyte differentiation. FEBS Lett, 2008.
 144. Iglesias, D.M., et al., *Canonical WNT signaling during kidney development*. Am J Physiol Renal Physiol, 2007. **293**(2): p. F494-500.
 145. Yu, J., et al., A Wnt7b-dependent pathway regulates the orientation of epithelial cell division and establishes the cortico-medullary axis of the mammalian kidney. Development, 2009. **136**(1): p. 161-71.
-

146. Lobov, I.B., et al., WNT7b mediates macrophage-induced programmed cell death in patterning of the vasculature. *Nature*, 2005. **437**(7057): p. 417-21.
147. Smith, K., et al., Up-regulation of macrophage wnt gene expression in adenoma-carcinoma progression of human colorectal cancer. *Br J Cancer*, 1999. **81**(3): p. 496-502.
148. Clevers, H., Wnt/beta-catenin signaling in development and disease. *Cell*, 2006. **127**(3): p. 469-80.
149. Speyer, C.L., et al., Regulatory effects of iNOS on acute lung inflammatory responses in mice. *Am J Pathol*, 2003. **163**(6): p. 2319-28.
150. Miyamoto, S., et al., Matrix metalloproteinase-7 triggers the matricrine action of insulin-like growth factor-II via proteinase activity on insulin-like growth factor binding protein 2 in the extracellular matrix. *Cancer Sci*, 2007. **98**(5): p. 685-91.
151. Decleves, A.E., et al., Dynamics of hyaluronan, CD44, and inflammatory cells in the rat kidney after ischemia/reperfusion injury. *Int J Mol Med*, 2006. **18**(1): p. 83-94.
152. Rouschop, K.M., et al., CD44 deficiency increases tubular damage but reduces renal fibrosis in obstructive nephropathy. *J Am Soc Nephrol*, 2004. **15**(3): p. 674-86.
153. Acharya, P.S., et al., Fibroblast migration is mediated by CD44-dependent TGF beta activation. *J Cell Sci*, 2008. **121**(Pt 9): p. 1393-402.
154. Medyouf, H. and J. Ghysdael, The calcineurin/NFAT signaling pathway: a novel therapeutic target in leukemia and solid tumors. *Cell Cycle*, 2008. **7**(3): p. 297-303.
155. Bourajaj, M., et al., NFATc2 is a necessary mediator of calcineurin-dependent cardiac hypertrophy and heart failure. *J Biol Chem*, 2008. **283**(32): p. 22295-303.
156. Maynard, C.L., et al., Contrasting roles for all-trans retinoic acid in TGF-beta-mediated induction of Foxp3 and Il10 genes in developing regulatory T cells. *J Exp Med*, 2009. **206**(2): p. 343-57.
157. Mucida, D., et al., Reciprocal TH17 and regulatory T cell differentiation mediated by retinoic acid. *Science*, 2007. **317**(5835): p. 256-60.
158. Klemann, C., et al., *Retinoid signals and Th17-mediated pathology*. *Nihon Rinsho Meneki Gakkai Kaishi*, 2009. **32**(1): p. 20-8.
159. Bartl, M.M., et al., Multiple receptors mediate apoJ-dependent clearance of cellular debris into nonprofessional phagocytes. *Exp Cell Res*, 2001. **271**(1): p. 130-41.
160. Liu, W., et al., *Regulation of gp330/megalin expression by vitamins A and D*. *Eur J Clin Invest*, 1998. **28**(2): p. 100-7.
161. Grimsrud, C.D., et al., Bone morphogenetic protein-7 in growth-plate chondrocytes: regulation by retinoic acid is dependent on the stage of chondrocyte maturation. *J Orthop Res*, 1998. **16**(2): p. 247-55.
162. Katoh, M., Transcriptional regulation of WNT2B based on the balance of Hedgehog, Notch, BMP and WNT signals. *Int J Oncol*, 2009. **34**(5): p. 1411-5.
163. Byers, S., et al., Retinoids increase cell-cell adhesion strength, beta-catenin protein stability, and localization to the cell membrane in a breast cancer cell line: a role for serine kinase activity. *Endocrinology*, 1996. **137**(8): p. 3265-73.

9 Supplementary data

Supplementary table 1: Oligonucleotides utilized for qPCR. Part 1

Assays on demand

Gene	Assay ID
Eukaryotic 18S rRNA	4310893E

Assays on demand

Gene ID	Gene Symbol	Assay ID
85272	<i>Bmp7</i>	Rn01528886_m1
84353	<i>Ctnnb1</i>	Rn00670330_m1
24508	<i>Irf1</i>	Rn00561424_m1
161452	<i>Lef1</i>	Rn00679641_m1
29216	<i>Lrp2</i>	Rn00667205_m1
25335	<i>Mmp7</i>	Rn00563467_m1
24599	<i>Nos2</i>	Rn00561646_m1
4851	<i>Notch1</i>	Rn01758625_m1
25124	<i>Stat1</i>	Rn00583505_m1
84382	<i>Tcf4</i>	Rn00584481_m1

Assays designed

Gene ID	Gene Symbol	Sense (5'->3')	Antisense (5'->3')
25712	<i>Irfng</i>	AACAGTAAAGCAAAAAAGGATGCATT Probe CGCCAAGTTCGAGGTGAACAACCC	TTCATTGACAGCTTTGTGCTGG

QuantiTec Primer Assays

Gene ID	Gene Symbol	Assay ID
83502	<i>Cdh1</i>	QT00176288
140589	<i>Gli1</i>	QT001586662
29146	<i>Jag1</i>	QT00193424
24514	<i>Jak2</i>	QT00189182
81818	<i>Vim</i>	QT00178724

Oligonucleotides for qPCR, self designed

Gene ID	Gene Symbol	Sense (5'->3')	Antisense (5'->3')
25365	<i>Actg2</i>	GGGATCCTGACCCTCAAATAC	AGGAGTGGTGCCAGATCTTCT
29134	<i>Axin2</i>	AAAACGGATTGAGATCCTTCAA	GTGGCTGGTGCAAAGACATA
25296	<i>Bmp4</i>	TCTGTCAAGACACCATGATTCC	TCCTAGCAGGACTTGGCATAA
24245	<i>Camk2b</i>	GTCAGCTAGAGATCACCAGAAGC	ATGGAGGCGTACAATGTTGG
24246	<i>Camk2d</i>	GGATCAAGGGCTCCACAG	CGTCCTTCAGGCACCAAG
24770	<i>Ccl2</i>	AGATGCAGTTAATGCCCCAC	CGACTCATTGGGATCATCTTG
25542	<i>Ccl3</i>	CTATGGACGGCAAATTCCAC	AGGCATTCAGTTCCAGCTC
81780	<i>Ccl5</i>	TGCTGCTTTGCTACCTCTC	CTTGAACCCACTTCTTCTCTGG
58919	<i>Ccnd1</i>	ATGCTAGAGGTCTGCGAGGA	CAGAGACAAGAAACGGTCCAG
25406	<i>Cd44</i>	CAGCAGCAGATCGATTTGAATA	CTGTAGCGGCCATTTTTTCTC
29393	<i>Col 1a1</i>	CTGGTACATCAGCCCAAACC	CGAACTGGAATCCATCGGTC
84032	<i>Col 11a1</i>	GAATGGTGGCTTTCAGTTTCCAG	GCTGGAAAGAAGTCTGAGGAAG
113927	<i>Csnk1a1</i>	ACCCAGCCTCGAAGACCT	ACTGATCATCTGGTCCAGCTAACAT
3627	<i>Cxcl10/lp10</i>	GCGGTGAGCCAAAGAAG	CAGGAGAAACAGGGACAGTTAGG
620711	<i>Dhh</i>	CCAACACTACAACCCCGACATAA	TGCAACGCTCTGTATCAG
171548	<i>Dkk3</i>	AGGTTACACAAGATAACCAACAACC	TTGCCTTCTCCATCCTCTACA
303811	<i>Dvl3_pred</i>	CTTCAATGGAACGCACAGG	TAGCATGAGGGTGAAGGAC

Supplementary table 1: Oligonucleotides utilized for qPCR. Part 2

Oligonucleotides for qPCR, self designed

Gene ID	Gene Symbol	Sense (5'→3')	Antisense (5'→3')
25661	<i>Fn1</i>	GCAAGCCAGTTTCCATCAAT	GACATCCGTACCTGCATC
24615	<i>Fsp1</i>	GCCTAGCTTCCTGGGGAGA	CTTCATTGTCCCTGTTGCTGT
84027	<i>Gsk3b</i>	TTCAACTTTACCACTCAAGAACTGTC	AGCATTAGTATCTGAGGCTGCTG
84399	<i>Ihh</i>	CCCAACTACAATCCCACAT	AGTTCAGACGGTCCCTTGCAG
25325	<i>Il10</i>	CTTTCAAAGAAGGACCAGCTG	GCAACCCAAGTAACCCTTAAAGT
24494	<i>IL1b</i>	TCGACAGTGAGGAGAATGACC	GGCTTGGAAGCAATCCTTAAT
24498	<i>Il6</i>	TGAGAAAAGAGTTGTGCAATGG	TTTTCTGACAGTGCATCATCG
314870	<i>Irak3_pred</i>	CCACCTAACTCGAAGCCTGT	CAGGAACAAGAACATTATCCACTG
50658	<i>Mapk9</i>	CCAAGGAATTGTTTGTGCTG	TCACGGTAGGCTCTCTTTGC
24577	<i>Myc</i>	GTGGAAAACCCGACAGTCAC	TGTTAGCGAAGCTCACGTTG
307231	<i>Nfat1_pred</i>	CCTCGTATCAGTGGGCAAAG	ATGAAGGCCTCATGTATGACGTT
307820	<i>Nfat5</i>	CCTTGAAAGCAATGAAAACGA	TGATCAGGGCATTAGGAAGG
361400	<i>Nfatc 3</i>	ACTCCTATATTTTCGCACATCTTCA	CACATTGTCCAAAGTGAGTTGG
305897	<i>Nfatc 4</i>	ATTGAGAGGGGCCTGAT	CCGCTTGTTGCTGTACTIONAG
311658	<i>Nfatc 2</i>	GCAGCTCCACGGCTACAT	ACTTGGTAGAAGGCGTGTGG
24617	<i>Serpine1/Pai-1</i>	TCCTCCACAGCCATTCTAGTC	CGAACCACAAAGAGAAAGGATC
24654	<i>Plcb1</i>	GCAGGTCCAAGTGTGATTG	ACTGACATCTGCCCTTTCTTG
25664	<i>Pparg</i>	TGTGGGGATGTCTCACAATG	GATCTCCGCCAACAGCTTC
24674	<i>Ppp3ca</i>	GGCACCTAACAGAGTATTTACAG	CCATACAGGGCGTCATAAACG
25023	<i>Prkcb1</i>	GCAAAGGGCTAATGACCAAA	AATGTCTCGTTCAAATTCAG
81749	<i>Prkch</i>	TCTGGGGAGTATTTGGGAAAC	GGCAAGTGCAGGCTGTAAC
89830	<i>Ptch1</i>	GATTTCCAAGGGGAAGGCTA	AACTTGCCGCAGTTCTTTTG
24705	<i>Rara</i>	GGGGAACCTACGAGAAGG	GCTGTTGTTGCTAGTGTACTTGC
81762	<i>Rock1</i>	TGGAAGACTTACGGAAAGCAAG	ATTGCTTCTTCTAACTGCTTCTG
25271	<i>Rxra</i>	ATCTTTGACAGGGTGTAAACG	AGCTCCGTCTTGTCCATCTG
361801	<i>Rxrb</i>	TTTTCTCCCTACCTCTGGAC	GGAGAAGGACGCAATGAGG
83574	<i>Rxrg</i>	GGGTCTCTGGTGAACACATC	CAGCTATACACCCCGTAGTGC
84402	<i>Sfrp1</i>	GAAGCCCCAAGGTACAACAG	GATGGCCTCCGATTTCAAC
310552	<i>Sfrp2</i>	TGCAAAACTAAGAACGAGGATG	GATTTTCAGTGCAGAGTCATTTT
89803	<i>Sfrp4</i>	TCGGTGCAAGTGCAAAAAG	TTTTGGCATGAATAACATAGCTG
309377	<i>Sfrp5_pred</i>	GTGCTCCAGCGACTTCGT	TCCCCATTGTCTATCTTGATCTC
29499	<i>Shh</i>	CAGGCTTCGACTGGGTCTAC	ACGGAGTTCTCTGCTTTTACA
29357	<i>Smad2</i>	CTCTCCGGCTGAACTGTCTC	GTAAGTGGCTGCAATCCAAG
25631	<i>Smad3</i>	CCAGTGCTACCTCCAGTGTTG	GGAAATGGCTGTAGTCATCCAG
50554	<i>Smad4</i>	TCACTATGAGCGGGTTGTCTC	CTTGGTGGAGCATTACTCTGC
116490	<i>Snai1</i>	CGTGTGTGGAGTTCACCTTC	CCAGGAGAGAGTCCCAGATG
24817	<i>Tcf1</i>	GATCACAGACACCAACCTCAG	GTGTCTGAGGTGAAGACCTGC
24253	<i>Tcf5</i>	ACGACTTCCTTTCCGACCTC	GGCTCACGTAACCGTAGTCG
59086	<i>Tgfb1</i>	CCAAGGAGACGGAATACAGG	GTTTGGGACTGATCCCATTG
81809	<i>Tgfb2</i>	GACATGCCGTCCCCTTC	CACTGAGCCAGAGGATGTTGTA
3851	<i>Tgfb3</i>	CCATAAATTCGACATGATCCAG	GACACATTGAAACGGAAAACC
24835	<i>Tnfa</i>	CCCAGACCCTCACACTCAG	TTTGCTACGACGTGGGCTA
29260	<i>Tlr4</i>	GATTTATCCAGGTGTGAAATTGAGA	TGTCAGTACCAAGTTGAGAGC
114557	<i>Wif1</i>	ATTCCCGTCAATATCCACTCC	GCCATGATGCCTTTATCCA
24881	<i>Wnt1</i>	GATGGTGGGGCATCGTG	GGGCTCTAGCACCCAGCTGTA
114487	<i>Wnt2</i>	GGTGGTACATGAGAGCGACAG	GACCTGGCACATTGTACAC
116466	<i>Wnt2b</i>	CGTCCTGGTGGTACATAGGG	AGACCCGGGATGTTGTAC
24882	<i>Wnt3</i>	CCCGCTCAGCTATGAACAAG	TCAGGTGCATGTGATCCAG

Supplementary table 1: Oligonucleotides utilized for qPCR. Part 3**Oligonucleotides for qPCR, self designed**

Gene ID	Gene Symbol	Sense (5'->3')	Antisense (5'->3')
303181	<i>Wnt3a</i>	CTCTGCCATGAACCGTCAC	CGGATAGTCCGTGGCATT
84426	<i>Wnt4</i>	CTGTGACCGGACAGTACACG	ATGTTGTCCGAGCATCCTG
64566	<i>Wnt5a</i>	TTCTTGGTGGTCCCTAGGTATG	GAGAAAGTCCCGCCAGTTG
282582	<i>Wnt5b</i>	GCACTGGGATGGGTTGAG	AGCGACCACCAGGAGTTG
316526	<i>Wnt6</i>	TTTCCGACGCTGGAAGT	AGCTGTCTCTCGAATGTCCTG
114850	<i>Wnt7a</i>	CCCGAACCCCTCATGAACCTAC	CATGGCACTTACACTCCAGTTTC
315196	<i>Wnt7b</i>	TCATGAACCTTACAACAATGAG	GTACATGAGCCCCGACTCC
291678	<i>Wnt8a</i>	CCCAAGGCCTATGTGACCTAC	TTACTACTTCCATGCCCATC
293990	<i>Wnt8b</i>	GGAGTGCTAACCAGGAGAC	CAGGGTGTACATAACTCCAGCAG
287357	<i>Wnt9a</i>	CCCTGGAGTGCCAGTACC	TCCTTGAAGCCTCGCTTG
303586	<i>Wnt9b</i>	GGCATCAAGGCTGTGAAGAG	CAGCACAGGAGCCTGACAC
316527	<i>Wnt10a</i>	CACGCATGAGACTCCACAAC	CTTTCGCCGCATGTTCTC
315294	<i>Wnt10b</i>	GCGGGTCTCCTGTTCTTG	GGCTCACCGGGAAGTTTTAG
140584	<i>Wnt11</i>	TGACATGCGCTGGAAGT	GGCATAACGAAGGCTGAC
500047	<i>Wnt16</i>	ACTGTATGGTCGCCACTGC	TGGTGCCGCTACTCAGTTC

Oligonucleotides for ChIP

Gene ID	Gene Symbol	Sense (5'->3')	Antisense (5'->3')
6352	CCL5	TGAGTTTGGACAAACCACAAGTGAATG	CGCCTGGTATCTTTATAGTCCTGTCCG
2597	GAPDH	GTTTCATCCAAGCGTGTAAAGG	GTCTTGAGGCCTGAGCTACG
3627	IP10/CXCL10	GCATTATAGTTAGAATGGATTGCAACC	CTCAGAAAACGTGGGCTAGTGTG
4843	NOS2	CTCTGTGCCAATAGCCTTCC	CCTCAGTTTTCGACTCGC

Supplementary table 2: Hedgehog pathway genes.

Gene_ID	Symbol	Microarray results						qPCR results						U34A
		PL			RA			PL			RA			
		7	14	56	7	14	56	7	14	56	7	14	56	
140589	Gli1							3.3	2.0	1.8	1.3	2.9	0.8	-
304729	Gli2													-
140588	Gli3													-
113927	Csnk1a1		1.4	1.3				n.s.	n.s.	n.s.	n.s.	n.s.	n.s.	✓
64462	Csnk1d									-1.7				✓
58822	Csnk1e													-
64086	Csnk1g1													-
65278	Csnk1g2													-
64823	Csnk1g3													-
29373	Bmp2				1.5									✓
25296	Bmp4	-2.0	-1.9	-1.9	-2.0	-1.9		-3.8	-4.7	-4.3	-5.1	-2.5	-2.4	✓
315824	Bmp5													-
25644	Bmp6													✓
85272	Bmp7	-1.5	-1.7	-1.8	-1.5	-1.5	-1.9	n.s.	-4.3	-4.0	-2.4	-2.8	n.s.	✓
680931	Bmp8a													-
301516	Stk36													-
84027	Gsk3b		1.2	1.3	1.6		1.7	n.s.	n.s.	n.s.	n.s.	n.s.	n.s.	✓
29499	Shh							-9.5	-15.7	-9.9	-9.6	-7.3	-3.2	✓
84399	Ihh							-4.4	-11.2	-33.3	-4.1	-3.0	-1.7	-
84380	Dhh							1.5	1.3	6.3	1.5	1.5	2.9	-
29216	Lrp2	-2.3	-4.1	-8.3	-2.1	-2.4	1.1	-3.1	-6.7	-36.1	-4.8	-4.3	-1.2	✓
25636	Prkaca													✓
293508	Prkacb			1.3	1.5	1.3	-1.1							✓
89830	Ptch1				-1.6		-2.0	3.8	4.1	5.3	3.4	4.9	-0.4	✓
25273	Smo													✓
361769	Sufu													-
24881	Wnt1													-
114487	Wnt2							n.s.	n.s.	n.s.	n.s.	n.s.	n.s.	-
116466	Wnt2b							-2.2	-2.8	-5.1	-2.2	-2.4	-1.6	-
24882	Wnt3							n.s.	n.s.	3.0	n.s.	n.s.	n.s.	-
84426	Wnt4							n.s.	n.s.	n.s.	n.s.	n.s.	n.s.	-
64566	Wnt5a							n.s.	n.s.	n.s.	n.s.	n.s.	n.s.	✓
282582	Wnt5b							n.s.	n.s.	n.s.	n.s.	-2.7	n.s.	-
316526	Wnt6							6.4	10.7	12.7	14.9	19.8	4.6	-
114850	Wnt7a							2.8	3.3	5.9	3.2	3.0	2.9	-
291678	Wnt8a							-2.6	-2.8	-3.4	-3.0	-3.8	-4.2	-
293990	Wnt8b							n.s.	n.s.	n.s.	n.s.	n.s.	n.s.	-
287357	Wnt9a							-2.3	-4.2	-3.7	-7.3	-6.7	-4.7	-
303586	Wnt9b							n.s.	n.s.	n.s.	n.s.	n.s.	n.s.	-
316527	Wnt10a							-6.1	-2.9	-2.3	-3.0	n.s.	n.s.	-
315294	Wnt10b							n.s.	n.s.	n.s.	n.s.	n.s.	n.s.	-
140584	Wnt11							n.s.	n.s.	n.s.	n.s.	n.s.	n.s.	-
500047	Wnt16													-

Supplementary table 2 summarizes the results of the microarray, as well as of the qPCR for genes associated with the hedgehog pathway. Genes were assigned in accordance with the KEGG database. Genes are represented by gene-IDs and official gene-symbols. Microarray and qPCR results are displayed per time point and treatment. Numbers denote fold changes, compared to the normal control kidneys. N.s.: non-significant regulation measured by qPCR. The last column displays if a gene is annotated to the array or not.

Supplementary table 3: Wnt canonical pathway genes.

Gene_ID	Symbol	Microarray data						qPCR data						U34A		
		PL		RA				PL		RA						
		7	14	56	7	14	56	7	14	56	7	14	56			
24185	Akt1	1.5	1.4													✓
25233	Akt2					1.3										✓
29414	Akt3			1.3												✓
24205	Apc		-1.2		-1.4	-1.2										✓
79257	Axin1		-1.3	-1.3			-1.7									✓
29134	Axin2		1.4	1.4	1.4			n.s.	n.s.	n.s.	n.s.	n.s.	n.s.			✓
84353	Ctnnb1							n.s.	n.s.	n.s.	n.s.	n.s.	n.s.			-
29373	Bmp2				1.5											✓
25296	Bmp4	-2.0	-1.9	-1.9	-2.0	-1.9		-3.8	-4.7	-4.3	-5.1	-2.5	-2.4			✓
25406	Cd44	2.9	3.0	2.7	3.5	3.0	2.1	23.8	20.2	24.2	15.1	19.3	4.2			✓
81650	Csnk2b				1.4	1.3	1.9									✓
29382	Ctbp1			-1.5			-2.4									✓
81717	Ctbp2															-
303811	Dvl3_pred							n.s.	n.s.	n.s.	n.s.	n.s.	n.s.			-
295445	Dkk4_pred															-
171548	Dkk3_pred							n.s.	n.s.	n.s.	n.s.	n.s.	n.s.			-
293897	Dkk1_pred															-
58868	Fzd1			-1.6	1.4		2.3									✓
64512	Fzd2															✓
266715	Fzd3															-
64558	Fzd4															-
317674	Fzd5															-
282581	Fzd6															-
266608	Fzd9															-
25661	Fn1	1.8	1.8	2.1	1.6	1.7	-1.7	2.6	2.6	3.5	n.s.	2.0	n.s.			✓
309377	Sfrp5							-7.0	-2.9	0.4	-8.8	-4.5	-3.8			-
89803	Sfrp4		2.1	2.4		1.7		n.s.	n.s.	n.s.	n.s.	n.s.	n.s.			✓
310552	Sfrp2							n.s.	n.s.	n.s.	n.s.	n.s.	n.s.			-
84402	Sfrp1							n.s.	n.s.	2.1	n.s.	n.s.	n.s.			-
84027	Gsk3b		1.2	1.3	1.6		1.7	n.s.	n.s.	n.s.	n.s.	n.s.	n.s.			✓
161452	Lef1	n.a.	n.a.	n.a.	n.a.	n.a.	n.a.	24.3	12.8	11.2	17.7	18.0	5.4			-
312781	Lrp6	n.a.	n.a.	n.a.	n.a.	n.a.	n.a.									-
24577	Myc	1.6	1.4	1.2	1.5	1.3	-1.7	3.4	n.s.	n.s.	n.s.	n.s.	-2.4			✓
24599	Nos2	1.9	1.6	1.6		-1.2	-1.6	661	360	332	472	192	15.2			✓
117104	Ppp2r2a		1.2	1.3	1.2		1.6									✓
60660	Ppp2r2b		-1.4	-1.6	-1.3	-1.3										✓
117281	Ppp2r1a			-1.5			-2.1									✓
246255	Ppp2r2d	n.a.	n.a.	n.a.	n.a.	n.a.	n.a.									-
24673	Ppp2cb			-1.5			-1.9									✓
24672	Ppp2ca															✓
117256	Ppp2r2c															✓
25682	Ppard				-1.3	-1.2	-1.5									✓
29192	Ps-1			-1.4		-1.3										✓
24705	Rara		-1.6	-1.7	-1.5		-1.8	n.s.	n.s.	n.s.	n.s.	n.s.	n.s.			✓
24525	Ras		1.4	1.4	1.7	1.4	1.8									✓
25631	Smad3							n.s.	n.s.	n.s.	n.s.	n.s.	n.s.			✓
29357	Smad2	1.5	1.4	1.3	1.5	1.5	-1.6	n.s.	n.s.	n.s.	n.s.	n.s.	n.s.			✓
50554	Smad4							n.s.	n.s.	n.s.	n.s.	n.s.	n.s.			✓
117526	Tbp		1.2	1.3	1.3											✓
24817	Tcf1		-1.4	-1.4	-1.4	-1.3		-2.5	-4.8	-9.0	-2.7	-1.9	-1.7			✓
84382	Tcf4		1.5	1.6	1.5			n.s.	n.s.	n.s.	n.s.	n.s.	n.s.			✓
24253	Cebpb			1.5												✓
25705	Tcf8		1.4	1.2	-1.5	-1.2										✓
25335	Mmp7		1.5	2.2				226	211	1009	186	299	62			✓
114557	Wif-1	n.a.	n.a.	n.a.	n.a.	n.a.	n.a.	n.s.	n.s.	n.s.	n.s.	n.s.	n.s.			-
24881	Wnt1	n.a.	n.a.	n.a.	n.a.	n.a.	n.a.									-
24882	Wnt3	n.a.	n.a.	n.a.	n.a.	n.a.	n.a.	n.s.	n.s.	3.0	n.s.	n.s.	n.s.			-
303181	Wnt3a	n.a.	n.a.	n.a.	n.a.	n.a.	n.a.	n.s.	n.s.	n.s.	n.s.	n.s.	n.s.			-
291678	Wnt8a	n.a.	n.a.	n.a.	n.a.	n.a.	n.a.	n.s.	n.s.	n.s.	n.s.	n.s.	n.s.			-
293990	Wnt8b	n.a.	n.a.	n.a.	n.a.	n.a.	n.a.	-2.3	-4.2	-3.7	-7.3	-6.7	-4.7			-
316527	Wnt10a	n.a.	n.a.	n.a.	n.a.	n.a.	n.a.	-6.1	-2.9	-2.3	-3.0	n.s.	n.s.			-
315294	Wnt10b	n.a.	n.a.	n.a.	n.a.	n.a.	n.a.									-

Supplementary table 3 summarizes the results of the microarray, as well as of the qPCR for genes associated with the WNT canonical pathway. Genes were assigned in accordance with the KEGG database. Genes are represented by gene-IDs and official gene-symbols. Microarray and qPCR results are displayed per time point and treatment. Numbers denote fold changes, compared to the normal control kidneys. N.s.: non-significant regulation measured by qPCR. The last column displays if a gene is annotated to the array or not.

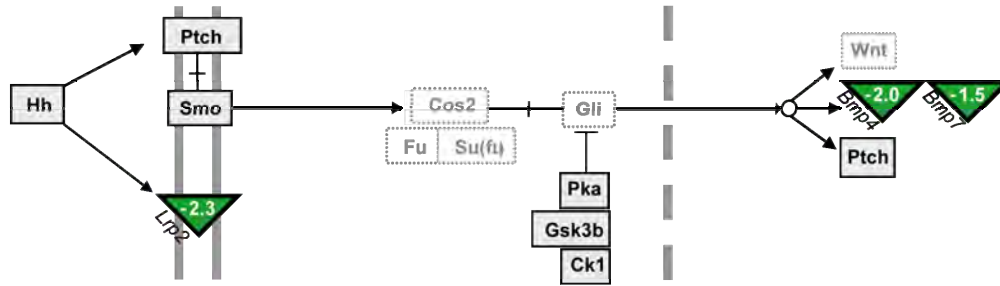
Supplementary table 4: Wnt - Ca+ pathway genes.

Gene_ID	Symbol	Microarray data						qPCR data						U34A		
		PL			RA			PL			RA					
		7	14	56	7	14	56	7	14	56	7	14	56			
171140	Camk2g															✓
25400	Camk2a															✓
24246	Camk2d							n.s.	n.s.	n.s.	n.s.	n.s.	n.s.	n.s.		✓
24245	Camk2b		1.3			-1.4		n.s.	n.s.	2.8	n.s.	n.s.	n.s.	n.s.		✓
171378	Ppp3cc															-
29749	Ppp3r2															✓
24674	Ppp3ca		1.4	1.4	1.4	1.3	1.7	n.s.	n.s.	n.s.	n.s.	n.s.	n.s.	n.s.		✓
24675	Ppp3cb		1.4	1.3	1.4											✓
29748	Ppp3r1			-1.4	1.3		-1.5									✓
266608	Fzd9															-
317674	Fzd5															-
266715	Fzd3															-
64512	Fzd2															✓
64558	Fzd4															-
282581	Fzd6															-
58868	Fzd1			-1.6	1.4		2.3									✓
24680	Prkca															✓
25023	Prkcb1	2.7	3.2	2.8	2.7	3.1	2.3	11.0	10.7	24.7	5.6	7.2	3.0			✓
170538	Prkcd	1.6	1.8	1.6	1.6	1.7	-1.6									✓
81749	Prkch	2.1	2.2	1.8	2.0	2.1		11.6	16.6	29.6	8.3	12.1	4.5			✓
25522	Prkcz	-1.5	-1.6	-1.6	-1.4	-1.4										✓
24654	Plcb1		-1.4	-1.7	-1.4	-1.3		n.s.	n.s.	n.s.	n.s.	n.s.	n.s.			✓
25031	Plcb4		1.3	1.3	1.5											✓
85240	Plcb2			1.3												✓
29322	Plcb3		1.3	1.3												✓
307231	Nfat1_pred							3.2	3.3	6.9	n.s.	2.9	n.s.			-
311658	Nfatc2							n.s.	n.s.	5.8	n.s.	2.8	2.6			-
361400	Nfatc3							n.s.	n.s.	n.s.	n.s.	n.s.	n.s.			-
305897	Nfatc4							n.s.	n.s.	n.s.	n.s.	n.s.	n.s.			-
307820	Nfat5							n.s.	n.s.	n.s.	n.s.	n.s.	n.s.			-
84426	Wnt4							n.s.	n.s.	n.s.	n.s.	n.s.	n.s.			-
64566	Wnt5a							n.s.	n.s.	n.s.	n.s.	n.s.	n.s.			✓
282582	Wnt5b							n.s.	n.s.	n.s.	n.s.	-2.7	n.s.			-
316526	Wnt6							6.4	10.7	12.7	14.9	19.8	4.6			-
114850	Wnt7a							2.8	3.3	5.9	3.2	3.0	2.9			-
315196	Wnt7b							-2.6	-2.8	-3.4	-3.0	-3.8	-4.2			-
140584	Wnt11							n.s.	n.s.	n.s.	n.s.	n.s.	n.s.			-

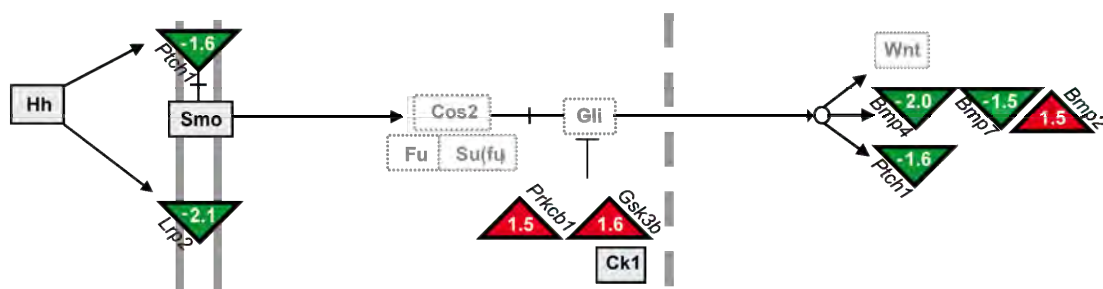
Supplementary table 2 summarizes the results of the microarray, as well as of the qPCR for genes associated with the WNT-Ca²⁺ pathway. Genes were assigned in accordance with the KEGG database. Genes are represented by gene-IDs and official gene-symbols. Microarray and qPCR results are displayed per time point and treatment. Numbers denote fold changes, compared to the normal control kidneys. N.s.: non-significant regulation measured by qPCR. The last column displays if a gene is annotated to the array or not.

Supplementary figure 1: HH pathway Placebo vs RA, day 7. Part 1

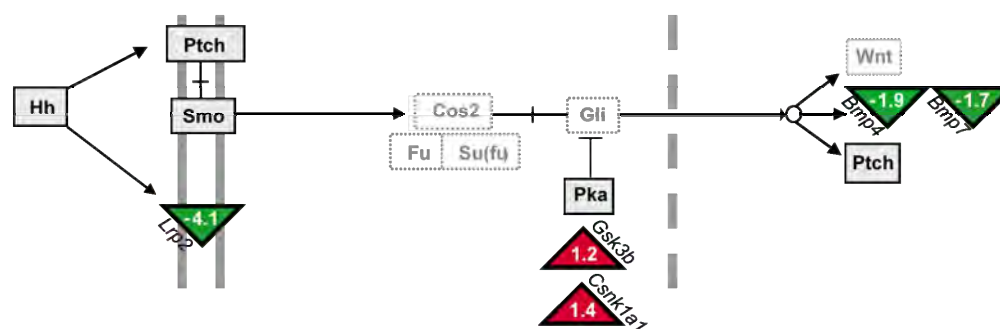
7 days Placebo



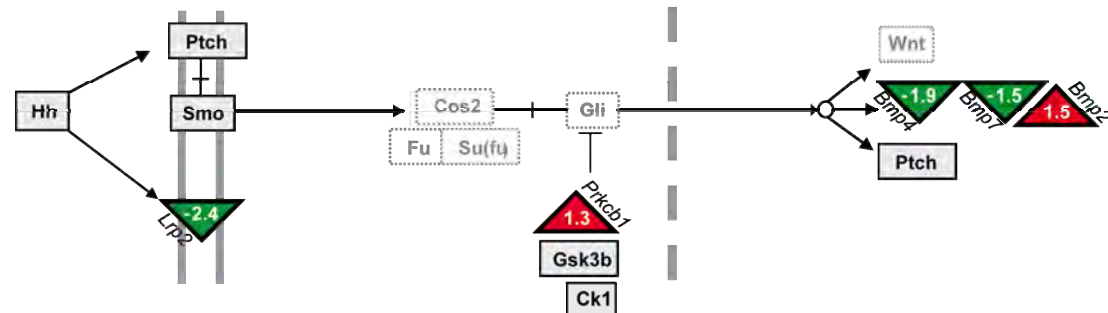
7 days RA



14 days Placebo



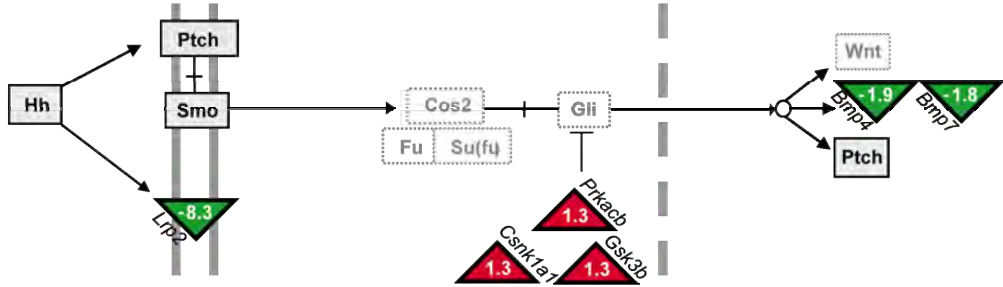
14 days RA



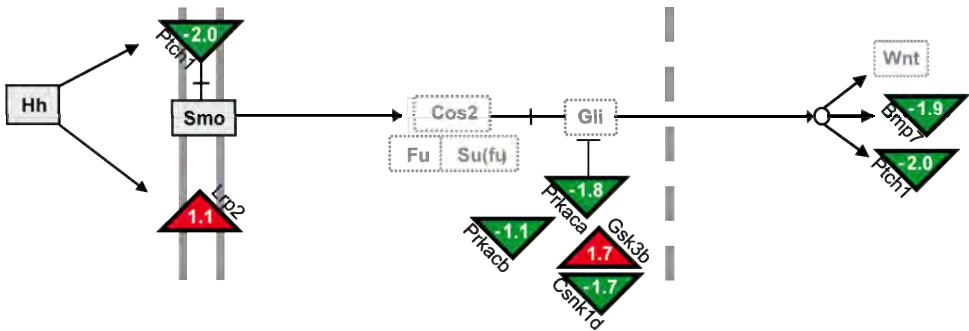
Microarray analysis of the hedgehog pathway. The scheme is a modified version of the pathway displayed on the KEGG database for rat . A white box marks a gene not annotated to the microarray. Triangles indicate the up or downregulation of genes in comparison to the control kidney. Red triangles indicate upregulation and green triangles indicate downregulation. The numbers displayed are ChipInspector generated fold changes (native scale, not log transformed).

Supplementary figure 1: HH pathway Placebo vs RA, day 14. Part 2

56 days Placebo

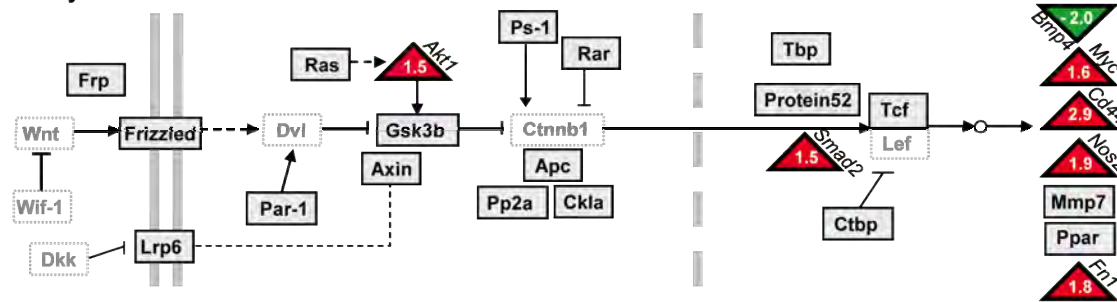


56 days RA

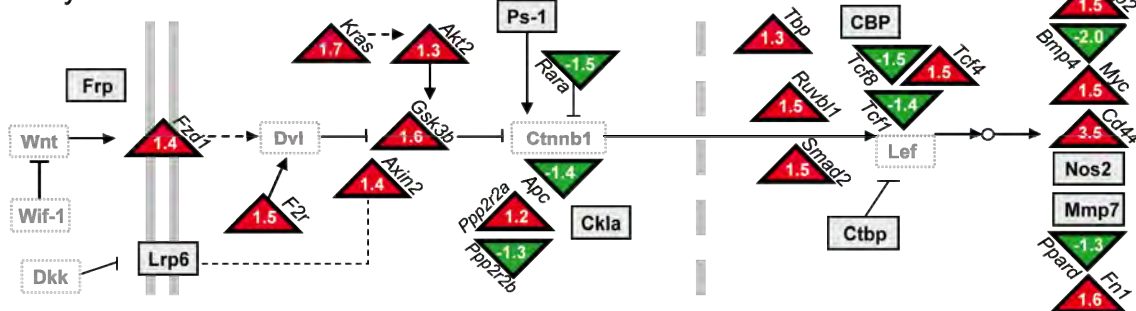


Supplementary figure 2: WNT canonical pathway Placebo vs RA, day 7. Part 1

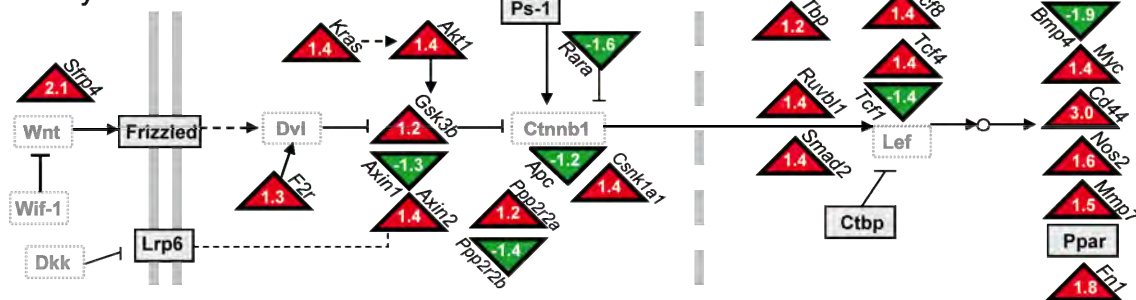
7 days Placebo



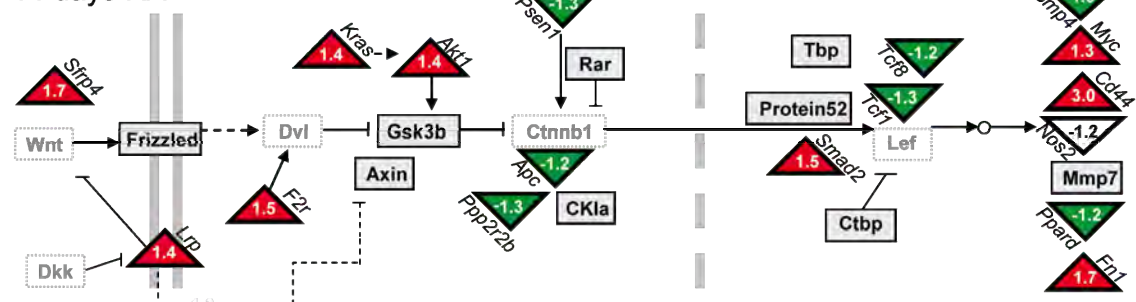
7 days RA



14 days Placebo



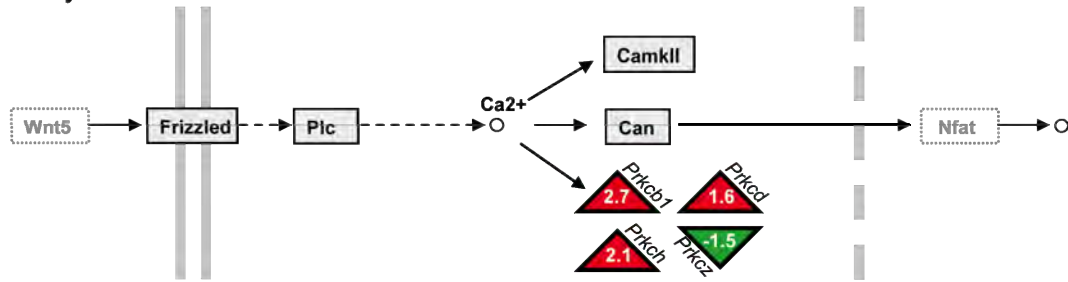
14 days RA



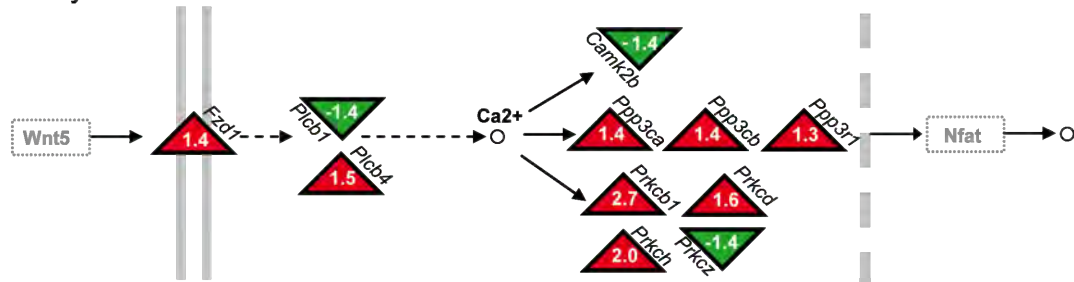
Microarray analysis of the Wnt canonical pathway. The scheme is a modified version of the pathway displayed on the KEGG database for rat. A white box marks a gene not annotated to the microarray. Triangles indicate the up or downregulation of genes in comparison to the control kidney. Red triangles indicate upregulation and green triangles indicate downregulation. The numbers displayed are ChipInspector generated fold changes (native scale, not log transformed).

Supplementary figure 3: WNT-Ca²⁺ pathway Placebo vs RA, day 7. Part 1

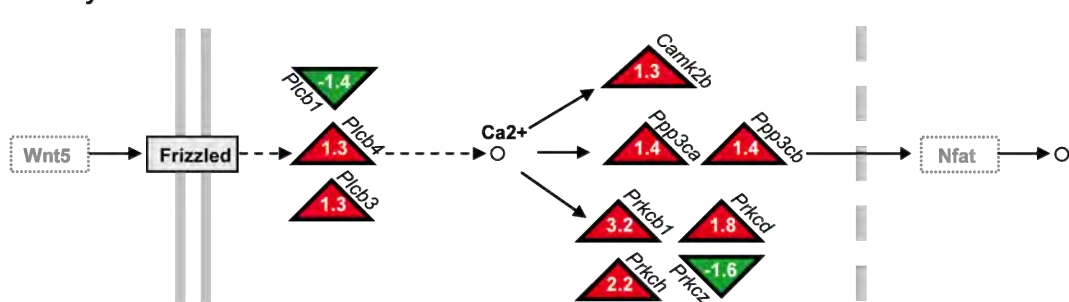
7 days Placebo



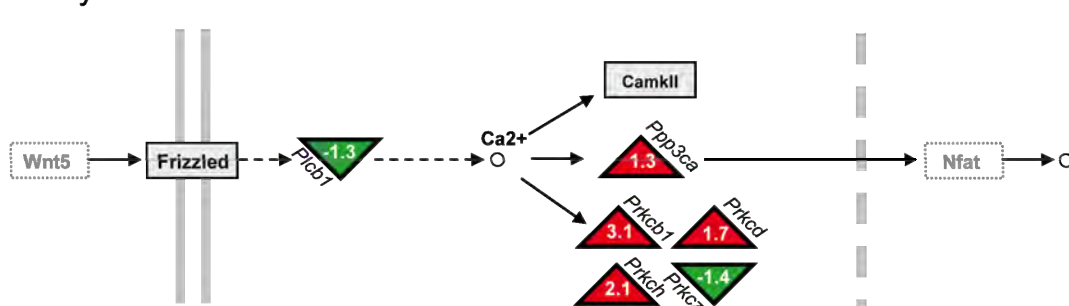
7 days RA



14 days Placebo



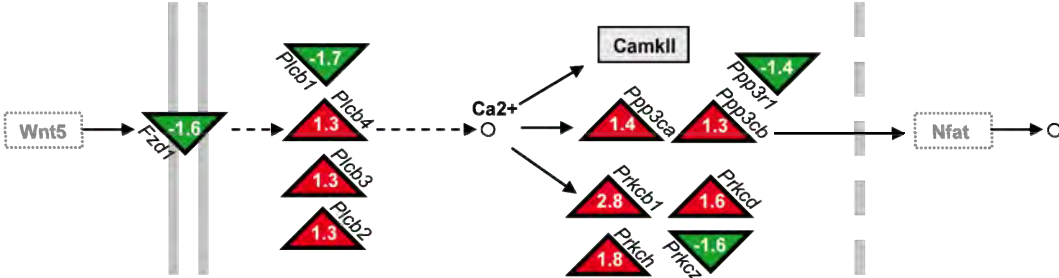
14 days RA



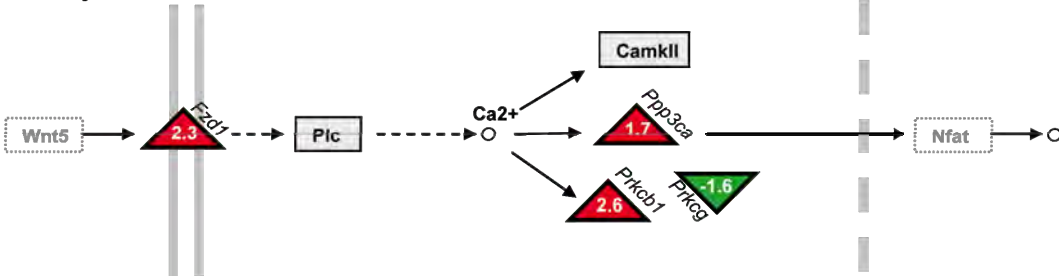
Microarray analysis of the Wnt-Ca²⁺ pathway. The scheme is a modified version of the pathway displayed on the KEGG database for rat . A white box marks a gene not annotated to the microarray. Triangles indicate the up or downregulation of genes in comparison to the control kidney. Red triangles indicate upregulation and green triangles indicate downregulation. The numbers displayed are ChiplInspector generated fold changes (native scale, not log transformed).

Supplementary figure 3: WNT-Ca²⁺ pathway Placebo vs RA, day 14. Part 2

56 days Placebo

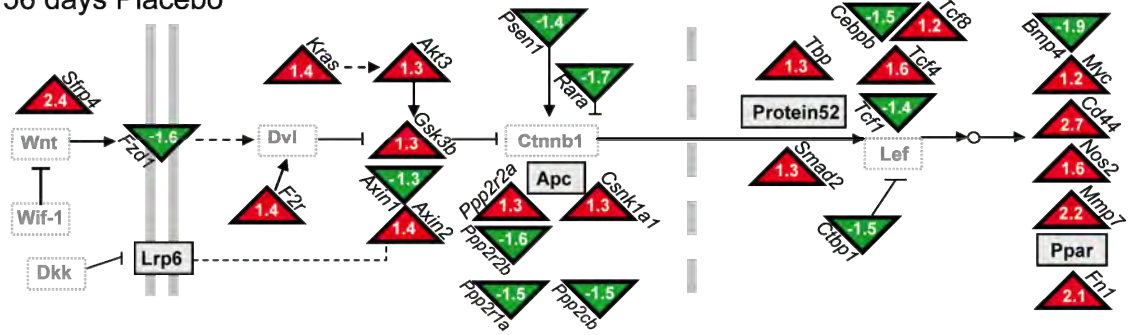


56 days RA

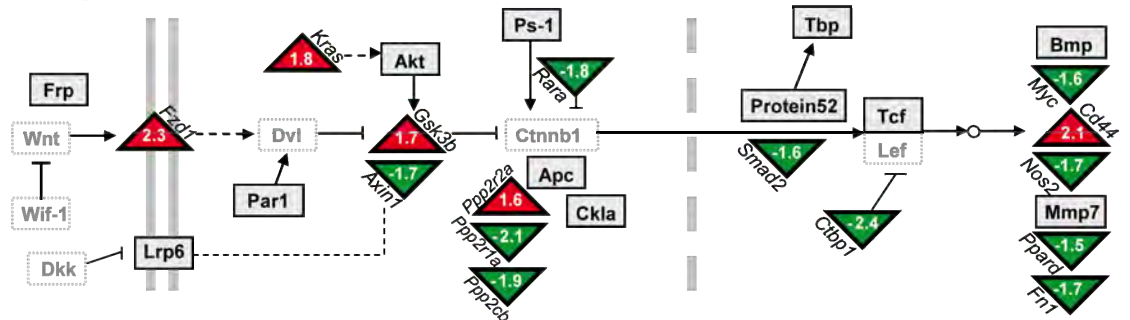


Supplementary figure 2: WNT canonical pathway Placebo vs RA, day 14. Part 2

56 days Placebo



56 days RA



10 Publications

Publications

Kumar D, Hosse J, **von Toerne C**, Noessner E, Nelson PJ. **JNK MAPK pathway regulates constitutive transcription of CCL5 by human NK cells through SP1**. J Immunol. 2009 Jan 15;182(2):1011–20.

Christine von Toerne, Claudia Schmidt, Judith Adams, Eva Kiss, Jens Bedke, Stefan Porubsky, Norbert Gretz, Maja T. Lindenmeyer, Clemens D. Cohen, Hermann–Josef Gröne and Peter J. Nelson **WNT Pathway Regulation in Chronic Renal Allograft Dysfunction** American Journal of Transplantation, in press

Publications in preparation

von Toerne, Christine, Schmidt, Claudia, Kiss, Eva, Loewe, Robert, Gröne, H.-J., Nelson, Peter **RA treatment influences Wnt and Hedghog regulatory in a model of chronic allograft damage**(in writing)

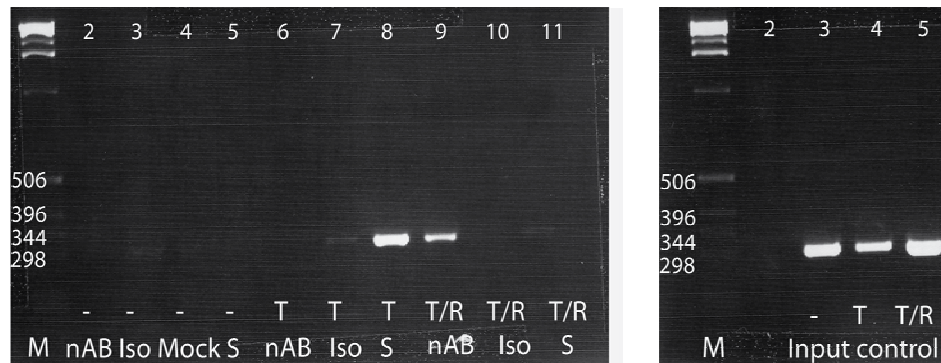
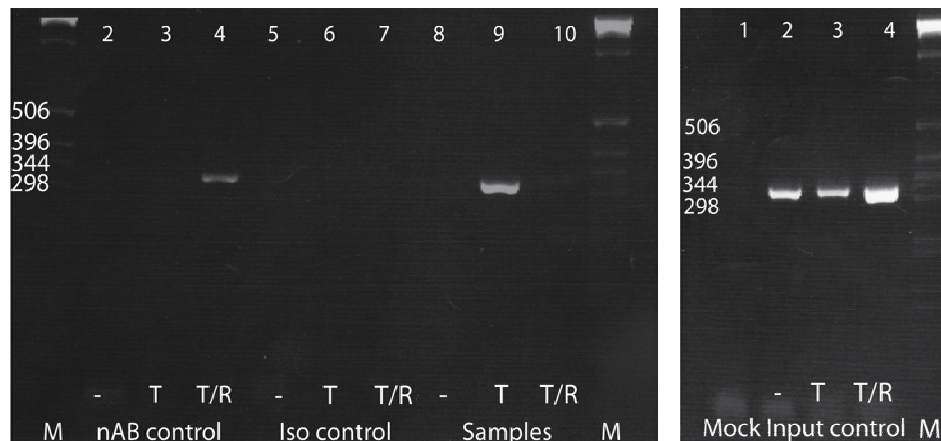
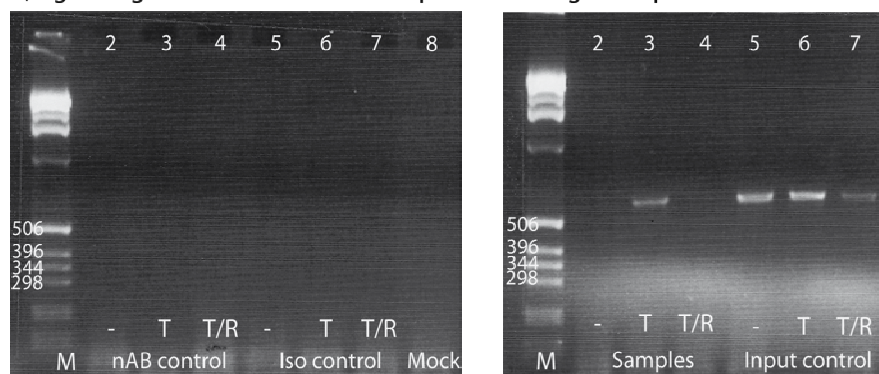
von Toerne, Christine, Diedrichs-Möhring, Maria, Sieg, Cornelia, Nelson, Peter J., Wildner, Gerhild **Differential gene expression in autoantigen-specific T cell lines causing monophasic or recurrent EAU in Lewis rats** (in writing)

Talks

Kongress für Nephrologie (38. Kongress der Gesellschaft für Nephrologie-GfN), 22.-25. September, **C. von Törne** et al. **Einfluss von 13-cis Retinsäure auf Signaltransduktionswege in fibrotischen und entzündlichen Vorgängen bei renalen allogenen Transplantationen**

Poster presentations

Cold Spring Harbor Laboratory Meeting: Epithelial-Mesenchymal Transition, March 17-20, 2008, **Christine von Toerne** et al. **Influence of WNT and TGF β pathway activation on EMT in fibrosis and inflammation**

Supplementary figure 4: Chromatin immunoprecipitation results**A) Agarose gel of PCR after the ChIP experiment using CCL5 primers****B) Agarose gel of PCR after the ChIP experiment using CXCL10/ IP10 primers****C) Agarose gel of PCR after the ChIP experiment using NOS2 primers**

This figure displays the original 2% agarose gels of the ChIP experiment discussed. Due to problems with the colour assignment after scanning the original photographs the colour information has been recalculated for black and white values only. PCR has been performed using (A) CCL5, (B) CXCL10/IP10, (C) NOS2 primer pairs as described in 4.4.5. Signals could be detected in all input samples, the actual samples of the TNFA treated group ((A) lane 8, (B) lane 9, (C) lane 3) and the no-antibody controls of the CCL5 ((A) lane 9) and the CXCL10/IP10 ((B) lane 4) PCRs.

Abbreviations: M: 1kb marker, nAB: no-antibody control, Iso/Iso control: isotype control, S/Samples: ChIP sample after precipitation with the NCOR antibody, -: unstimulated sample, T: TNFA stimulated sample, T/R: TNFA plus RA stimulated sample, Mock: mock control for buffers, containing no chromatin sample, Input: input control 1% of total DNA. .

11 Acknowledgements

I would like to thank

Prof. Dr. Schlöndorff for giving me the opportunity to work in his Institute

Prof. Dr. Elisabeth Weiß for the supervision of my PhD thesis and Prof. Dr. Peter Becker as my second supervisor

My boss, PD Dr. Peter Nelson for teaching me what is possible to accomplish with liberty granted and trust placed

Prof. Dr. Hermann-Josef Gröne at the DKFZ Heidelberg and his lab members for the close collaboration that made my work possible

Prof. Dr. Gerhild Wildner for the great collaboration and the warm support of my work, my carrer and me as person

PD Dr. Bruno Luckow for his time and advice

My colleges in the lab for fun, the necessary pampering and the sharing of great ideas

My family and friends for encouraging me

Philipp, for making me do the best I can

Hiermit erkläre ich, dass ich die vorliegende Dissertation selbstständig und unter ausschließlicher Verwendung der ausdrücklich bezeichneten Hilfsmittel angefertigt habe.

Christine von Törne

München, Juli 2009